Polish Academy of Sciences
Institute of Fundamental Technological Research

Archives of Mechanics

Archiwum Mechaniki Stosowanej

volume 55 issue 3

DRUKARNIA BRACI GRODZICKICH

SUBSCRIPTIONS

Address of the Editorial Office: Archives of Mechanics
Institute of Fundamental Technological Research, Świętokrzyska 21
PL 00-049 Warsaw, Poland
Tel. 48 (*prefix*) 22 826 60 22, Fax 48 (*prefix*) 22 826 98 15,
e-mail:publikac@ippt.gov.pl

Subscription orders for all journals edited by IFTR may be sent directly to the Editorial Office of the Institute of Fundamental Technological Research

Subscription rates

Annual subscription rate (2003) including postage is US $ 240.
Please transfer the subscription fee to our bank account: Payee: IPPT PAN,
Bank: PKO SA. IV O/Warszawa,
Account number 12401053-40054492-3000-401112-001.

All journals edited by IFTR are available also through:

- Foreign Trade Enterprise ARS POLONA Krakowskie Przedmieście 7,
  00-068 Warszawa, Poland fax 48 (*prefix*) 22 826 86 73

- RUCH S.A. ul. Towarowa 28,
  00-958 Warszawa, Poland fax 48 (*prefix*) 22 620 17 62

- International Publishing Service Sp. z o.o. ul. Noakowskiego 10 lok. 38
  00-664 Warszawa, Poland tel./fax 48 (*prefix*) 22 625 16 53, 625 49 55

Warunki prenumeraty

Redakcja przyjmuje prenumeratę na wszystkie czasopisma wydawane przez IPPT PAN. Bieżące numery można nabyć, a także zaprenumerować roczne wydanie Archiwum Mechaniki Stosowanej bezpośrednio w Dziale Wydawnictw IPPT PAN, Świętokrzyska 21, 00-049 Warszawa, Tel. 48 (*prefix*) 22 826 60 22; Fax 48 (*prefix*) 22 826 98 15.
Cena rocznej prenumeraty z bonifikatą (na rok 2003) dla krajowego odbiorcy wynosi 300 PLN

Również można je nabyć, a także zamówić (przesyłka za zaliczeniem pocztowym) we Wzorcowni Ośrodka Rozpowszechniania Wydawnictw Naukowych PAN,
00-818 Warszawa, ul. Twarda 51/55, tel. 48 (*prefix*) 22 697 88 35.
Wpłaty na prenumeratę przyjmują także jednostki kolportażowe RUCH S.A. Oddział Krajowej Dystrybucji Prasy, 00-958 Warszawa, ul. Towarowa 28. Konto: PBK. S.A. XIII Oddział Warszawa nr 11101053-16551-2700-1-67. Dostawa odbywa się pocztą lotniczą, której koszt w pełni pokrywa zleceniodawca. Tel. 48 (*prefix*) 22 620 10 39, Fax 48 (*prefix*) 22 620 17 62

Arkuszy wydawniczych 7,0. Arkuszy drukarskich 5,25.
Papier offset. kl III 70g. B1.
Druk ukończono w czerwcu 2003 r.
Skład w systemie TEX: E. Jaczyńska.
Druk i oprawa: Drukarnia Braci Grodzickich, Piaseczno ul. Geodetów 47A.

Arch. Mech., 55, 3, pp. 243–256, Warszawa 2003

Experimental research on development of the controllable disturbances in the wake at supersonic flow around the plate

V. I. LYSENKO, A. D. KOSINOV, Yu. G. YERMOLAEV

Russian Academy of Sciences,
Institute of Theoretical and Applied Mechanics,
Novosibirsk 630090, Russia.
e-mail: vl@itam.nsc.ru

THE DEVELOPMENT of the artificial disturbances in the boundary layer on the flat part of a plate, the boundary layer on the opposite wedge (model stern) behind a fan of expansion waves and the wake was investigated at Mach number 2.

1. Introduction

RESEARCH ON the flow in the wake behind an object is the important problem of aerodynamics. The base drag of bodies of revolution at supersonic speeds can be up to 30% of their complete drag (and particularly for cones – up to 50%; MIHALEV [1]; KOVENYA and LEBEDEV [2]), i.e. the flow in a wake can determine the aerodynamics of the flying apparatus. In addition, the value of the base drag can differ by more than 100% at laminar and turbulent regimes (MIHALEV [1]). Incidentally the condition of the boundary layer on a streamlined body renders influence on the position of transition in the wake.

In the system "boundary layer – wake" the process of turbulence origin in the wake behind a body has been investigated rarely so far. In the experiments (BEHRENS [3], DEMETRIADES [4], BEHRENS and KO [5], BEHRENS *et al.* [6], MCLAUGHLIN *et al.* [7], MCLAUGHLIN [8], LYSENKO [9–11]) on the stability of a wake at supersonic flow, the development of the natural disturbances is studied, therefore there are not the enough complete spatial characteristics of the wave field of oscillations. These characteristics can be obtained at the study of the controllable artificial disturbances, simulating the process of development of the natural ones (KOSINOV and MASLOV [12]). While there are many works (KOSINOV and MASLOV [12], KOSINOV *et al.* [13–15] and other), in which development of the artificial disturbances in a supersonic boundary layer was studied, the works on development of the artificial oscillations in a supersonic wake, on the whole, are absent. The main limitation of application of the method of controllable oscillations at the research on wave processes in a wake is the non-uniformity of flow, that hinders the definition of wave characteristics of unstable

disturbances, however the wave approach in a number of cases can be applied. In particular, in a quasi-two-dimensional task the non-uniformity of flow is present along a flow only, then it is possible to determine wave spectra on transversal wave number, and in linear approximation – to determine the transmission characteristics on wave numbers. Thus, the practical implementation of controllable experiments in a wake depends on the flow character.

According to LEES and GOLD [16], in a wake both symmetric (varicose) and antisymmetric (sinuous) disturbances can develop. And according to theoretical work by CHEN *et al.* [17], in the supersonic wake the two-dimensional waves of antisymmetric mode are the most unstable. Their phase velocity is about 0.8. The two-dimensional character of the most unstable disturbances of this mode remains at sub-, super- and hypersonic speeds of a flow. For the symmetric mode at supersonic speeds the three-dimensional waves are the most unstable, and the phase velocity increases with increasing Mach number. At $M = 2$ it is approximately equal to 0.6. The symmetric mode (by character of instability and values of phase velocity) is similar to the eigen-disturbances of supersonic boundary layer.

The influence of disturbances in the model boundary layer on disturbances in the wake is obviously possible, as their wave characteristics are close. At the same time it is necessary to take into account the circumstance, that the formation of a wake is accompanied by non-uniformity of flow in longitudinal direction, that results in the change of discrete spectrum on wave numbers to the continuous one.

The purpose of the present work was the study of development of the artificial disturbances (initiated on the surface of a flat plate) in the system "boundary layer on the flat part of a plate – boundary layer on the opposite wedge (model stern) behind a fan of expansion waves – wake" at supersonic free-flow velocities.

2. Research methods and equipment

The present experiments were carried out in the wind tunnel T-325 (BAGAEV *et al.* [18]) at free-flow Mach number $M_\infty = 2.0$, unit Reynolds number $Re_{1\infty} = 5.4 \cdot 10^6 \mathrm{m}^{-1}$, flow stagnation temperature 290 K.

As the basic test model (model 1), an insulated steel symmetric flat plate (Fig. 1) of 80 mm length (from the leading edge up to the back edge), 10 mm thickness, 200 mm width, having the bow and stern as wedges with bevel half-angle of the leading and back edges of 14°, was used. The length of both the bow and stern parts was 20 mm. For realization of an additional experiment, the model 2 (modified model 1) was used. For model 2 the stern looked like the opposite wedge with bevel half-angle of 10°. Accordingly, the length of the stern part has increased from 20 up to 28 mm, and the length of the central site has

decreased down to 32 mm (on model 1 it was equal to 40 mm). Other differences between models 1 and 2 were absent.

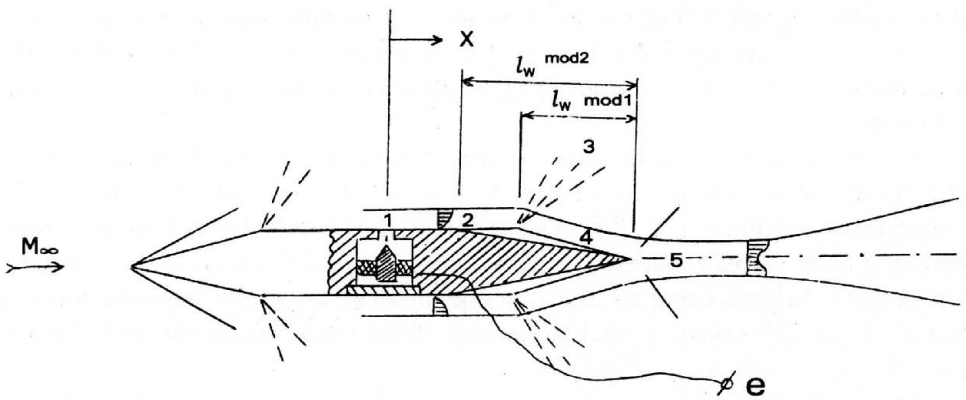

FIG. 1. The scheme of the model flowing around: (1) source of controllable disturbances, (2) plate flat-part boundary layer, (3) fan of expansion waves, (4) opposite-wedge boundary layer, (5) wake.

The plate was fixed rigidly to the lateral walls of the wind tunnel's test section and was established under a zero angle of attack. Inside of the model in the center, a source of controllable disturbances (similar to KOSINOV *et al.* [15, 19]) was placed. For excitation of the disturbances, the high-frequency electrical discharge device was used. The artificial disturbances penetrated through the hole of 0.4 mm diameter, 40 mm from the leading edge, into the boundary layer on the top surface of the plate. At glow discharge, in the interspace between an electrode and model surface (under the hole on the plate surface), the pressure and temperature oscillations arose, which disturbed the boundary layer, penetrating into it through this hole. A design and detailed description of the disturbance generator are adduced in KOSINOV *et al.* [19]. From the hole of disturbance generator, the longitudinal x and transversal z coordinates were measured.

The scheme of ignition of high-frequency electrical discharge consists of the generator of signals G3-112/1, power amplifier, raising transformer and electrodes (this scheme is described also in KOSINOV *et al.* [19]). The process of glow discharge was inspected by the oscillograph C1-96.

In the first section $x = 8$ mm, measured in the boundary layer, the parameter of excess of the maximum disturbance amplitude above the natural background was about 10, and in the wake it was about 2. The results presented in the paper are obtained for oscillations of frequency $f = 20$ kHz.

For measurement of disturbances, the constant-temperature hot-wire anemometer and the probe (with the tungsten wire of diameter of 5 microns and length of 1.2 mm) were used. The overheating of the probe wire was 0.8, and therefore it is possible to assert that the fluctuations of mass flow were mainly measured. The selective amplifier U2-8 was used as a frequent filter. With its help the amplitude of a signal on frequency $f = 20$ kHz in the bandwidth of 1% was measured.

The researches on development of disturbances in the model boundary layer and in the wake behind model 2 were conducted in the layer, in which the fluctuations are maximum. The measurements in the wake behind model 1 were executed at $E = \text{const}$, where E – mean voltage in the diagonal of the hot-wire-anemometer bridge, equal to mean voltage at boundary-layer measurements in the model end (it corresponded to moving of the sensor along the line of equal mass flow).

The fluctuating and average characteristics of the flow were measured with the help of the automated measuring system (KOSINOV *et al.* [19]) of the wind tunnel T-325. The fluctuating and average hot-wire voltages were recorded by a computer (DVK-3.2) using a ten-bit amplitude-digital converter (ADC) with 1 MHz reading frequency. The ADC was started synchronously with the generator setting the frequency of the introduced disturbances. For increase of the signal/noise ratio, the synchronous summation of a signal on 200 realizations was carried out. The time length of each realization was 200 microseconds. The averaged oscillograms of a fluctuation signal were controlled during the experiment. It allowed to determine the bounds of the introduced wave packet on z rather precisely. In experiments the oscillograms in several cross-sections on x were measured.

The complete spectral processing of digital oscillograms was carried out by an IBM PC. For spectral processing of experimental data, the discrete Fourier-transformation was used

$$e_{\beta\omega}(x,y) = \frac{2}{T}\sum_{j,k} e(x,\ y,\ z_j,\ t_k)\exp\left(-i\left[\beta z_j - \omega t_k\right]\right),$$

where $e(x,y,z_j,t_k)$ is the pulsation signal from the hot-wire anemometer, averaged through realizations, T – the length of realization in time, $\omega = 2\pi f$ – circular frequency of a disturbance, β – wave number in z-direction, j – list on coordinate z, k – list on time. Amplitude and phase of disturbances (in their notation we shall omit the index ω, as the selective amplifier was adjusted to one frequency) were found from the formulas

$$A^*_\beta = \{\mathrm{Re}^2[e_{\beta\omega}(x,y)] + \mathrm{Im}^2[e_{\beta\omega}(x,y)]\}^{0.5},$$

$$\Phi_\beta = \mathrm{arctg}\{\mathrm{Im}[e_{\beta\omega}(x,y)]/\mathrm{Re}[e_{\beta\omega}(x,y)]\}.$$

The wave-to-the basic flow inclination angle $\chi = \text{arctg}\,[\beta/\alpha_r(\beta)]$, where the wave number in x-direction α_r was determined from the relation $\alpha_r(\beta) = \Delta\Phi_\beta(x)/\Delta x$ due to linear phase dependence $\Phi_\beta(x)$.

The phase velocity of disturbances was determined by the formula $c_x = \lambda_x f/U_e$, where $\lambda_x = 2\pi/\alpha_r$ is the wavelength of a disturbance, U_e – flow velocity at the layer border.

3. Results

In conformity with the conditions of flowing round the model, the boundary-layer flow had a non-uniformity streamwise, connected with two fans of expansion waves. The first fan started near to the place of change of the nose wedge to the central (flat) model site, the second one – near to the place of change of the central site to the opposite wedge. In KOSINOV *et al.* [14] (this work was executed on the model "cone–cylinder") it was found, that behind a fan of expansion waves the pressure becomes constant at the distance equal to twenty values of the boundary-layer thickness. For conditions of the present experiments, it corresponds to about 6 mm from the first "fracture" of the model, moreover for the model "wedge–plate" this distance should be even smaller. Thus, in the present experiments the source of disturbances was placed in gradientless (on x) flow. In this case we should expect the development of disturbances on the central part of model, similarly to the results of experiments in the boundary layer on the flat plate (KOSINOV *et al.* [14]).

In this work, the development of controlled disturbances was investigated on 3 ranges: (I) on the central (flat) part of the plate, (II) at passage through a fan of expansion waves and on the opposite wedge, and (III) in the wake.

3.1. On the central (flat) part of the plate

For definition of the character of development of the introduced spatial wave packet ($f = 20$ kHz), the measurements of distributions (on transversal coordinate z) of mass-flow fluctuations in the boundary layer were executed at $x = 8, 13$ and 18 mm. The analysed range corresponds approximately to one disturbance wavelength. After the data processing, the wave amplitude-phase spectra on β and dispersion relations $\alpha_r(\beta)$ and $\chi(\beta)$ were obtained. In Fig. 2 the amplitude spectra A^*_β on β for $x = 8$, 13 and 18 mm are shown, normalized by the average value of mass flow in measurement positions. Thus, it was confirmed that on the flat part of the model, as well as in case of the flat plate (KOSINOV *et al.* [15]), the inclined disturbances with $\beta = \pm 1$ rad/mm are the most unstable. The asymmetry in spectra is caused by properties of the disturbance generator; this is confirmed after normalization of, amplitude spectra on β by the initial

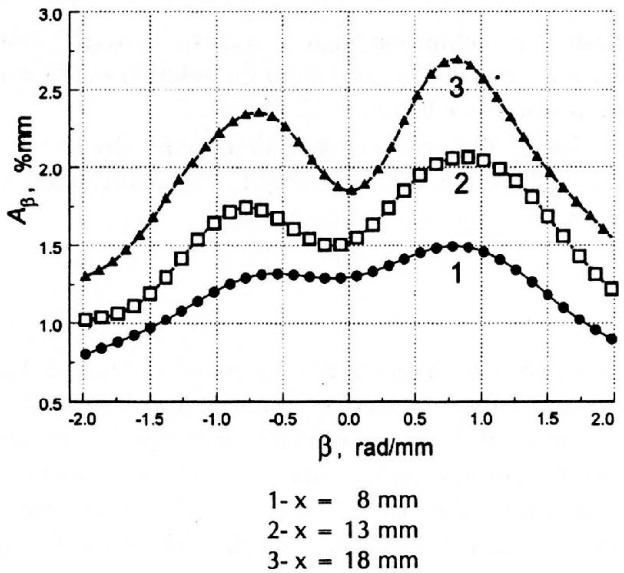

FIG. 2. Amplitude spectra for $x = 8$, 13 and 18 mm (flat part of model).

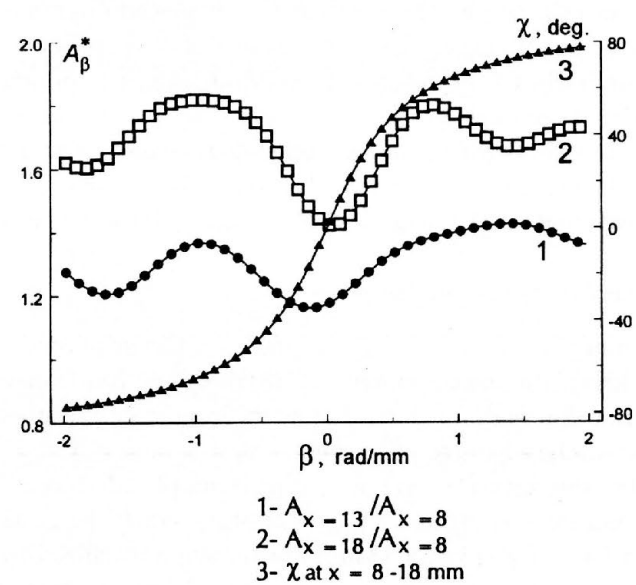

FIG. 3. Normalized amplitude spectra for $x = 8$, 13 and 18 mm, and dispersion dependence for $x = 8$–18 mm (flat part of model).

the initial(at $x = 8$ mm) spectrum. It is demonstrated in Fig. 3, where the examples of normalized amplitude spectra A^*_β for $x = 13$ and 18 mm (curves 1 and 2), depending on β, and the dispersion dependence $\chi(\beta)$ (curve 3) are given, where χ is the angle of the inclination of the wave front to the basic flow. It was found, that on the flat part of the plate the phase velocity of propagation of disturbances $c_x \approx 0.55$, the wave number in the streamwise direction $\alpha_r \approx 0.45$ rad/mm, and the inclined disturbances with $\chi \approx 60°$ are the most unstable. All the data, obtained in the boundary layer on the flat range of the plate, are in a good agreement with the researches on a flat plate (KOSINOV and MASLOV [12], KOSINOV *et al.* [13, 15]).

3.2. At passage through a fan of expansion waves and on the opposite wedge

The measurements of distributions of controllable oscillations on z on the opposite wedge are executed at $x = 25.2$; 30 and 35 mm. In Fig. 4 the amplitude spectra A^*_β on β for these values of longitudinal coordinate, normalized by the initial spectrum of disturbances at $x = 8$ mm, are exhibited. Figure 4 (curve 1, $x = 25.2$ mm) shows the considerable stabilization of disturbances at passage through a fan of expansion waves (i.e. at the negative gradient of pressure).

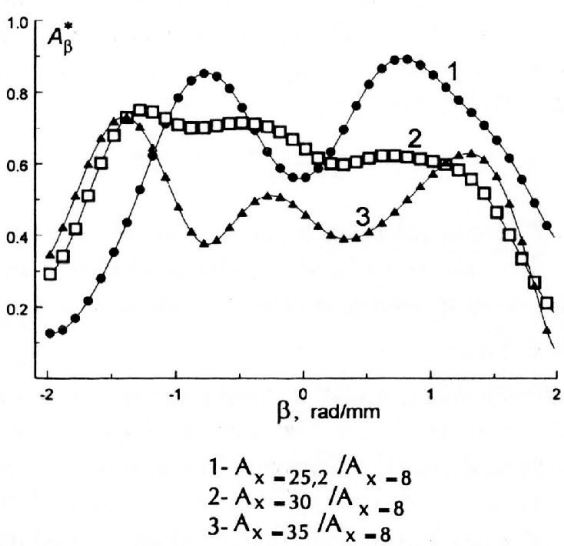

FIG. 4. Normalized amplitude spectra for x=25.2; 30 and 35 mm (opposite wedge).

This statement is in a complete conformity with the results of the theoretical works (GAPONOV and MASLOV [20], LYSENKO [21–22], GAPONOV and PETROV [23]) and the experiments (KOSINOV *et al.* [14], GAPONOV, KOSINOV *et al.* [24]),

in which the investigations were carried out on the "cone-cylinder" model. As a whole, on the opposite wedge after the fan of expansion waves (in the range $x = 25.2 - 35$mm), a certain decrease of the disturbance level was found. The obtained data correspond to the statements of GAPONOV and PETROV [23], GAPONOV, KOSINOV *et al.* [24] that the stability, arising under influence of the flow turn, is kept at large distance after its end, and correspond to the conclusion of KOSINOV *et al.* [14] that at some distance after recovery (after flow turn) of a boundary layer to the equilibrium condition, it remains stable. However it is important to notice, that the work by GAPONOV and PETROV [23] and part of the work by GAPONOV, KOSINOV *et al.* [24] are theoretical, and in experimental work by KOSINOV *et al.* [14] and in the experimental part of the work by GAPONOV, KOSINOV *et al.* [24] the "cone-cylinder" model is analysed.

As it was already indicated, the measurements of distributions on z were executed in a maximum of controllable fluctuations across the boundary layer. Before the turn of flow ($x = 20$ mm) this maximum was at $\frac{\rho U}{\rho_\infty U_\infty} = 0.9$, after the turn – at $\frac{\rho U}{\rho_\infty U_\infty} = 0.55$. It was found, that the flow was homogeneous on z down to $x = 30$ mm, and at $x = 35$ mm the essential (up to 5–10% concerning the mass flow in the free stream) distortion of flow in transversal direction was revealed, which was close to periodic. This periodicity corresponded approximately to 2 mm. Probably, the appearance of such non-uniformity on z is caused by influence of the wake.

3.3. In the wake

As measurements of controllable oscillations in the near wake behind the model have shown, the scale and non-uniformity level of flow in transversal direction remained the same, as well as on the opposite wedge at $x = 35$ mm. The measurements of distributions on z were executed at $\frac{\rho U}{\rho_\infty U_\infty} = 0.55$. In Fig. 5 the normalized amplitude spectrum A^*_β on wavenumber β in the wake for $x = 43$ mm is presented. One can see that in the wake, additional peaks in spectra on β occur. The data, obtained in this experiment for $x = 48$ mm, have turned out to be distorted, as this cross-section is already in the zone of strong nonlinear development of disturbances in the wake (and at about $x = 53$ mm, as the oscillograms have shown, in the wake the laminar-turbulent transition starts). This is why the additional investigation on changed model (model 2, with shorter flat part of the plate – 32 mm instead of 40 – and longer model stern – 28 mm instead of 20) was carried out to observe more confidently the development of disturbances in a wake. Such change of model stabilizes these disturbances. At first, as it was shown in the paper by LYSENKO [11], with increase of the length

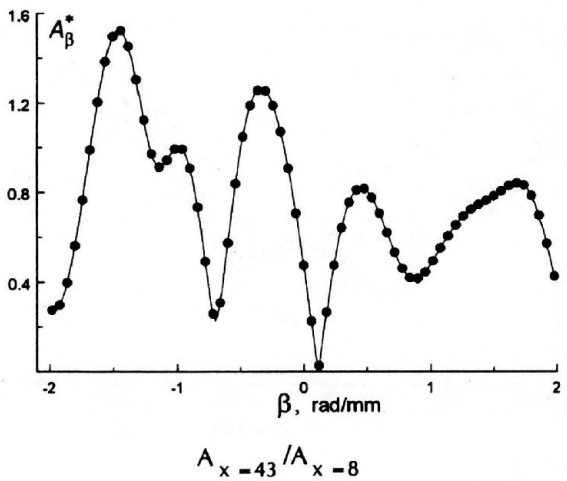

FIG. 5. Normalized amplitude spectrum for $x = 43$ mm (wake, model 1).

of the model stern part, the position of transition in a wake displaces downstream, and the stability of this wake slightly increases. Secondly, the decrease of bevel angle of the stern part (when it is an opposite wedge) from 14° to 10° and, naturally, the flow turn angle before a wake leads to reduction of intensity of the appropriate shock wave, which can be the generator of disturbances (similarly to the fan of expansion waves, which in works by KOSINOV *et al.* [14] and GAPONOV, KOSINOV *et al.* [24] resulted in the growth of sound oscillations). And with decreasing of shock-wave intensity the generated disturbances can decrease accordingly. Thus, the above-stated factors should result (at investigation on model 2) in considerable lengthening of the laminar site of disturbance development in the wake and transition delay.

In Figs. 6–7 the amplitude spectra A^*_β on β and χ in the wake behind the model 2 for $x = 41.5$; 51.5 and 61.5 mm, normalized by the wave spectrum at $x = 9$ mm are presented. These results demonstrate the evolution of disturbances in the wake and differ from the data shown in Fig. 5. At first, the relative amplitude is essentially (6–7 times) less than for the first model; secondly, spectra are more smooth, with smaller modulation of amplitude. Apparently, it is connected with changes of the flow character, becoming less unstable, and with essentially smaller non-uniformity of flow in transversal direction. In Fig. 8 the phase spectra Φ^*_β on β for $x = 41.5$; 51.5 and 61.5 mm are presented. These spectra resemble the phase spectra in the boundary layer. The dependences 2 and 3 are similar to each other, that proves the similar correspondence of α_r and β.

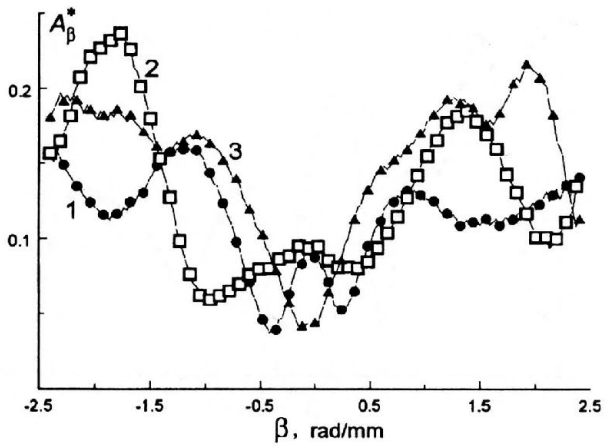

FIG. 6. Normalized amplitude spectra for $x = 41.5$; 51.5 and 61.5 mm (wake, model 2).

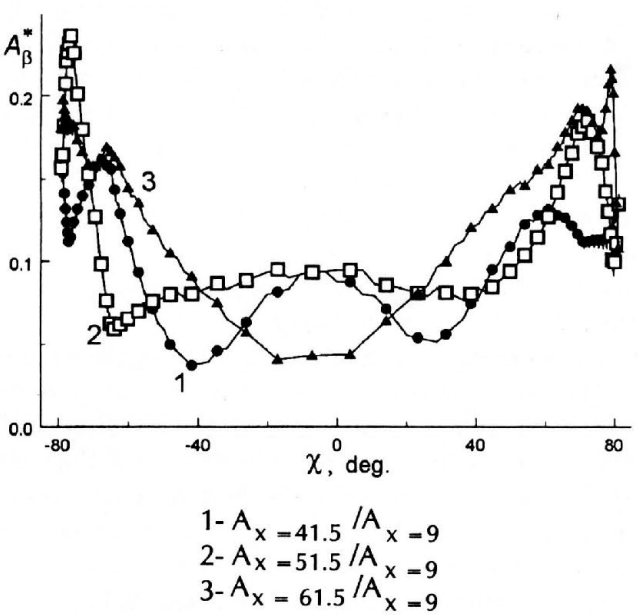

FIG. 7. Normalized amplitude spectra on the angle of inclination of wave vector to a flow for $x = 41.5$; 51.5 and 61.5 mm (wake, model 2).

The estimation of the phase velocity of disturbances in the wake ($x = 51.5$–61.5 mm), given in Fig. 9 (curve 1) depending on the angle of inclination of a wave vector to the flow, allows to conclude that in the experiments discussed the evolution of the wake symmetric mode is mainly observed, which is close, on phase velocities, to the eigen-waves of supersonic boundary layer. The curve 2 in Fig. 9, represented the dependence of amplitude of waves on the angle of inclination (for $x = 61.5$ mm), shows that the disturbances with angles of inclination more than 60° have the greatest relative amplitude. More complex evolution of disturbances in the wake behind the first model can be connected with greater instability and non-uniformity of flow. In principle, in any special case, the last circumstance can result in strong detuning of disturbances on wave numbers in longitudinal direction and generation of quasi two-dimensional antisymmetric mode.

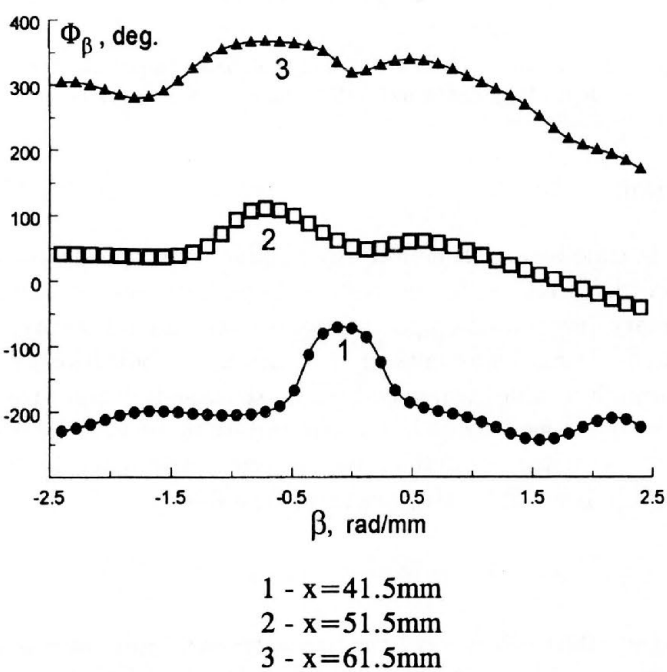

FIG. 8. Phase spectra for $x = 41.5$; 51.5 and 61.5 mm (wake, model 2).

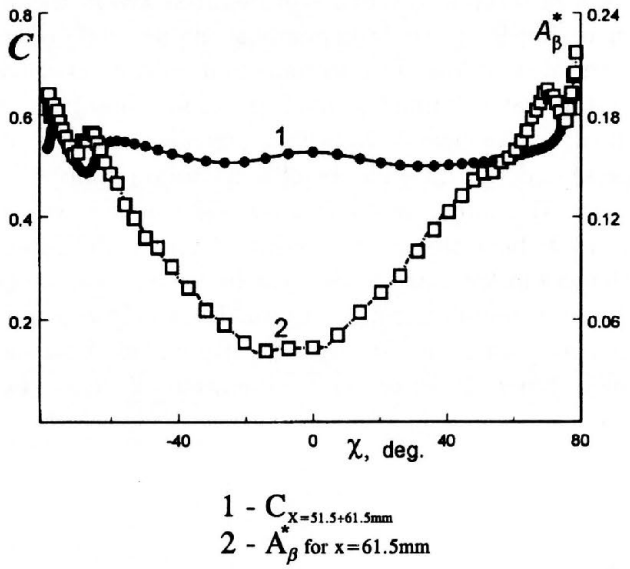

FIG. 9. Phase velocity (for $x = 51.5 - 61.5$ mm) and wave amplitude (for $x = 61.5$ mm) depending on the inclination angle (wake, model 2).

4. Conclusions

For the first time by experimental way at supersonic speeds, the development of the artificial disturbances in the system "boundary layer on the flat part of a plate – boundary layer on the opposite wedge (the model stern) after a fan of expansion waves – wake" was investigated. Strong stabilization of disturbances at passage through a fan of expansion waves at transition from the flat plate to the opposite wedge was confirmed. It was found, that the wake disturbances have a complex wave structure and that for the symmetric mode in the supersonic wake the three-dimensional waves are most unstable.

References

1. A. N. MIHALEV, *About influence of Reynolds number on the parameters of a near wake behind supersonic cones* [in Russian], [in:] Physical-Gasdynamical Ballistic Researches, Nauka, Leningrad 1980, 88–98.

2. V. M. KOVENYA, A. S. LEBEDEV, *Numerical modelling of viscous separated flow in a near wake* [in Russian], Zh. Prikl. Mekh. Tekh. Fiz., **5**, 53–59, 1989.

3. W. BEHRENS, *Far wake behind cylinders at hypersonic speeds: II. Stability*, AIAA J., **6**, 2, 225–232, 1968.

4. A. DEMETRIADES, *Hot-wire measurements in the hypersonic wakes of slender bodies*, AIAA J., **2**, 2, 245–250, 1964.

5. W. BEHRENS, D. R. S. KO, *Experimental stability studies in wakes of two-dimensional slender bodies at hypersonic speeds*, AIAA J., **5**, 851–857, 1971.

6. W. BEHRENS, J. E. LEWIS, W. H. WEBB, *Transition and turbulence phenomena in supersonic wakes of wedges*, AIAA J., **9**, 10, 2083–2084, 1971.

7. D. K. MCLAUGHLIN, J. E. CARTER, M. FINSTON, A. FORNEY, *Experimental investigation of the mean flow of the laminar supersonic cone wake*, AIAA J., **9**, 3, 479–484, 1971.

8. D. K. MCLAUGHLIN, *Experimental investigation of the stability of the laminar supersonic cone wake*, AIAA J., **9**, 4, 696–702, 1971.

9. V. I. LYSENKO, *Experimental research on stability and transition in high-speed wakes. Part 1. Research on the transition position in supersonic and hypersonic wakes, and the effects of temperature and other factors*, Engn.Trans., **46**, 3–4, 243–250, 1998.

10. V. I. LYSENKO, *Experimental research on stability and transition in high-speed wakes. Part 2. Influence of parameters of supersonic free flow on development of disturbances in a wake*, Engn.Trans., **46**, 3–4, 251–260, 1998.

11. V. I. LYSENKO, *Experimental research on stability and transition in high-speed wakes. Part 3. Influence of thickness of a flat plate and length of its stern on stability of a supersonic wake*,Engn.Trans., **46**, 3–4, 261–269, 1998.

12. A. D. KOSINOV, A. A. MASLOV, *The development of the artificially caused disturbances in the supersonic boundary layer* [in Russian], Izv. Akad. Nauk SSSR, Mekh. Zhid. Gaza, 5, 37–43, 1984.

13. A. D. KOSINOV, A. A. MASLOV, S. G. SHEVELKOV, *An experimental research of wave structure of the supersonic boundary layer* [in Russian], Zh. Prikl. Mekh. Tekh. Fiz., 5, 107–112, 1986.

14. A. D. KOSINOV, A. A. MASLOV, S. G. SHEVELKOV, *Stability of a supersonic boundary layer after a fan of waves of rarefaction* [in Russian], Zh. Prikl. Mekh. Tekh. Fiz., 3, 113–117, 1989.

15. A. D. KOSINOV, A. A. MASLOV, S. G. SHEVELKOV, *Experiments on the stability of supersonic laminar boundary layers*, J. Fluid Mech., **219**, 621–633, 1990.

16. L. LEES, H. GOLD, *Stability of laminar boundary layers and wakes at hypersonic speeds. Part 1. Stability of laminar wakes*, [in:] Fund. Phenom. in Hypersonic Flow, 4, 310–337, Cornell Univ. Press, Buffalo, N.Y. 1964.

17. J. H. CHEN, B. J. CANTWELL, N. N. MANSOUR, *The effect of Mach number on the stability of a plane supersonic wake*, Phys. Fluids A, **2**, 6, 984–1004, 1990.

18. G. I. BAGAEV, V. A. LEBIGA, V. G. PRIDANOV, V. V. CHERNYH, *A supersonic wind tunnel T-325 with low-degree turbulence* [in Russian], [in:] Aerodynamic researches, Novosibirsk 1972, 11–13.

19. A. D. KOSINOV, N. V. SEMIONOV, S. G. SHEVELKOV, *Investigation of supersonic boundary layer stability and transition using controlled disturbances*, [in:] Methods of Aerophysical Research, Proc. 7-th Intern. Conference, **2**, 159–166, Novosibirsk 1994.

20. S. A. GAPONOV, A. A. MASLOV, *Stability of a supersonic boundary layer with gradient of pressure and suction* [in Russian], [in:] Development of disturbances in a boundary layer, Inst. Theor. Appl. Mechanics, Novosibirsk 1979, 95–103.

21. V. I. LYSENKO, *Characteristics of stability of a supersonic boundary layer and its connection with the position of transition of a laminar boundary layer into a turbulent one* [in Russian], Izv. SO AN SSSR, Ser. Tekh. Nauk, **1**, 4, 79–86, 1985.

22. V. I. LYSENKO, *About a role of the first and second modes of disturbances in the process of transition of a supersonic boundary layer* [in Russian], Zh. Prikl. Mekh. Tekh. Fiz., 6, 58–62, 1985.

23. S. A. GAPONOV, G. V. PETROV, *Stability of a supersonic boundary layer at turn of flow* [in Russian], Izv. SO AN SSSR, Ser. Tekh. Nauk, **5**, 18, 25–30, 1987.

24. S. A. GAPONOV, A. D. KOSINOV, A. A. MASLOV, S. G. SHEVELKOV, *About influence of a fan of rarefaction waves on the development of disturbances in a supersonic boundary layer* [in Russian], Zh. Prikl. Mekh. Tekh. Fiz., 2, 52–55, 1992.

Received April 24, 2001; revised version February 11, 2003.

Arch. Mech., **55**, 3, pp. 257–274, Warszawa 2003

On Bénard convection in a porous medium in the presence of throughflow and rotation in hydromagnetics

SUNIL[(1)], P. K. BHARTI[(1)], R. C. SHARMA[(2)]

[(1)] *Department of Applied Sciences,*
National Institute of Technology,
Hamirpur, (H.P.)–177 005, India.

[(2)] *Department of Mathematics,*
Himachal Pradesh University,
Summer Hill, Shimla–171 005, India.

THE EFFECT OF THROUGHFLOW on a layer of a rotating fluid heated from below in porous medium in the presence of a vertical magnetic field is considered. For the case of stationary convection, the rotation has always a stabilizing effect. The medium permeability has always a destabilizing effect whereas the magnetic field and the throughflow have always a stabilizing effects in the absence of rotation. But in the presence of rotation, the medium permeability is found to have a destabilizing effect whereas the magnetic field and the throughflow have a stabilizing effects under certain conditions. Graphs have been plotted by giving numerical values to the parameters, to depict the stability characteristics. The magnetic field and rotation introduce oscillatory modes in the system, which were nonexistent in their absence. The sufficient conditions for non-existence of the overstability are also obtained.

Key words: Thermal instability, throughflow, magnetic field, rotation, porous medium.

1. Introduction

THE DETERMINATION of the criterion for the onset of convection in a horizontal fluid layer heated uniformly from below is a classical problem associated with Lord Rayleigh and H. Bénard. The steady state conduction solution becomes unstable, and convection begins when the Rayleigh number R exceeds a certain critical value R_c. A comprehensive account of the onset of Bénard convection, under varying assumptions of hydromagnetics, has been given by CHANDRASEKHAR [1]. In the classical problem, there is no flow of fluid across the horizontal boundaries. A slightly modified problem when a layer of fluid subjected to an adverse vertical temperature gradient with an imposed constant vertical motion downward/upward through the layer, called throughflow, produced by injection at one boundary and removal of fluid at the other boundary, is studied by SHVARTSBLAT [2, 3, 4] and his results were summarized by

GERSHUNI and ZHUKHOVITSKII [5]. The throughflow is measured by a Péclet number P_e.

Shvartsblat pointed out that the problem is of interest because of the importance of possibility in controlling the convective instability by adjustment of the transverse throughflow and importance in control of convection by the adjustment of transverse throughflow and also due to its relevance in meteorology. He also found, for the case of conducting rigid permeable boundaries, that R_c was independent of the sign of P_e, and increased markedly with P_e increasing, i.e. the throughflow is stabilizing and is independent of the direction of the flow. GERSHUNI and ZHUKHOVITSKII ([5], p. 236) wrote that the stabilizing effect may be explained as follows. With increasing injection velocity, a temperature boundary layer forms at one of the boundaries. This decreases the effective thickness of the stratified layer of fluid which (at sufficiently large P_e) is of order $d_{\text{eff}} \sim d/P_e$, where d is the layer depth. On the other hand, the characteristic temperature difference across the layer remains fixed. The critical Rayleigh number defined in terms of d is thus of the order of $R_c \sim (d/d_{\text{eff}})^3$, so that it increases with the Péclet number according to $R_c \sim P_e^3$.

The effect of throughflow is in general quite complex. Not only is the basic temperature profile altered, but also in the perturbation equations certain contributions arise from the convection of both the temperature and velocity, and there is an interaction between all is these contributions. The meteorologists KRISHNAMURTI [6, 7, 8] and SOMERVILLE and GAL-CHEN [9] have discussed the effects of small amounts of throughflow, but their main interest in it was the measure of a vertical asymmetry and associated stability of hexagonal cells. NIELD [10] has studied the effect of vertical throughflow on the onset of convection in a fluid layer by considering the boundaries which are either rigid or free and either insulating or conducting. The effect of magnetic field on the stability of thermal flow is of interest to geophysics, particularly in the study of earth's core, when earth's mantle, which consists of conducting fluid, behaves like a porous medium that can become convectively unstable as a result of differential diffusion. Another application of the results of flow through a porous medium in the presence of a magnetic field is the study of stability of the convective geothermal flow.

The effect of vertical throughflow in a porous medium has not been extensively discussed so far, in spite of its natural occurrence in many geothermal and deep-sea hydrodynamic problems. The flow through porous media is of considerable interest for petroleum engineers and for specialists in geophysical fluid dynamics as stated in a book by CHIN [11]. A great number of applications in geophysics may be found in a book by PHILLIPS [12]. When the fluid slowly percolates through the pores of a rock, the gross effect is represented by Darcy's law. As a result of this macroscopic law, the usual viscous term in the equations of

fluid motion is replaced by the resistance term $\left[-\frac{\mu}{k_1}\mathbf{q}\right]$, where μ is the viscosity of the fluid, k_1 is the medium permeability and $\mathbf{q}$ is the Darcian (filter) velocity of the fluid. HOMSY and SHERWOOD [13] and NIELD [14] have also studied the convective instability in porous medium with throughflow.

The purpose of the present study is to discuss the effect of throughflow (so-called mass-discharge) on thermal instability of the fluid in a porous medium in the presence of rotation in hydromagnetics by using the linearized stability theory and the normal mode analysis method. Earlier SPARROW [15] presented an experimental study of the heat transfer and temperature field in an enclosure in the presence of rotation and coolant throughflow. The *in-situ* processing of energy resources such as coal, oil shale, or geothermal energy, often involves the non-isothermal flow of fluids through porous medium. This throughflow is an integrated feature of in-situ processing, and it is of interest to assess its effect on the stability limits. Many operations and processes involving the thermal flow of rotating fluid through porous medium with throughflow commonly occur in geophysics, packed-bed processing, *in-situ* coal gasification and other problems.

2. Formulation of the problem and perturbation equations

Here we consider an infinite, horizontal, incompressible fluid layer of thickness d, with the uniform and prescribed vertical velocity w_0 at the horizontal boundaries, heated from below, so that the temperatures and densities at the bottom surface $z = 0$ are T_0 and ρ_0, and at the upper surface $z = d$ they are T_d and ρ_d, respectively, and that a uniform temperature gradient $\beta\,(= |dT/dz|)$ is maintained. Here w_0, the imposed vertical velocity is the magnitude of the throughflow. The gravity field $\mathbf{g} = (0,\ 0,\ -g)$, a uniform vertical magnetic field $\mathbf{H} = (0,\ 0,\ H)$ and a uniform vertical rotation $\mathbf{\Omega} = (0,\ 0,\ \Omega)$ act on the system. This fluid layer is flowing through an isotropic and homogeneous porous medium of porosity ε and medium permeability k_1.

Let ρ, p, T and $\mathbf{q} = (u, v, w)$ denote the fluid density, pressure, temperature and filter velocity, respectively. Then the momentum balance, mass balance and energy balance equations of fluid flowing through porous medium, following the Boussinesq approximation, are given by

$$\frac{\rho_0}{\varepsilon}\left[\frac{\partial \mathbf{q}}{\partial t} + \frac{1}{\varepsilon}(\mathbf{q}.\nabla)\,\mathbf{q}\right] = -\nabla p + (\rho_0 + \delta\rho)\,\mathbf{g} - \frac{\mu}{k_1}\mathbf{q} + \frac{\mu_e}{4\pi}(\nabla \times \mathbf{H}) \times \mathbf{H} + \frac{2\rho_0}{\varepsilon}(\mathbf{q} \times \mathbf{\Omega}), \tag{2.1}$$

$$\nabla.\mathbf{q} = 0, \tag{2.2}$$

$$E\frac{\partial T}{\partial t} + (\mathbf{q}.\nabla)\, T = \kappa \nabla^2 T. \tag{2.3}$$

Here $E = \varepsilon + (1-\varepsilon)\left(\frac{\rho_s c_s}{\rho_0 c_v}\right)$ is a constant, while ρ_s, c_s and ρ_0, c_v stand for the density and heat capacity of the solid (porous matrix) material and the fluid, respectively.

The Maxwell equations yield

$$\varepsilon\frac{d\mathbf{H}}{\mathrm{dt}} = (\mathbf{H}.\nabla)\,\mathbf{q} + \varepsilon\eta\nabla^2\mathbf{H}, \tag{2.4}$$

$$\nabla.\mathbf{H} = 0 \tag{2.5}$$

where $\frac{d}{dt} = \frac{\partial}{\partial t} + \frac{1}{\varepsilon}\mathbf{q}.\nabla$ stands for the convective derivative.

The equation of state is

$$\rho = \rho_0\left[1 - \alpha\left(T - T_0\right)\right], \tag{2.6}$$

where the subscript zero refers to values at the reference level $z = 0$. In writing Eq. (2.1), use has been made of the Boussinesq approximation, which states that the density variations are ignored in all the terms in the equation of motion except the external force term.

The basic solution is

$$\mathbf{q} = (0,\ 0,\ w_0), \qquad T = -\beta z + T_0, \qquad \rho = \rho_0\left(1 + \alpha\beta z\right), \tag{2.7}$$

where w_0 is the magnitude of the throughflow.

Here we use the linearized stability theory and the normal mode analysis method. Assume small perturbations around the basic solution, and let $\delta\rho$, δp, θ, $\mathbf{h}(h_x, h_y, h_z)$ and $\mathbf{q}' = (u, v, w)$, denote, respectively, the perturbations in fluid density ρ, pressure p, temperature T, magnetic field $\mathbf{H}$ $(0,\ 0,\ H)$ and velocity $\mathbf{q} = (0,\ 0,\ w_0)$. The change in density $\delta\rho$, caused mainly by the perturbation of the temperature θ, is given by

$$\delta\rho = -\alpha\rho_0\theta. \tag{2.8}$$

Then the linearized perturbation equations of the fluid reduce to:

$$\frac{1}{\varepsilon}\left[\frac{\partial u}{\partial t} + \frac{1}{\varepsilon}w_0\frac{\partial u}{\partial z}\right] = -\frac{1}{\rho_0}\frac{\partial}{\partial x}\delta p - \frac{\nu}{k_1}u + \frac{\mu_e H}{4\pi\rho_0}\left(\frac{\partial h_x}{\partial z} - \frac{\partial h_z}{\partial x}\right) + \frac{2}{\varepsilon}v\Omega, \tag{2.9}$$

$$\frac{1}{\varepsilon}\left[\frac{\partial v}{\partial t}+\frac{1}{\varepsilon}w_0\frac{\partial v}{\partial z}\right]=-\frac{1}{\rho_0}\frac{\partial}{\partial y}\delta p-\frac{\nu}{k_1}v+\frac{\mu_e H}{4\pi\rho_0}\left(\frac{\partial h_y}{\partial z}-\frac{\partial h_z}{\partial y}\right)-\frac{2}{\varepsilon}u\Omega, \tag{2.10}$$

$$\frac{1}{\varepsilon}\left[\frac{\partial w}{\partial t}+\frac{1}{\varepsilon}w_0\frac{\partial w}{\partial z}\right]=-\frac{1}{\rho_0}\frac{\partial}{\partial z}\delta p+g\alpha\theta-\frac{\nu}{k_1}w, \tag{2.11}$$

$$\frac{\partial u}{\partial x}+\frac{\partial v}{\partial y}+\frac{\partial w}{\partial z}=0, \tag{2.12}$$

$$E\frac{\partial\theta}{\partial t}+w_0\frac{\partial\theta}{\partial z}=\beta w+\kappa\nabla^2\theta, \tag{2.13}$$

$$\frac{\partial h_x}{\partial x}+\frac{\partial h_y}{\partial y}+\frac{\partial h_z}{\partial z}=0, \tag{2.14}$$

$$\varepsilon\frac{\partial h_x}{\partial \mathrm{t}}=H\frac{\partial u}{\partial z}+\varepsilon\eta\nabla^2 h_x, \tag{2.15}$$

$$\varepsilon\frac{\partial h_y}{\partial \mathrm{t}}=H\frac{\partial v}{\partial z}+\varepsilon\eta\nabla^2 h_y, \tag{2.16}$$

$$\varepsilon\frac{\partial h_z}{\partial \mathrm{t}}=H\frac{\partial w}{\partial z}+\varepsilon\eta\nabla^2 h_z. \tag{2.17}$$

Applying the operator $-\dfrac{\partial}{\partial x}$ to Eq. (2.9), and $-\dfrac{\partial}{\partial y}$ to Eq. (2.10), using (2.12) and adding, we get

$$\frac{1}{\varepsilon}\left[\frac{\partial}{\partial t}\left(\frac{\partial w}{\partial z}\right)+\frac{1}{\varepsilon}w_0\frac{\partial^2 w}{\partial z^2}\right]=\frac{1}{\rho_0}\left(\frac{\partial^2}{\partial x^2}+\frac{\partial^2}{\partial y^2}\right)\delta p-\frac{\nu}{k_1}\frac{\partial w}{\partial z}+\frac{\mu_e H}{4\pi\rho_0}\nabla^2 h_z-\frac{2\Omega}{\varepsilon}\zeta, \tag{2.18}$$

where $\zeta=\dfrac{\partial v}{\partial x}-\dfrac{\partial u}{\partial y}$ is z-component of vorticity.

Now applying $\frac{\partial}{\partial z}$ to Eq. (2.18) and $\left(\frac{\partial^2}{\partial x^2}+\frac{\partial^2}{\partial y^2}\right)$ to Eq. (2.11) and adding, we get

$$\left[\frac{1}{\varepsilon}\frac{\partial}{\partial t}+\frac{w_0}{\varepsilon^2}\frac{\partial}{\partial z}+\frac{\nu}{k_1}\right]\nabla^2 w = g\alpha\left(\frac{\partial}{\partial x^2}+\frac{\partial}{\partial y^2}\right)\theta+\frac{\mu_e H}{4\pi\rho_0}\frac{\partial}{\partial z}\nabla^2 h_z-\frac{2\Omega}{\varepsilon}\frac{\partial\zeta}{\partial z}. \tag{2.19}$$

Applying $-\frac{\partial}{\partial y}$ to Eq. (2.9) and $\frac{\partial}{\partial x}$ to Eq. (2.10) using (2.12) and adding, we get

$$\left[\frac{1}{\varepsilon}\frac{\partial}{\partial t}+\frac{w_0}{\varepsilon^2}\frac{\partial}{\partial z}+\frac{\nu}{k_1}\right]\zeta=\frac{2\Omega}{\varepsilon}\frac{\partial w}{\partial z}+\frac{\mu_e H}{4\pi\rho_0}\frac{\partial\xi}{\partial z}, \tag{2.20}$$

where $\xi=\frac{\partial h_y}{\partial x}-\frac{\partial h_x}{\partial y}$ stand for the z-component of the current density.

Now applying $-\frac{\partial}{\partial y}$ to Eq. (2.15) and $\frac{\partial}{\partial x}$ to Eq. (2.16) and adding, we get

$$\left[\varepsilon\frac{\partial}{\partial t}-\varepsilon\eta\nabla^2\right]\xi=H\frac{\partial\zeta}{\partial z}. \tag{2.21}$$

3. The dispersion relation

Analyzing the disturbances appearing in two-dimensional waves, and considering the disturbances characterized by a particular wave number, we assume that the perturbation quantities are of the form

$$[w,\ h_z,\ \theta,\ \zeta,\ \xi] = [W(z),\ K(z),\ \Theta(z),\ \mathrm{Z(z)},\ \mathrm{X(z)}]\exp\left(ik_x x+ik_y y+nt\right), \tag{3.1}$$

where k_x, k_y are the wave numbers along the x- and y- directions, respectively, $k=\sqrt{(k_x^2+k_y^2)}$ is the resultant wave number and n is the growth rate which is, in general, a complex constant.

Expressing the coordinates x, y, z in the new unit of length d and letting $a=kd$, $\sigma=\frac{nd^2}{\nu}$, $p_1=\frac{\nu}{\kappa}$, $p_2=\frac{\nu}{\eta}$, $P_\ell=\frac{k_1}{d^2}$, $P_e'=\frac{w_0 d}{\kappa}$ and $D=\frac{d}{dz}$,

Eqs. (2.19), (2.13), (2.17), (2.20) and (2.21), using (3.1) become

$$\left[\frac{\sigma}{\varepsilon}+\frac{1}{P_\ell}+\frac{P_e'}{\varepsilon^2 p_1}D\right](D^2-a^2)W = -\frac{g\alpha a^2 d^2}{\nu}\Theta+\frac{\mu_e H d}{4\pi\rho_0\nu}(D^2-a^2)DK-\frac{2\Omega d^3}{\varepsilon\nu}DZ, \tag{3.2}$$

$$(D^2-a^2-Ep_1\sigma)\Theta-P_e'D\Theta=-\left(\frac{\beta d^2}{\kappa}\right)W, \tag{3.3}$$

$$(D^2-a^2-p_2\sigma)K=-\left(\frac{Hd}{\varepsilon\eta}\right)DW, \tag{3.4}$$

$$\left[\frac{\sigma}{\varepsilon}+\frac{1}{P_\ell}+\frac{P_e'}{\varepsilon^2 p_1}D\right]Z=\left(\frac{\mu_e H d}{4\pi\rho_0\nu}\right)DX+\left(\frac{2\Omega d}{\nu\varepsilon}\right)DW, \tag{3.5}$$

$$(D^2-a^2-p_2\sigma)X=-\left(\frac{Hd}{\varepsilon\eta}\right)DZ. \tag{3.6}$$

Eliminating Θ, K, X and Z between Eqs. (3.2) – (3.6), we get

$$\begin{aligned}&\left[(D^2-a^2-Ep_1\sigma-P_e'D)(D^2-a^2-p_2\sigma)\left(\frac{\sigma}{\varepsilon}+\frac{1}{P_\ell}+\frac{P_e'}{\varepsilon^2 p_1}D\right)\right.\\&\left.\left\{\left(\frac{\sigma}{\varepsilon}+\frac{1}{P_\ell}+\frac{P_e'}{\varepsilon^2 p_1}D\right)(D^2-a^2-p_2\sigma)+QD^2\right\}\right](D^2-a^2)W\\&+(D^2-a^2-Ep_1\sigma-P_e'D)(D^2-a^2)\\&\left\{\left(\frac{\sigma}{\varepsilon}+\frac{1}{P_\ell}+\frac{P_e'}{\varepsilon^2 p_1}D\right)(D^2-a^2-p_2\sigma)+QD^2\right\}QD^2W\\&+T_A(D^2-a^2-Ep_1\sigma-P_e'D)(D^2-a^2-p_2\sigma)^2D^2W\\&=(D^2-a^2-p_2\sigma)\left\{\left(\frac{\sigma}{\varepsilon}+\frac{1}{P_\ell}+\frac{P_e'}{\varepsilon^2 p_1}D\right)(D^2-a^2-p_2\sigma)+QD^2\right\}Ra^2W,\end{aligned} \tag{3.7}$$

where $R = \dfrac{g\alpha\beta d^4}{\nu\kappa}$ is the Rayleigh number, $Q = \dfrac{\mu_e H^2 d^2}{4\pi\rho_0\nu\varepsilon\eta}$ is the Chandrasekhar number, $T_A = \left(\dfrac{2\Omega d^2}{\varepsilon\nu}\right)^2$ is the modified Taylor number, $p_1 = \dfrac{\nu}{\kappa}$ is the Prandtl number and $P_e' = \dfrac{w_0 d}{\kappa}$ is the Péclet number accounting for the throughflow effect.

Consider the case when both boundaries are free as well as perfect conductors of heat, while the adjoining medium is perfectly conducting. The case of two free boundaries is slightly artificial but it enables us to find analytical solutions and to make some qualitative conclusions. The appropriate boundary conditions, with respect to which Equations (3.2)–(3.6) must be solved, are

$$W = D^2 W = 0, \quad \Theta = 0, \quad DZ = 0, \tag{3.8}$$

at $z = 0$ and $z = 1$, $K = 0$ on the perfectly conducting boundaries, and h_x, h_y, h_z are continuous.

Using the above boundary conditions, it can be shown that all the even-order derivatives of W must vanish for $z = 0$ and 1 and hence the proper solution of W characterizing the lowest mode is

$$W = W_0 \sin \pi z, \tag{3.9}$$

where W_0 is a constant.

Substituting the proper solution $W = W_0 \sin \pi z$ in the resultant equation, we obtain the dispersion relation

$$\begin{aligned} R_1 = {} & \left(\frac{1+x}{x}\right)(1 + x + iEp_1\sigma_1 + P_e \cot \pi z) \\ & \times \left[\left(\frac{i\sigma_1}{\varepsilon} + \frac{1}{P} + \frac{P_e}{\varepsilon^2 p_1}\cot \pi z\right) + \frac{Q_1}{(1 + x + ip_2\sigma_1)}\right] \\ & + T_1 \left[\frac{(1 + x + iEp_1\sigma_1 + P_e \cot \pi z)(1 + x + ip_2\sigma_1)}{x\left\{\left(\dfrac{i\sigma_1}{\varepsilon} + \dfrac{1}{P} + \dfrac{P_e}{\varepsilon^2 p_1}\cot \pi z\right)(1 + x + ip_2\sigma_1) + Q_1\right\}}\right], \end{aligned} \tag{3.10}$$

where $R_1 = \dfrac{R}{\pi^4}$, $Q_1 = \dfrac{Q}{\pi^2}$, $T_1 = \dfrac{T_A}{\pi^4}$, $x = \dfrac{a^2}{\pi^2}$, $P = \pi^2 P_\ell$, $P_e = \dfrac{P'_e}{\pi}$ and $i\sigma_1 = \dfrac{\sigma}{\pi^2}$.

Equation (3.10) is the required dispersion relation including the effects of throughflow, magnetic field, rotation and medium permeability on the thermal instability of fluid in a porous medium.

4. The stationary convection

When the instability sets in as stationary convection, the marginal state will be characterized by $\sigma = 0$. Putting $\sigma = 0$, the dispersion relation (3.10) reduces to

$$(4.1) \qquad R_1 = \left(\frac{1+x}{x}\right)(1+x+P_e\cot\pi z) \times \left(\left(\frac{1}{P}+\frac{P_e}{\varepsilon^2 p_1}\cot\pi z\right)+\frac{Q_1}{1+x}+\frac{T_1}{\left\{\left(\frac{1}{P}+\frac{P_e}{\varepsilon^2 p_1}\cot\pi z\right)(1+x)+Q_1\right\}}\right)$$

which expresses the modified Rayleigh number R_1 as a function of the dimensionless wave number x and the parameters P_e, Q_1, T_1 and p_1. The meaning of this relation (4.1) is that for all Rayleigh numbers less than that given by (4.1), disturbances in the wave number x will be stable; these disturbances will become marginally stable when the Rayleigh number equals the value given by (4.1); and when the Rayleigh number exceeds the value given by (4.1), the same disturbances will be unstable.

In order to investigate the effects of rotation, medium permeability, magnetic field and throughflow, we examine the natures of $\frac{dR_1}{dT_1}$, $\frac{dR_1}{dP}$, $\frac{dR_1}{dQ_1}$ and $\frac{dR_1}{dP_e}$ analytically. Equation (4.1) yields

$$(4.2) \qquad \frac{dR_1}{dT_1} = \frac{(1+x)(1+x+P_e\cot\pi z)}{x\left\{\left(\frac{1}{P}+\frac{P_e}{\varepsilon^2 p_1}\cot\pi z\right)(1+x)+Q_1\right\}}.$$

This shows that rotation has always a stabilizing effect on the thermal instability of a rotating fluid in a porous medium in the presence of throughflow.

Also Eq. (4.1) yields

$$(4.3) \qquad \frac{dR_1}{dP} = -\left(\frac{1+x}{x}\right)\frac{(1+x+P_e\cot\pi z)}{P^2}\left[1-\frac{T_1(1+x)}{\{X_1(1+x)+Q_1\}^2}\right],$$

$$(4.4) \qquad \frac{dR_1}{dQ_1} = \frac{(1+x+P_e\cot\pi z)}{x}\left[1-\frac{T_1(1+x)}{\{X_1(1+x)+Q_1\}^2}\right],$$

$$\frac{dR_1}{dP_e} = \left(\frac{1+x}{x}\right)\cot \pi z \left[\left(\frac{1}{P} + \frac{2P_e}{\varepsilon^2 p_1}\cot \pi z\right) + \frac{(1+x)}{\varepsilon^2 p_1}\left\{1 - \frac{T_1(1+x)}{\{X_1(1+x)+Q_1\}^2}\right\}\right] + \frac{Q_1}{(1+x)} + \frac{T_1}{\{X_1(1+x)+Q_1\}^2}\{(1+x)+Q_1 P\}, \tag{4.5}$$

where

$$\left(\frac{P_e \cot \pi z}{\varepsilon^2 p_1} + \frac{1}{P}\right) = X_1.$$

Thus for stationary convection, the medium permeability has always a destabilizing effect, whereas the magnetic field and the throughflow have always a stabilizing effects on the thermal instability of fluid in a porous medium in the absence of rotation. But in the presence of rotation, the medium permeability is found to have a destabilizing effect whereas the magnetic field and the throughflow have a stabilizing effect if

$$T_1 < \frac{\{(1+x)(\varepsilon^2 p_1 + PP_e \cot \pi z) + Q_1 \varepsilon^2 p_1 P\}^2}{\varepsilon^4 p_1^2 P^2 (1+x)}. \tag{4.6}$$

If

$$T_1 > \frac{\{(1+x)(\varepsilon^2 p_1 + PP_e \cot \pi z) + Q_1 \varepsilon^2 p_1 P\}^2}{\varepsilon^4 p_1^2 P^2 (1+x)}, \tag{4.7}$$

then the medium permeability has always a stabilizing effect and the magnetic field has always a destabilizing effect, whereas the throughflow has a stabilizing or destabilizing effect on the system.

The dispersion relation (4.1) is analyzed numerically. In Fig. 1, R_1 is plotted against the wave number x for $p_1 = 7$, $P_e = 4$, $Q_1 = 2$, $P = 4$, $\varepsilon = 0.7$, $z = 0.25$ and $T_1 = 10, 20, 30, 40$. It is clear that the rotation has always a stabilizing effect as the Rayleigh number increases with the increase in the rotation parameter. In Fig. 2, R_1 is plotted against the wave number x for $p_1 = 7$, $P_e = 4$, $Q_1 = 2$, $T_1 = 0$, $\varepsilon = 0.7$, $z = 0.25$ and $P = 1, 2, 3, 4$. It is clear that the medium permeability has a destabilizing effect in the absence of rotation whereas in the presence of rotation parameter ($T_1 = 20$) (Fig. 3), medium permeability has a stabilizing effect for small wave numbers and destabilizing effect for higher wave numbers. This is because, in their simultaneous presence, there is a competition

between the stabilizing role of rotation and destabilizing role of the medium permeability, and the rotation parameter succeeds in stabilizing a certain wave number range.

In Fig. 4, R_1 is plotted against the wave number x for $p_1 = 7$, $P = 4$, $\varepsilon = 0.7$, $z = 0.25$, $P_e = 4$, $T_1 = 0$ and $Q_1 = 1, 2, 3, 4$. It is observed that the magnetic field has always a stabilizing effect in the absence of rotation, whereas in the presence of rotation parameter ($T_1 = 20$) (Fig. 5), magnetic field has a destabilizing effect for small wave numbers and a stabilizing effect for higher wave numbers. This is because, in their simultaneous presence of medium permeability, rotation and magnetic field, there is a competition between the stabilizing role of rotation and magnetic field and a destabilizing role of medium permeability, and each parameter succeeds in stabilizing a certain wave number range. In Fig. 6, R_1 is plotted against the wave number x for $p_1 = 7$, $P = 4$, $Q_1 = 10$, $T_1 = 0$, $\varepsilon = 0.7$, $z = 0.25$ and $P_e = 4, 5, 6, 7$. It is observed that the throughflow has a stabilizing effect as the Rayleigh number increases with the increase in the throughflow parameter in the absence of rotation, whereas in the presence of rotation parameter ($T_1 = 100$) (Fig. 7), throughflow has a stabilizing effect or destabilizing effect on the system.

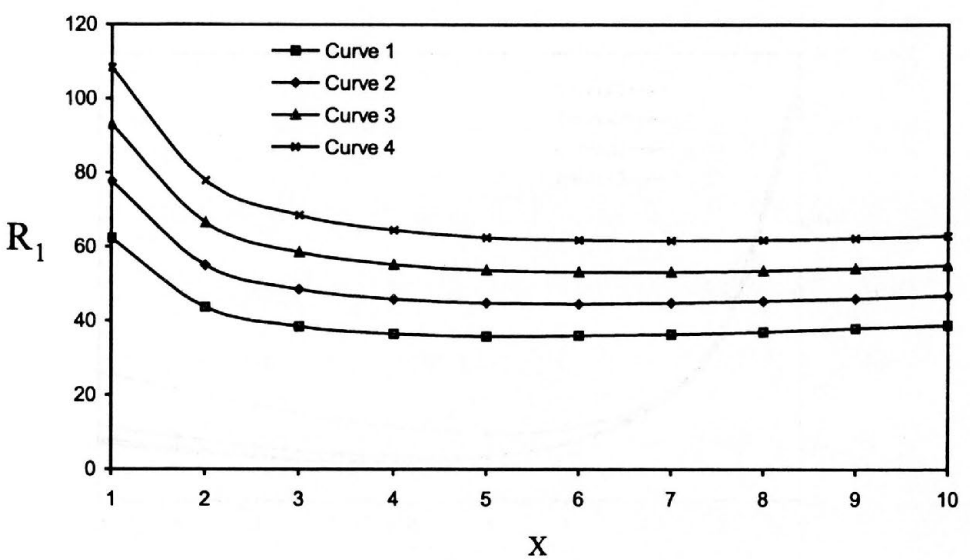

FIG. 1. The variation of Rayleigh number (R_1) with wave number (x) for $p_1 = 7$, $Q_1 = 5$, $P = 4$, $P_e = 4$, $\varepsilon = 0.7$, $z = 0.25$; $T_1 = 10$ for curve 1, $T_1 = 20$ for curve 2, $T_1 = 30$ for curve 3 and $T_1 = 40$ for curve 4.

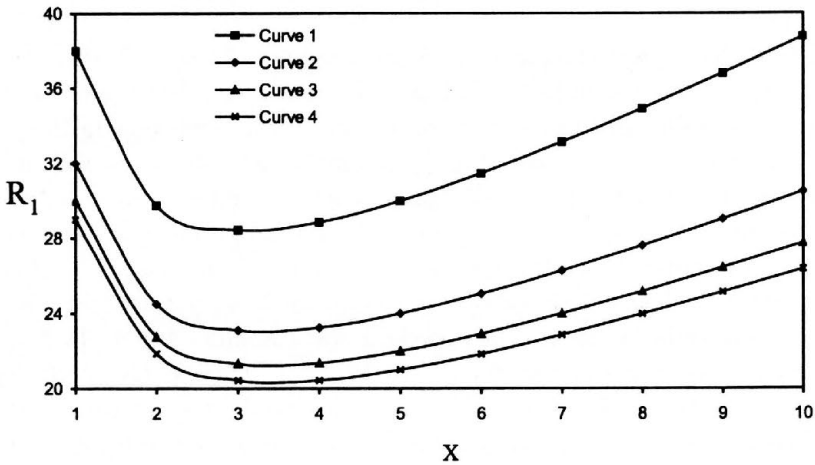

FIG. 2. The variation of Rayleigh number (R_1) with wave number (x) for $p_1 = 7$, $Q_1 = 2$, $T_1 = 0$, $P_e = 4$, $\varepsilon = 0.7$ $z = 0.25$; $P = 1$ for curve 1, $P = 2$ for curve 2, $P = 3$ for curve 3 and $P = 4$ for curve 4.

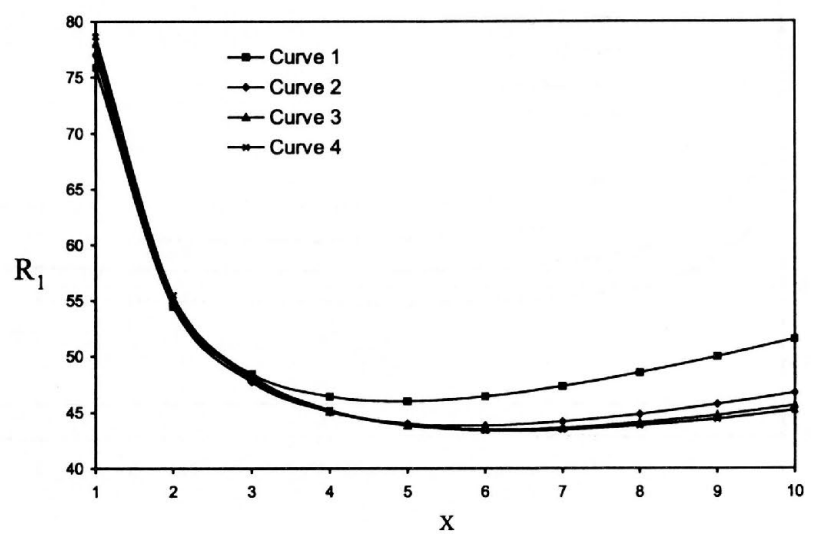

FIG. 3. The variation of Rayleigh number (R_1) with wave number (x) for $p_1 = 7$, $Q_1 = 2$, $T_1 = 20$, $P_e = 4$, $\varepsilon = 0.7$, $z = 0.25$; $P = 1$ for curve 1, $P = 2$ for curve 2, $P = 3$ for curve 3 and $P = 4$ for curve 4.

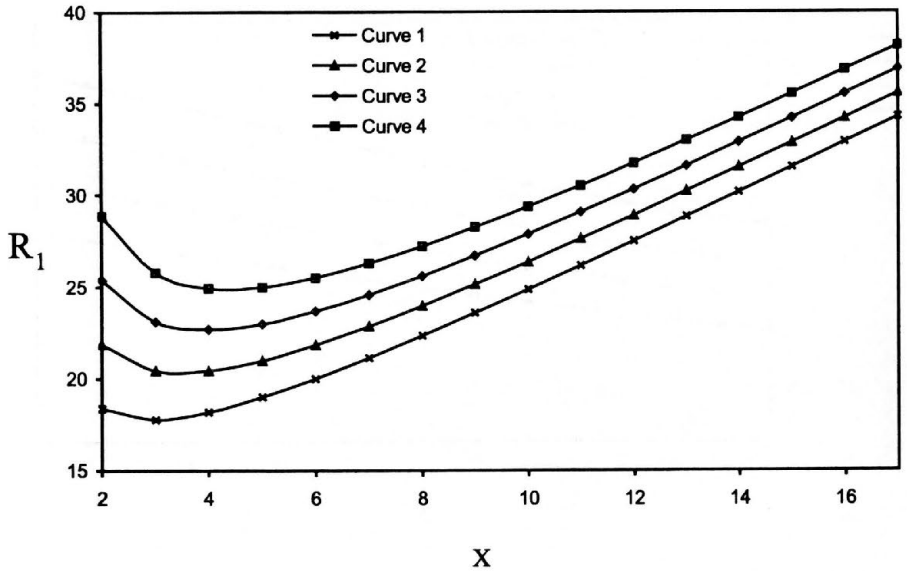

FIG. 4. The variation of Rayleigh number (R_1) with wave number (x) for $p_1 = 7$ $P_e = 4$, $T_1 = 0$, $P = 4$, $\varepsilon = 0.7$, $z = 0.25$; $Q_1 = 1$ for curve 1, $Q_1 = 2$ for curve 2, $Q_1 = 3$ for curve 3 and $Q_1 = 4$ for curve 4.

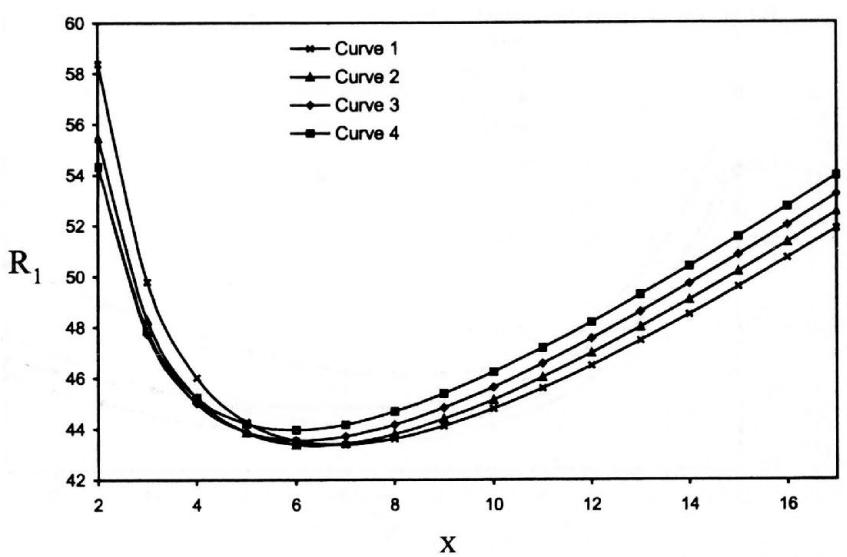

FIG. 5. The variation of Rayleigh number (R_1) with wave number (x) for $p_1 = 7$, $P_e = 4$, $T_1 = 20$, $P = 4$, $\varepsilon = 0.7$, $z = 0.25$; $Q_1 = 1$ for curve 1, $Q_1 = 2$ for curve 2, $Q_1 = 3$ for curve 3 and $Q_1 = 4$ for curve 4.

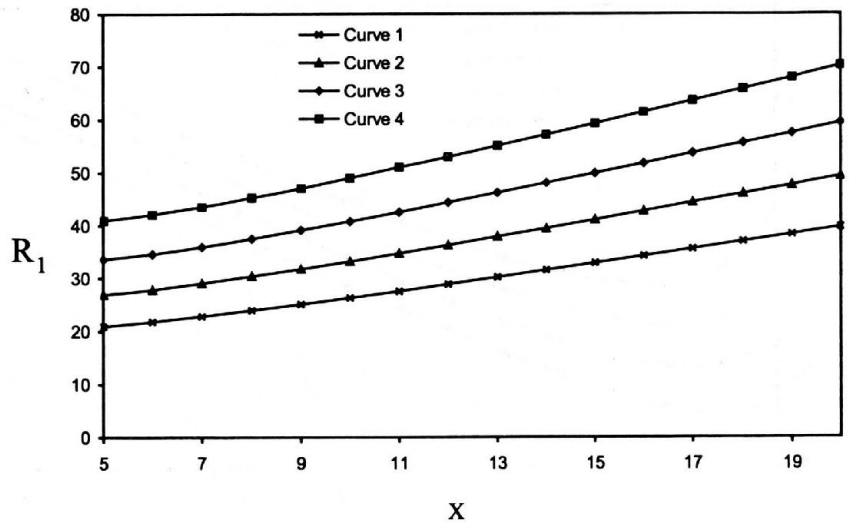

FIG. 6. The variation of Rayleigh number (R_1) with wave number (x) for $p_1 = 7$, $Q_1 = 2$, $T_1 = 0$, P = 4, $\varepsilon = 0.7$, z = 0.25; $P_e = 4$ for curve 1, $P_e = 5$ for curve 2, $P_e = 6$ for curve 3 and $P_e = 7$ for curve 4.

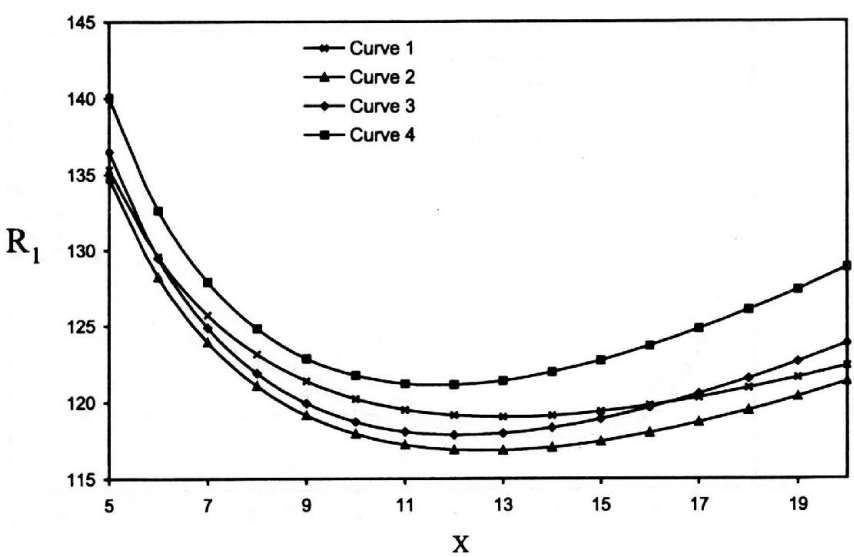

FIG. 7. The variation of Rayleigh number (R_1) with wave number (x) for $p_1 = 7$, $Q_1 = 2$, $T_1 = 100$, $P = 4$, $\varepsilon = 0.7$, z = 0.25; $P_e = 4$ for curve 1, $P_e = 5$ for curve 2, $P_e = 6$ for curve 3 and $P_e = 7$ for curve 4.

5. The case of oscillatory modes

Here we examine the possibility of oscillatory modes, if any, in the stability problem due to the presence of throughflow, magnetic field and medium permeability. Multiplying (3.2) by W^*, the complex conjugate of W, and using Eqs. (3.3) - (3.7) together with the boundary conditions (3.8), we obtain

$$(5.1)\quad \left(\frac{\sigma}{\varepsilon}+\frac{1}{P_\ell}\right)\left\langle |DW|^2+a^2|W|^2\right\rangle - \frac{g\alpha a^2\kappa}{\nu\beta}$$
$$\left[\left\langle |D\Theta|^2+a^2|\Theta|^2\right\rangle + Ep_1\sigma^*\left\langle |\Theta|^2\right\rangle - P_e'\langle D\Theta\,\Theta^*\rangle\right]$$
$$+d^2\left[\left(\frac{\sigma^*}{\varepsilon}+\frac{1}{P_\ell}\right)\left\langle |Z|^2\right\rangle - \frac{P_e'}{\varepsilon^2 p_1}[\langle DZ^*\,Z\rangle]\right]$$
$$+\frac{\mu_e\eta\varepsilon}{4\pi\rho_0\nu}\left[\left\langle\left(|D^2K|^2+2a^2|DK|+a^4|K|^2\right)\right\rangle + p_2\sigma^*\left\langle\left(|DK|^2+a^2|DK|\right)\right\rangle\right]$$
$$-\frac{P_e'}{\varepsilon^2 p_1}\left[\langle D^2W^*\,\mathrm{DW}\rangle + a^2\langle DW^*\,\mathrm{W}\rangle\right] = 0,$$

where $\langle\ldots\ldots\rangle = \int_0^1 (\ldots\ldots)\,dz$.

Putting $\sigma = i\sigma_i$, where σ_i is real and equating the imaginary parts of Eq. (4.6), we obtain

$$(5.2)\qquad \sigma_i\left[\begin{array}{l}\frac{1}{\varepsilon}\left\langle |DW|^2+a^2|W|^2\right\rangle + \frac{g\alpha a^2\kappa}{\nu\beta}Ep_1\left\langle |\Theta|^2\right\rangle \\ -\frac{d^2}{\varepsilon}\left\langle |Z|^2\right\rangle - \frac{\mu_e\eta\varepsilon}{4\pi\rho_0\nu}p_2\left\langle |DK|^2+a^2|K|^2\right\rangle\end{array}\right] = 0.$$

It is clear from (5.2) that σ_i may be zero or non-zero, meaning that the modes may be non-oscillatory or oscillatory. But in the absence of magnetic field and rotation, (5.2) reduces to

$$(5.3)\qquad \sigma_i\left[\frac{1}{\varepsilon}\left\langle |DW|^2+a^2|W|^2\right\rangle + \frac{g\alpha a^2\kappa}{\nu\beta}Ep_1\left\langle |\Theta|^2\right\rangle\right] = 0.$$

Here the quantity inside the brackets is positive definite. Hence

$$(5.4)\qquad \sigma_i = 0.$$

This shows that whenever $\sigma_r = 0$ implies that $\sigma_i = 0$, then the stationary (cellular) pattern of flow prevails in the onset of instability. In other words, the principle of exchange of stabilities is valid for the fluid heated from below in porous medium with throughflow in the absence of magnetic field and rotation. The oscillatory modes are introduced due to the presence of magnetic field and rotation, which were non-existent in their absence.

6. The case of overstability

The present section is devoted to find the possibility as to whether instability may occur as overstability. Since we wish to determine the critical Rayleigh number for the onset of instability via a state of pure oscillations, it suffices to find the conditions for which (3.10) will admit solutions with σ_i real.

Equating real and imaginary parts of (3.10) and eliminating R_1 between them, we obtain

$$A_3 c_1^3 + A_2 c_1^2 + A_1 c_1 + A_0 = 0, \tag{6.1}$$

where we have put $c_1 = \sigma_1^2$, $\left(\frac{P_e \cot \pi z}{\varepsilon^2 p_1} + \frac{1}{P}\right) = X_1$, $(b + P_e \cot \pi z) = X_2$, $b = 1 + x$ and

$$\begin{aligned} A_0 = {} & \left[\frac{1}{\varepsilon}\left(\frac{\varepsilon E p_1}{P^3} - T_1\right) + \left(\frac{P_e \cot \pi z}{\varepsilon^2 p_1}\right) E p_1 \left\{\left(\frac{P_e \cot \pi z}{\varepsilon^2 p_1}\right)^2 + \frac{2X_1}{P}\right\}\right] b^5 \\ & + \left[E p_1 Q_1 X_1 \{2X_1 + 1\} + T_1 \left\{\frac{P_e \cot \pi z}{\varepsilon}(E - \varepsilon) + \frac{E p_1}{P}\right\}\right] b^4 \\ & + \left[\frac{1}{\varepsilon} X_1^2 X_2 \left(b^2 - \varepsilon Q_1 p_2\right)\right] b^3 \\ & + \left[\frac{2Q_1}{\varepsilon} X_1 X_2 \left(b^2 - \varepsilon Q_1 p_2\right) + Q_1^3 (E p_1 - p_2) + p_2 Q_1 T_1 X_2\right] b^2 \\ & + \left[\frac{1}{\varepsilon} Q_1^2 P_e \cot \pi z \left(b^2 - \varepsilon Q_1 p_2\right)\right] b, \end{aligned} \tag{6.2}$$

$$A_3 = \frac{p_2^4}{\varepsilon^3}\left[b^2 + \left\{\frac{P_e \cot \pi z}{\varepsilon}(E + \varepsilon) + \frac{\varepsilon E p_1}{P}\right\} b\right]. \tag{6.3}$$

Since σ_1 is real for overstability, the three values of $c_1 (= \sigma_1^2)$ are positive. So the product of roots of (6.1) is positive, but this is impossible if $A_0 > 0$ and

$A_3 > 0$ $\left(\text{since the product of the roots of Eq. (6.1) is } -\frac{A_0}{A_3}\right)$. $A_0 > 0$ and $A_3 > 0$ are, therefore, sufficient conditions for the nonexistence of overstability.

It is clear from Eq. (6.2) and (6.3) that A_0 and A_3 are always positive if

$$(6.4) \qquad Ep_1 > p_2, \quad \frac{\varepsilon E p_1}{P^3} > T_1 \quad \text{and} \quad b > \sqrt{Q_1 \varepsilon p_2},$$

which implies that

$$(6.5) \qquad \frac{E\nu}{\kappa} > \frac{\nu}{\eta}, \quad \kappa < E\left(\frac{\nu\varepsilon}{k_1}\right)^3\left(\frac{d^2}{4\Omega^2\pi^2}\right) \quad \text{and} \quad (1+x) > \left(\frac{\mu_e}{4\pi\rho_0}\right)^{1/2}\frac{Hd}{\eta\pi},$$

i. e.

$$(6.6) \qquad E\eta > \kappa, \quad \kappa < E\left(\frac{\nu\varepsilon}{k_1}\right)^3\left(\frac{d^2}{4\Omega^2\pi^2}\right) \text{ and } \left(1+\frac{k^2d^2}{\pi^2}\right) > \left(\frac{\mu_e}{4\pi\rho_0}\right)^{1/2}\frac{Hd}{\eta\pi}.$$

Thus, $E\eta > \kappa$, $\kappa < E\left(\frac{\nu\varepsilon}{k_1}\right)^3\left(\frac{d^2}{4\Omega^2\pi^2}\right)$ and $\left(1+\frac{k^2d^2}{\pi^2}\right) > \left(\frac{\mu_e}{4\pi\rho_0}\right)^{1/2}\frac{Hd}{\eta\pi}$

are the sufficient conditions for the nonexistence of overstability, the violation of which does not necessarily imply the occurrence of overstability.

Acknowledgement

The financial assistance to Dr. Sunil in the form of Research and Development Project [No. 25(0129)/02/EMR-II] of the Council of Scientific and Industrial Research (CSIR), New Delhi, is gratefully acknowledged.

References

1. S. CHANDRASEKHAR, *Hydrodynamic and hydromagnetic stability*, Dover Publications, New York 1981.

2. D. L. SHVARTSBLAT, *The spectrum of perturbations and convective instability of a plane horizontal fluid layer with permeable boundaries*, J. Appl. Mech. (PMM), **32**, 266–271, 1968.

3. D. L. SHVARTSBLAT, *Steady convective motions in a plane horizontal fluid layer with permeable boundaries*, Fluid Dyn., **4**, 54–59, 1969. (Translation from Izv. Akad. Nauk SSSR, Fiz. Zhidkosti i Gaza.)

4. D. L. SHVARTSBLAT, *Numerical analysis of a steady convective flow in a plane horizontal fluid layer* [in Russian], Uchen. Zap. Perm Univ. No. 248, Gidrodinamika, **3**, 97, 1971.

5. G. Z. GERSHUNI, and E. M. ZHUKHOVITSKII, *Convective stability of incompressible fluids*, Jerusalem: Keter Publishing House, 1976.

6. R. KRISHNAMURTI, *On cellular cloud patterns. Part 1: Mathematical model*, J. Atmos. Sci., **32**, 1353–1363, 1975.

7. R. KRISHNAMURTI, *On cellular cloud patterns. Part 2: Mathematical model*, J. Atmos. Sci., **32**, 1364–1372, 1975.

8. R. KRISHNAMURTI, *On cellular cloud patterns. Part 3: Mathematical model*, J. Atmos. Sci., **32**, 1373–1383, 1975.

9. R. C. SOMERVILLE and T. GAL-CHEN, *Numerical simulation of convection with vertical motion*, J. Atmos. Sci., **36**, 805–815, 1979.

10. D. A. NIELD, *Throughflow effects in the Rayleigh-Bénard convection instability problem*, J. Fluid Mech., **185**, 353–360, 1987.

11. W. C. CHIN, *Wave propagation in petroleum engineering*, Gulf Publishing Company, Houston, USA, 1993.

12. O. M. PHILLIPS, *Flow and reaction in permeable rocks*, Cambridge University Press, Cambridge, 1991.

13. G. M. HOMSY and A. E. SHERWOOD, *Convective instabilities in porous medium with through flow*, A.I.Ch.E., **22**, 1, 168–174, 1976.

14. D. A. NIELD, *Convective instability in porous medium with throughflow*, A. I. Ch. E., **33**, 7, 1222–1224, 1987.

15. E. M. SPARROW and L. GOLDSTEI, *Effect of rotation and coolant throughflow on the heat transfer and temperature field in an enclosure*, J. Heat Transfer, **98**, 387–394, 1976.

Received December 5, 2002; revised version April 7, 2003.

Arch. Mech., **55**, 3, pp. 275–304, Warszawa 2003

Penny-shaped crack in a piezoceramic cylinder under Mode I loading

F. NARITA, S. LIN, Y. SHINDO

Department of Materials Processing, Graduate School of Engineering, Tohoku University, Aoba-yama 02, Sendai 980-8579, Japan.
e-mail: narita@material.tohoku.ac.jp

THE ELECTROELASTIC response of a penny-shaped crack in a piezoelectric cylinder of finite radius is investigated in this study. Fourier and Hankel transforms are used to reduce the problem to the solution of a pair of dual integral equations. They are then reduced to a Fredholm integral equation of the second kind. Numerical values of the stress intensity factor, energy release rate and energy density factor for piezoelectric ceramics are obtained to show the influence of applied electrical loads.

1. Introduction

MECHANICAL RELIABILITY and durability of piezoelectric ceramics offer important considerations in the design of smart structures and devices. In recent years, significant efforts have been made to the study of fracture behavior of piezoelectric ceramics [1, 2]. In the theoretical studies of the piezoelectric crack problems, the electrical boundary condition imposed across the crack surface remains a debating issue. There are two commonly used electrical boundary conditions. PAK [3] has assumed the crack face to be free of surface charge (the so-called condition of impermeability) while SHINDO *et al.* [4] have assumed that the normal component of the electric displacement and the tangential component of the electric field are continuous across the crack face (the permeable crack boundary condition). The impermeable crack is an inappropriate model [1, 5]. Recently, NARITA and SHINDO [6] obtained a crack growth rate equation of a plane strain slit-like permeable crack parallel to the edges of a narrow piezoelectric ceramic body under Mode I loading. The results indicated that under applied uniform strain, positive electrical fields (electrical fields in poling direction) impede crack propagation while negative electrical fields (electrical fields applied opposite to the poling direction) aid the crack propagation. SHINDO *et al.* [7] also made a finite element analysis (FEA) for the single-edge precracked piezoelectric ceramics for various electric fields to calculate the total potential energy release rate and mechanical strain energy release rate for permeable and impermeable cracks, and performed the

single-edge precracked beam tests on piezoceramics to verify the theoretical predictions of the influence of the applied electric field on the fracture behavior of piezoceramics. They concluded that for applied displacements, the total potential energy release rate and mechanical strain energy release rate for the applied positive electric field under the permeable boundary condition are lower in magnitude than those for the applied negative electric field. This explains an increase in the fracture initiation load in the presence of a positive electric field as observed in the experimental studies. For applied load, the positive (negative) electric field increases (decreases) the total energy release rate and mechanical energy release rate. The FEA results for applied force are in agreement with experimental findings of PARK and SUN [8] and SHINDO *et al.* [9].

The strain energy density theory has opened the door to a new and fruitful area of research in fracture mechanics [10]. In recent works, the energy density criterion was applied to determine the piezoelectric crack growth segments for conditions of positive, negative and zero electric field based on the impermeable assumption. Failure stresses of Mode I and II cracking were also obtained [11]. It is evident that this assumption is valid only for modeling flaws of finite thickness.

This paper considers the electroelastic problem of a penny-shaped crack in a piezoelectric circular cylinder under tensile loading. The method of solution involves the use of Fourier and Hankel transforms to reduce the mixed boundary value problem to a pair of dual integral equations. The solution is then given in terms of a Fredholm integral equation of the second kind. The stress intensity factor, energy release rate and energy density factor are determined and numerical results are shown graphically to demonstrate the influence of applied electric loads.

2. Problem statement and basic equations

Consider a penny-shaped crack of radius a embedded in a long circular piezoelectric cylinder of radius b ($b > a$). It is assumed that the center of the crack is located on the axis of the piezoelectric cylinder and its plane is normal to that axis. Figure 1 shows the geometry of the problem where the position of a point is defined by the cylindrical coordinates (r, θ, z). In this coordinate system, the crack occupies the region $z = 0$, $0 \leq \theta \leq 2\pi$, $0 \leq r < a$. The piezoelectric cylinder is transversely isotropic with hexagonal symmetry; it is subjected to a far-field normal stress $\sigma_{zz} = \sigma_\infty$. Two possible cases of electrical boundary conditions are considered at infinity. The first case is a uniform electric displacement, $D_z = D_\infty$; and the second is a uniform electric field, $E_z = E_\infty$.

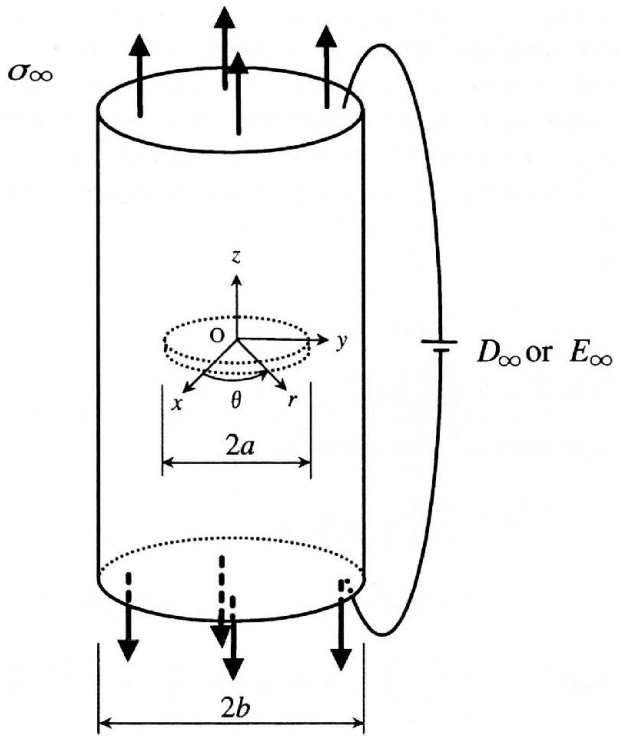

FIG. 1. Geometry and loading of a piezoelectric cylinder with a penny-shaped crack.

The constitutive equations for piezoceramics poled in the z-direction can be written as

$$\left.\begin{aligned}
\sigma_{rr} &= c_{11}u_{r,r} + c_{12}\frac{u_r}{r} + c_{13}u_{z,z} - e_{31}E_z \\
\sigma_{\theta\theta} &= c_{12}u_{r,r} + c_{11}\frac{u_r}{r} + c_{13}u_{z,z} - e_{31}E_z \\
\sigma_{zz} &= c_{13}u_{r,r} + c_{13}\frac{u_r}{r} + c_{33}u_{z,z} - e_{33}E_z \\
\sigma_{zr} &= c_{44}(u_{r,z} + u_{z,r}) - e_{15}E_r
\end{aligned}\right\} \tag{2.1}$$

$$\left.\begin{aligned}
D_r &= e_{15}(u_{r,z} + u_{z,r}) + \epsilon_{11}E_r \\
D_z &= e_{31}\left(u_{r,r} + \frac{u_r}{r}\right) + e_{33}u_{z,z} + \epsilon_{33}E_z
\end{aligned}\right\} \tag{2.2}$$

In Eqs. (2.1) and (2.2), $\sigma_{rr}, \sigma_{\theta\theta}, \sigma_{zz}, \sigma_{zr}$ are components of the stress tensor; D_r and D_z the components of electric displacement vector; u_r and u_z the components of displacement vector; E_r and E_z the components of electric field vector; $c_{11}, c_{12}, c_{13}, c_{33}, c_{44}$ the elastic moduli measured in a constant electric field; $\epsilon_{11}, \epsilon_{33}$ the dielectric permittivities measured at constant strain; and e_{15}, e_{31}, e_{33} the piezoelectric constants. A comma implies partial differentiation with respect to the coordinates. The electric field components are related to the electric potential $\phi(r, z)$ by

$$\left.\begin{aligned} E_r &= -\phi_{,r} \\ E_z &= -\phi_{,z} \end{aligned}\right\} \tag{2.3}$$

The governing equations can be written as:

$$\left.\begin{aligned} &c_{11}\left(u_{r,rr} + \frac{u_{r,r}}{r} - \frac{u_r}{r^2}\right) + c_{44}u_{r,zz} \\ &\qquad + (c_{13} + c_{44})u_{z,rz} + (e_{31} + e_{15})\phi_{,rz} = 0 \\ &(c_{13} + c_{44})\left(u_{r,rz} + \frac{u_{r,z}}{r}\right) + c_{33}u_{z,zz} + c_{44}\left(u_{z,rr} + \frac{u_{z,r}}{r}\right) \\ &\qquad + e_{15}\left(\phi_{,rr} + \frac{\phi_{,r}}{r}\right) + e_{33}\phi_{,zz} = 0 \end{aligned}\right\} \tag{2.4}$$

$$(e_{31} + e_{15})\left(u_{r,rz} + \frac{u_{r,z}}{r}\right) + e_{15}\left(u_{z,rr} + \frac{u_{z,r}}{r}\right) + e_{33}u_{z,zz} - \epsilon_{11}\left(\phi_{,rr} + \frac{\phi_{,r}}{r}\right) - \epsilon_{33}\phi_{,zz} = 0. \tag{2.5}$$

In a vacuum, the constitutive equations (2.2) and the governing equations (2.5) become

$$\left.\begin{aligned} D_r &= \epsilon_0 E_r, \\ D_z &= \epsilon_0 E_z; \end{aligned}\right\} \tag{2.6}$$

$$\phi_{,rr} + \frac{\phi_{,r}}{r} + \phi_{,zz} = 0, \tag{2.7}$$

where ϵ_0 is the electric permittivity of the vacuum.

Referring to the semi-infinite region $z \geq 0$, $0 \leq r \leq b$, $0 \leq \theta \leq 2\pi$, the boundary conditions can be expressed in the form

$$\sigma_{zr}(r,0) = 0 \quad (0 \leq r \leq b), \tag{2.8}$$

$$\begin{aligned} \sigma_{zz}(r,0) &= 0 \quad (0 \leq r < a), \\ u_z(r,0) &= 0 \quad (a \leq r \leq b), \end{aligned} \tag{2.9}$$

$$\begin{aligned} E_r(r,0) &= E_r^c(r,0) \quad (0 \leq r < a), \\ \phi(r,0) &= 0 \quad (a \leq r \leq b), \end{aligned} \tag{2.10}$$

$$D_z(r,0) = D_z^c(r,0) \quad (0 \leq r < a), \tag{2.11}$$

$$\sigma_{rr}(b,z) = 0, \tag{2.12}$$

$$\sigma_{rz}(b,z) = 0, \tag{2.13}$$

$$D_r(b,z) = 0, \tag{2.14}$$

$$\text{Case I}: \quad \sigma_{zz}(r,z) = \sigma_\infty, \quad D_z(r,z) = D_\infty \quad (0 \leq r \leq b, z \to \infty), \tag{2.15}$$

$$\text{Case II}: \quad \sigma_{zz}(r,z) = \sigma_\infty, \quad E_z(r,z) = E_\infty \quad (0 \leq r \leq b, z \to \infty), \tag{2.16}$$

where the superscript c stands for the electric field quantity in the void inside the crack. The far-field normal stress σ_∞ is expressed as

$$\sigma_\infty = \begin{cases} c_1\sigma_0 - e_1 D_\infty & \text{(Case I)}, \\ \sigma_0 - e_2 E_\infty & \text{(Case II)}, \end{cases} \tag{2.17}$$

where

$$c_1 = \frac{(c_{11}+c_{12})\{(c_{11}+c_{12})\bar{c}_{33} - 2(c_{13}^2 + 2c_{13}e_{33}e_{31}/\epsilon_{33} - c_{33}e_{31}^2/\epsilon_{33})\}}{(\bar{c}_{11}+\bar{c}_{12})\{c_{33}(c_{11}+c_{12}) - 2c_{13}^2\}}, \tag{2.18}$$

$$e_1 = \frac{(c_{11}+c_{12})e_{33}/\epsilon_{33} - 2c_{13}e_{31}/\epsilon_{33}}{\bar{c}_{11}+\bar{c}_{12}}, \tag{2.19}$$

$$e_2 = \frac{(c_{11}+c_{12})e_{33} - 2c_{13}e_{31}}{c_{11}+c_{12}}. \tag{2.20}$$

Note that σ_0 is a uniform normal stress for a closed-circuit condition with the potential forced to remain zero (grounded) and $\bar{c}_{11} = c_{11} + e_{31}^2/\epsilon_{33}$, $\bar{c}_{12} = c_{12} + e_{31}^2/\epsilon_{33}$, $\bar{c}_{33} = c_{33} + e_{33}^2/\epsilon_{33}$ are the piezoelectric stiffened elastic constants.

3. Solution procedure

Assume that the solutions u_r, u_z and ϕ are of the form

$$u_r(r,z) = \frac{2}{\pi}\sum_{j=1}^{3}\int_0^\infty [a_j A_j(\alpha)\exp(-\gamma_j\alpha z)J_1(\alpha r) + a_j' B_j(\alpha) I_1(\gamma_j'\alpha r)\cos(\alpha z)]d\alpha + a_\infty r,$$

$$u_z(r,z) = \frac{2}{\pi}\sum_{j=1}^{3}\int_0^\infty \left\{\frac{1}{\gamma_j}A_j(\alpha)\exp(-\gamma_j\alpha z)J_0(\alpha r) + \frac{1}{\gamma_j'}B_j(\alpha)I_0(\gamma_j'\alpha r)\sin(\alpha z)\right\} d\alpha + b_\infty z, \tag{3.1}$$

$$\phi(r,z) = \frac{2}{\pi}\sum_{j=1}^{3}\int_0^\infty \left\{-\frac{b_j}{\gamma_j}A_j(\alpha)\exp(-\gamma_j\alpha z)J_0(\alpha r) + \frac{b_j'}{\gamma_j'}B_j(\alpha)I_0(\gamma_j'\alpha r)\sin(\alpha z)\right\} d\alpha - c_\infty z, \tag{3.2}$$

where $A_j(\alpha)$ and $B_j(\alpha)$ $(j = 1,2,3)$ are the unknowns to be determined, $J_0()$ and $J_1()$ are the zero and first order Bessel functions of the first kind, and $I_0()$ and $I_1()$ are the zero and first order modified Bessel functions of the first kind, respectively. The real constants a_∞, b_∞ and c_∞ will be determined from the far-field loading conditions, and $\gamma_j^2, \gamma_j'^2, a_j, b_j, a_j', b_j'$ $(j = 1,2,3)$ are given in Appendix A. Application of the Fourier transform to Eq. (2.7) yields

$$\phi^c = \frac{2}{\pi}\int_0^\infty C(\alpha)\sinh(\alpha z)J_0(\alpha r)d\alpha \quad (0 \le \gamma < a) \tag{3.3}$$

where $C(\alpha)$ is also unknown. The stresses, electric field intensities and electric displacements can be obtained by making use of Eqs. (2.1)–(2.3), (3.1) and (3.2). The electric field intensities and electric displacements in the void inside the crack can also be obtained from Eqs. (2.3), (2.6) and (3.3).

By applying the far-field loading conditions, the constants a_∞, b_∞ and c_∞ are evaluated as

CASE I.

$$
\begin{aligned}
a_\infty &= \frac{1}{\delta}\{-(e_{31}e_{33}+c_{13}\epsilon_{33})\sigma_\infty-(c_{13}e_{33}-c_{33}e_{31})D_\infty\},\\
b_\infty &= \frac{1}{\delta}\Big[\{(c_{11}+c_{12})\epsilon_{33}+2e_{31}^2\}\sigma_\infty+\{(c_{11}+c_{12})e_{33}-2c_{13}e_{31}\}D_\infty\Big],\\
c_\infty &= \frac{1}{\delta}\Big[\{2c_{13}e_{31}-(c_{11}+c_{12})e_{33}\}\sigma_\infty+\{(c_{11}+c_{12})c_{33}-2c_{13}^2\}D_\infty\Big],\\
\delta &= (c_{11}+c_{12})(c_{33}\epsilon_{33}+e_{33}^2)+2(-c_{13}^2\epsilon_{33}+c_{33}e_{31}^2-2c_{13}e_{31}e_{33}).
\end{aligned}
\tag{3.4}
$$

CASE II.

$$
\begin{aligned}
a_\infty &= \frac{1}{2c_{13}^2-c_{33}(c_{11}+c_{12})}\Big\{c_{13}\sigma_\infty+(c_{13}e_{33}-c_{33}e_{31})E_\infty\Big\},\\
b_\infty &= \frac{1}{2c_{13}^2-c_{33}(c_{11}+c_{12})}\Big[-(c_{11}+c_{12})\sigma_\infty\\
&\qquad +\Big\{2c_{13}e_{31}-(c_{11}+c_{12})e_{33}\Big\}E_\infty\Big],\\
c_\infty &= E_\infty.
\end{aligned}
\tag{3.5}
$$

The boundary conditions of Eqs. (2.8) and (2.10) lead to the following relations between unknown functions:

$$\frac{f_1}{\gamma_1}A_1(\alpha)+\frac{f_2}{\gamma_2}A_2(\alpha)+\frac{f_3}{\gamma_3}A_3(\alpha)=0, \tag{3.6}$$

$$\frac{b_1}{\gamma_1}A_1(\alpha)+\frac{b_2}{\gamma_2}A_2(\alpha)+\frac{b_3}{\gamma_3}A_3(\alpha)=0, \tag{3.7}$$

where

$$f_j = c_{44}(a_j\gamma_j^2+1)-e_{15}b_j \qquad (j=1,2,3). \tag{3.8}$$

Application of the mixed boundary conditions in Eqs. (2.9) gives rise to a pair of dual integral equations:

$$\int_0^\infty \alpha F D(\alpha) J_0(\alpha r) d\alpha - \sum_{j=1}^{3} \int_0^\infty \alpha g_j \gamma_j B_j(\alpha) I_0(\gamma_j' \alpha r) d\alpha$$

$$= -\frac{\pi}{2}\sigma_\infty \quad (0 \le r < a),$$

(3.9)

$$\int_0^\infty D(\alpha) J_0(\alpha r) d\alpha = 0 \quad (a \le r \le b),$$

where

$$D(\alpha) = \frac{A_1(\alpha)}{d_1} = \frac{A_2(\alpha)}{d_2} = \frac{A_3(\alpha)}{d_3}, \tag{3.10}$$

$$F = \sum_{j=1}^{3} g_j d_j \tag{3.11}$$

$$d_1 = \gamma_1(b_2 f_3 - b_3 f_2), \quad d_2 = \gamma_2(b_3 f_1 - b_1 f_3), \quad d_3 = \gamma_3(b_1 f_2 - b_2 f_1), \tag{3.12}$$

$$g_j = c_{13} a_j - c_{33} + e_{33} b_j \quad (j = 1, 2, 3). \tag{3.13}$$

Through Eqs. (2.12)–(2.14), the unknowns $B_j(\alpha)(j = 1, 2, 3)$ are related to the new parameter $D(\alpha)$ and are given in Appendix B. Note that the only unknown in Eqs. (3.9) is $D(\alpha)$ since $A_j(\alpha), B_j(\alpha)(j = 1, 2, 3)$ are related to $D(\alpha)$ through Eqs. (3.10) and (B.1) in Appendix B.

The solution of a pair of dual integral equations (3.9) may be obtained by using a new function $\Phi(\xi)$ and the result is

$$D(\alpha) = -\frac{\sigma_\infty}{F} a^2 \int_0^1 \Phi(\xi) \sin(a\alpha\xi) d\xi. \tag{3.14}$$

The function $\Phi(\xi)$ is governed by the following Fredholm integral equation of the second kind:

$$\Phi(\xi) + \int_0^1 \Phi(\eta) K(\xi, \eta) d\eta = \xi. \tag{3.15}$$

The kernel function $K(\xi,\eta)$ is

$$K(\xi,\eta)=\frac{4}{\pi^2 F}\sum_{j=1}^{3} g_j\gamma_j^2\int_0^{\infty}\frac{1}{\Delta(\alpha)}\sum_{i=1}^{3} d_i\gamma_i'\{\gamma_i'\alpha M_{ji}(\alpha)K_0(\gamma_i'\alpha b) \tag{3.16}$$

$$-N_{ji}(\alpha)K_1(\gamma_i'\alpha b)\}\sinh(\gamma_i'a\alpha\eta)\sinh(\gamma_j'a\alpha\xi)d\alpha$$

in which $K_0()$ and $K_1()$ are, respectively, the zero and first order modified Bessel function of the second kind, and $M_{ji}(\alpha)$, $N_{ji}(\alpha)$ $(i,j=1,2,3)$, $\Delta(\alpha)$ are given in Appendix B.

The displacement components u_r, u_z and electric potential ϕ near the crack border are

$$\begin{aligned} u_r &= \frac{k_1\sqrt{r_1}}{F}\sum_{j=1}^{3} a_j d_j\{(\cos^2\theta_1+\gamma_j^2\sin^2\theta_1)^{1/2}+\cos\theta_1\}^{1/2}, \\ u_z &= -\frac{k_1\sqrt{r_1}}{F}\sum_{j=1}^{3}\frac{d_j}{\gamma_j}\{(\cos^2\theta_1+\gamma_j^2\sin^2\theta_1)^{1/2}-\cos\theta_1\}^{1/2}, \end{aligned} \tag{3.17}$$

$$\phi = \frac{k_1\sqrt{r_1}}{F}\sum_{j=1}^{3}\frac{b_j d_j}{\gamma_j}\{(\cos^2\theta_1+\gamma_j^2\sin^2\theta_1)^{1/2}-\cos\theta_1\}^{1/2}, \tag{3.18}$$

and the singular parts of the strains, electric field intensities, stresses and electric displacements in the neighborhood of the crack border are

$$\begin{aligned} \varepsilon_{rr} &= \frac{k_1}{2F\sqrt{r_1}}\sum_{j=1}^{3} a_j d_j R_j^c(\theta_1), \\ \varepsilon_{rz}=\varepsilon_{zr} &= -\frac{k_1}{4F\sqrt{r_1}}\sum_{j=1}^{3}\frac{d_j(a_j\gamma_j^2+1)}{\gamma_j}R_j^s(\theta_1), \\ \varepsilon_{zz} &= -\frac{k_1}{2F\sqrt{r_1}}\sum_{j=1}^{3} d_j R_j^c(\theta_1); \end{aligned} \tag{3.19}$$

$$\begin{aligned} E_r &= -\frac{k_1}{2F\sqrt{r_1}}\sum_{j=1}^{3}\frac{b_j d_j}{\gamma_j}R_j^s(\theta_1), \\ E_z &= -\frac{k_1}{2F\sqrt{r_1}}\sum_{j=1}^{3} b_j d_j R_j^c(\theta_1); \end{aligned} \tag{3.20}$$

$$\sigma_{rr} = \frac{k_1}{2F\sqrt{r_1}} \sum_{j=1}^{3} m_j d_j R_j^c(\theta_1),$$

$$\sigma_{zz} = \frac{k_1}{2F\sqrt{r_1}} \sum_{j=1}^{3} g_j d_j R_j^c(\theta_1), \tag{3.21}$$

$$\sigma_{zr} = -\frac{k_1}{2F\sqrt{r_1}} \sum_{j=1}^{3} \frac{f_j d_j}{\gamma_j} R_j^s(\theta_1);$$

$$D_r = -\frac{k_1}{2F\sqrt{r_1}} \sum_{j=1}^{3} \frac{n_j d_j}{\gamma_j} R_j^s(\theta_1),$$

$$D_z = \frac{k_1}{2F\sqrt{r_1}} \sum_{j=1}^{3} h_j d_j R_j^c(\theta_1), \tag{3.22}$$

where

$$h_j = e_{31} a_j - e_{33} - \epsilon_{33} b_j, \tag{3.23}$$

$$R_j^c(\theta_1) = \left\{ \frac{(\cos^2\theta_1 + \gamma_j^2 \sin^2\theta_1)^{1/2} + \cos\theta_1}{\cos^2\theta_1 + \gamma_j^2 \sin^2\theta_1} \right\}^{1/2},$$

$$R_j^s(\theta_1) = -\left\{ \frac{(\cos^2\theta_1 + \gamma_j^2 \sin^2\theta_1)^{1/2} - \cos\theta_1}{\cos^2\theta_1 + \gamma_j^2 \sin^2\theta_1} \right\}^{1/2} \tag{3.24}$$

and the polar coordinates r_1 and θ_1 are defined as

$$r_1 = \{(r-a)^2 + z^2\}^{1/2}, \tag{3.25}$$

$$\theta_1 = \arctan\left(\frac{z}{r-a}\right). \tag{3.26}$$

The stress intensity factor k_1 for the permeable crack is obtained as

$$k_1 = \lim_{r \to a^+} \left\{2(r-a)\right\}^{1/2} \sigma_{zz}(r,0) = \frac{2}{\pi} \sigma_\infty \sqrt{a} \Phi(1). \tag{3.27}$$

The electric displacement intensity factor k_D is also given by

$$k_D = \lim_{r\to a^+} \left\{2(r-a)\right\}^{1/2} D_z(r,0) = \left(\frac{1}{F}\sum_{j=1}^{3} h_j d_j\right) k_1. \tag{3.28}$$

The stress and electric displacement intensity factors for the impermeable crack are discussed in Appendix C.

By using the concept of crack closure energy and the asymptotic behavior of stresses, displacements, electric displacement and electric potential near the crack border, the total potential energy release rate G may be expressed as

$$G = \lim_{\Delta a\to 0} \frac{1}{\Delta a} \int_0^{\Delta a} \{\sigma_{zz}(r_1)u_z(\Delta a - r_1) + \sigma_{zr}(r_1)u_r(\Delta a - r_1) + D_z(r_1)\phi(\Delta a - r_1)\}dr_1, \tag{3.29}$$

where Δa is the assumed crack extension. Expression relating G for the permeable crack to k_1 is obtained by substituting representations for the stresses, displacements, electric displacement and electric potential in the vicinity of the crack into Eq. (3.29) and taking the limit. The result is

$$G = -\frac{\pi}{2F^2}\left(F\sum_{j=1}^{3}\frac{d_j}{\gamma_j} - \sum_{j=1}^{3} h_j d_j \sum_{j=1}^{3}\frac{b_j d_j}{\gamma_j}\right) k_1^2. \tag{3.30}$$

The mechanical strain energy release rate G_M includes only the mechanical energy released as the crack extends and is given by

$$G_M = \lim_{\Delta a\to 0} \frac{1}{\Delta a} \int_0^{\Delta a} \left\{\sigma_{zz}(r_1)u_z(\Delta a - r_1) + \sigma_{zr}(r_1)u_r(\Delta a - r_1)\right\}dr_1. \tag{3.31}$$

Writing the mechanical strain energy release rate expression for the permeable crack in terms of the stress intensity factor, we obtain:

$$G_M = -\left(\frac{\pi}{2F}\sum_{j=1}^{3}\frac{d_j}{\gamma_j}\right) k_1^2. \tag{3.32}$$

The total potential and mechanical strain energy release rates for the impermeable crack are also given in Appendix C.

When the stress intensity factor k_1 and the electric displacement intensity factor k_D are present along the crack border, the fracture criterion should depend

on a combination of k_1 and k_D reaching a critical value. Such a criterion can be developed by referring to the amount of energy stored in a volume element ahead of the crack. The critical value of this energy density will be used to determine whether the piezoceramic has reached the state of failure or not [10, 11]. For the piezoceramic, the energy stored in the volume element dV is

$$dW = \left\{\frac{1}{2}(\sigma_{rr}\varepsilon_{rr} + \sigma_{zr}\varepsilon_{zr} + \sigma_{rz}\varepsilon_{rz} + \sigma_{zz}\varepsilon_{zz}) + \frac{1}{2}(D_r E_r + D_z E_z)\right\} dV. \tag{3.33}$$

Substituting Eqs. (3.19)–(3.22) into Eq. (3.33) yields the quadratic form for the energy density function

$$\frac{dW}{dV} = \frac{1}{r_1}(a_M + a_E)k_1^2 = \frac{S}{r_1} \tag{3.34}$$

in which the coefficients a_M and a_E depend on the angle θ_1 and they are given by

$$a_M = \frac{1}{8F^2}\left\{\sum_{j=1}^{3} m_j d_j R_j^c(\theta_1) \sum_{j=1}^{3} a_j d_j R_j^c(\theta_1) + \sum_{j=1}^{3} \frac{f_j d_j}{\gamma_j} R_j^s(\theta_1) \sum_{j=1}^{3} \frac{d_j(a_j\gamma_j^2 + 1)}{\gamma_j} R_j^s(\theta_1) - \sum_{j=1}^{3} g_j d_j R_j^c(\theta_1) \sum_{j=1}^{3} d_j R_j^c(\theta_1)\right\}, \tag{3.35}$$

$$a_E = \frac{1}{8F^2}\left\{\sum_{j=1}^{3} \frac{n_j d_j}{\gamma_j} R_j^s(\theta_1) \sum_{j=1}^{3} \frac{b_j d_j}{\gamma_j} R_j^s(\theta_1) - \sum_{j=1}^{3} h_j d_j R_j^c(\theta_1) \sum_{j=1}^{3} b_j d_j R_j^c(\theta_1)\right\}. \tag{3.36}$$

The magnitude, S, of the $1/r_1$ energy field in Eq. (3.34) will be referred to as the energy density factor for the permeable crack. The energy density factor for the impermeable crack is also given in Appendix C.

For a penny-shaped crack under tensile loading, fracture will always occur in the normal plane. SIH [10] has assumed that crack initiation starts in a radial direction along which the energy density is a minimum. Necessary and sufficient conditions for S to have a minimum value are

$$\frac{dS}{d\theta_1} = 0, \qquad \frac{d^2S}{d\theta_1^2} > 0. \tag{3.37}$$

Rapid crack growth occurs when the minimum energy density factor reaches a critical value:

$$S_{min} = S_c = r_{1c}\left(\frac{dW}{dV}\right)_c, \tag{3.38}$$

where r_{1c} represents the last ligament of slow crack growth, just prior to the onset of rapid fracture. Each increment of stable crack growth $r_{11}, r_{12}, ..., r_{1j}, ..., r_{1c}$ up to the rapid crack propagation is determined by the condition

$$\left(\frac{dW}{dV}\right)_c = \frac{S_1}{r_{11}} = \frac{S_2}{r_{12}} = \cdots = \frac{S_j}{r_{1j}} = \cdots = \frac{S_c}{r_{1c}}. \tag{3.39}$$

If the fracture process due to increasing electromechanical load is unstable, then each increment of crack growth will increase monotonically, i.e.

$$r_{11} < r_{12} < \cdots < r_{1j} < \cdots < r_{1c}. \tag{3.40}$$

The corresponding energy density factors will also increase according to $S_j/r_{1j} = \text{const}$:

$$S_1 < S_2 < \cdots < S_j < \cdots < S_c. \tag{3.41}$$

A stable fracture process corresponds to decreasing increments of the crack growth:

$$r_{11} > r_{12} > \cdots > r_{1j} > \cdots > r_{1a}, \tag{3.42}$$

where r_{1a} is the last increment of growth before the crack arrest. A corresponding decrease in the energy density factors takes place:

$$S_1 > S_2 > \cdots > S_j > \cdots > S_a. \tag{3.43}$$

In the piezoceramic, a combination of the conditions described by Eqs. (3.40) and (3.42) can exist. That is, the increments of crack growth may either increase or decrease, depending on the material properties and the nature of combined electromechanical loading.

4. Numerical results and discussion

The determination of the stress intensity factor, energy release rate and energy density factor for the permeable crack requires the solution of the function $\Phi(\xi)$. The solution of the Fredholm integral equation of the second kind (3.15)

governing $\Phi(\xi)$ has been computed numerically by the use of Gaussian quadrature formulas. Once this is done, k_1, G and S can be found from Eqs. (3.27), (3.30), (3.31) and (3.34). The simultaneous Fredholm integral equations of the second kind (C.11) were also solved numerically to yield the values of the functions $\Phi_1(1)$ and $\Phi_2(1)$. These values were then inserted into Eqs. (C.13) and (C.14) to determine the stress and electric displacement intensity factors for the impermeable crack. The energy release rate and energy density factor were calculated by using Eqs. (C.15), (C.16) and (C.18)–(C.20). The piezoelectric materials are assumed to be the commercially available piezoceramic P-7. The elastic, piezoelectric and dielectric properties of material are listed in Table 1.

Table 1. Material properties of a piezoelectric ceramic P-7.

	Elastic stiffnesses ($\times 10^{10}$N/m^2)					Piezoelectric coefficients (C/m^2)			Dielectric constants ($\times 10^{-10}$C/Vm)	
	c_{11}	c_{33}	c_{44}	c_{12}	c_{13}	e_{31}	e_{33}	e_{15}	ϵ_{11}	ϵ_{33}
P-7	13.0	11.9	2.5	8.3	8.3	−10.3	14.7	13.5	171	186

Figure 2 shows the normalized stress intensity factor $\pi k_1/2\sigma_0 a^{1/2}$ as a function of the crack-radius to cylinder-radius ratio a/b for different values of the normalized electric displacement $e_1 D_\infty/c_1\sigma_0$ (Case I) and for the permeable (exact) and impermeable (approximate) cracks. The data are normalized by the stress intensity factor $2\sigma_0 a^{1/2}/\pi$ of an infinite P-7 piezoelectric ceramic for $D_\infty = 0$ C/m^2 corresponding to the applied uniform displacement. A similar phenomenon was observed for the stress intensity factor of the permeable and impermeable cracks. Note that an increase of a/b causes an increase in the stress intensity factor. When electric displacement is applied, which is equivalent to applying a surface charge, $\pi k_1/2\sigma_0 a^{1/2}$ increases or decreases depending on the direction of the electric displacement. The stress intensity factor k_1 normalized by $2\sigma_\infty a^{1/2}/\pi$ corresponding to the applied uniform stress for the permeable and impermeable crack models is independent of the normalized electric displacement $e_1 D_\infty/c_1\sigma_\infty$. A similar explanation applies to the results shown in Fig. 3 for Case II as the normalized electric field $e_2 E_\infty/\sigma_0$ is varied. In the case of electric field loading, which can be more readily achieved in the laboratory by applying a constant potential difference across the piezoceramic cylinder, applying the field in the positive direction decreases the stress intensity factor, whereas the negative electric field increases it. For $e_1 D_\infty/c_1\sigma_0 \to 1.0$ or $e_2 E_\infty/\sigma_0 \to 1.0$, $\pi k_1/2\sigma_0 a^{1/2}$ approaches zero. The stress intensity factor is also studied for different conditions of the electric potential at infinity of the piezoceramic cylinder:

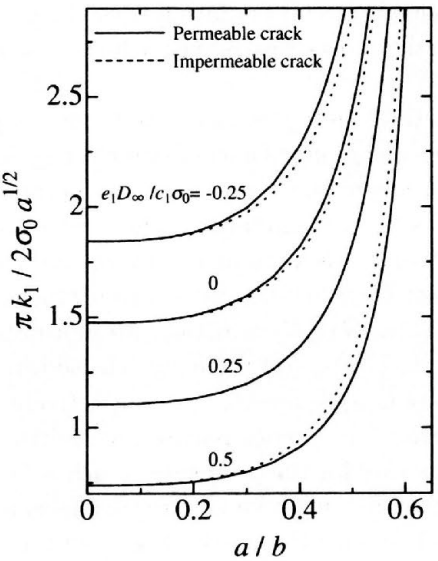

FIG. 2. Stress intensity factor versus a/b for different electric displacement $e_1 D_\infty / c_1 \sigma_0$ (Case I).

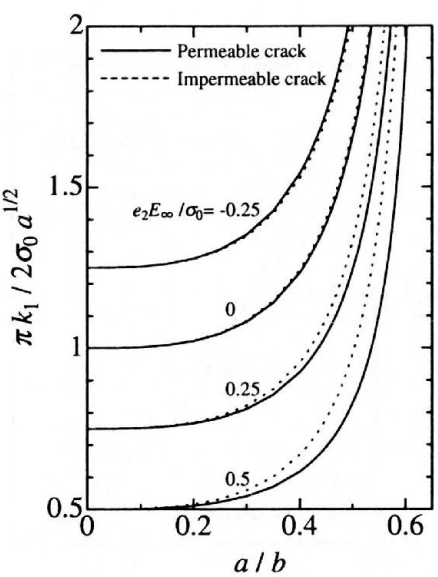

FIG. 3. Stress intensity factor versus a/b for different electric field $e_2 E_\infty / \sigma_0$ (Case II).

an open-circuit condition where the electric potential remains free (zero electric displacements) and a closed-circuit condition with the potential forced to remain zero (grounded). Note that the stress intensity factor for $E_\infty = 0$ is smaller than the one for $D_\infty = 0$.

Figure 4 shows the total energy release rate G for the permeable crack under applied uniform displacement versus normalized electric displacement $e_1 D_\infty / c_1 \sigma_0$ (Case I) for $a/b = 0.5$, where the result has been normalized by the energy release rate G_{D0} for $D_\infty = 0$. For comparison, the mechanical strain energy release rate G_M for the permeable crack, total energy release rate G_I and mechanical strain energy release rate G_{MI} for the impermeable crack are also included in the figure. Energy release rates G_M, G_I and G_{MI} are normalized by the mechanical strain energy release rate G_{MD0}, total energy release rate G_{ID0} and mechanical strain energy release rate G_{MID0} for $D_\infty = 0$, respectively. Comparing the results from the total and mechanical energy release rates, little difference is observed. The total energy release rate for the permeable crack is lower for positive electric displacements and higher for negative electric displacements. Hence, a positive electrical load will tend to slow the crack growth and a negative electrical load will tend to enhance the crack growth. The numerical results for the permeable crack are found to be in excellent agreement with the observations of SHINDO *et al.* [7]. On the other hand, when a positive electrical load is larger, a negative total energy release rate is produced for the impermeable crack. The impermeable assumption leads to an overly attractive prediction regarding the crack

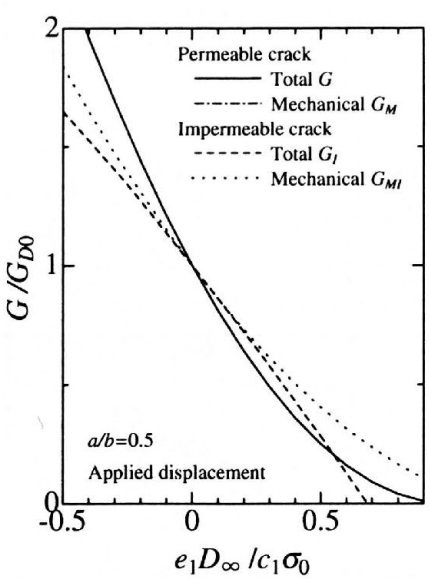

FIG. 4. Energy release rate versus electric displacement $e_1 D_\infty / c_1 \sigma_0$ (Case I).

arresting ability of electrical loads in cracked piezoceramics. Figure 5 shows the corresponding result for Case II. Here the data G, G_M, G_I and G_{MI} have been normalized by the energy release rates G_{E0}, G_{ME0}, G_{IE0} and G_{MIE0} for $E_\infty = 0$, respectively. The presentation of data for the impermeable crack causes confusion in using the electrical boundary conditions on the crack face. Figure 6 gives the plot of the normalized total energy release rate G_I/G_{ID0} for the permeable and impermeable cracks under applied uniform stress versus normalized electric displacement $e_1 D_\infty/c_1\sigma_\infty$ (Case I) for $a/b = 0.5$. Also shown is the normalized mechanical energy release rate G_{IM}/G_{IMD0}.

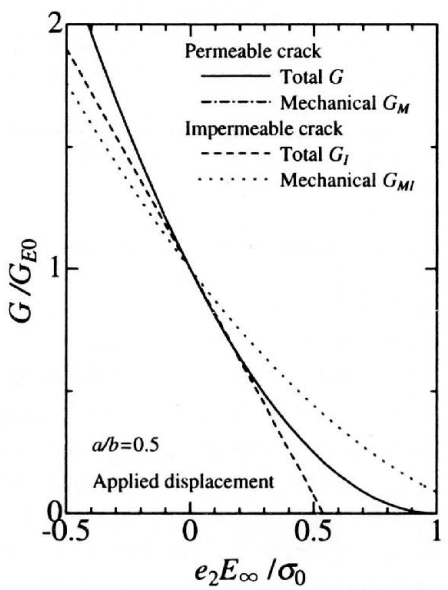

FIG. 5. Energy release rate versus electric field $e_2 E_\infty/\sigma_0$ (Case II).

Figure 7 shows the corresponding result for Case II. Appling the electrical load in either direction decreases the total energy release rate for the impermeable crack and eventually arrests the crack growth. However, experimental investigation does not confirm this crack-arresting behavior. The total and mechanical energy release rates for the permeable crack are independent of the electrical loading.

Figure 8 gives the variation of the normalized energy density factor $\pi^2 S/4a\sigma_0^2$ with angle θ_1 for different values of $e_1 D_\infty/c_1\sigma_0$ (Case I) and $a/b = 0.5$. Excluding the extreme values at the crack boundaries, all curves for the permeable and impermeable cracks possess minimum at $\theta_1 = 0$. The variation of $\pi^2 S/4a\sigma_0^2$ with

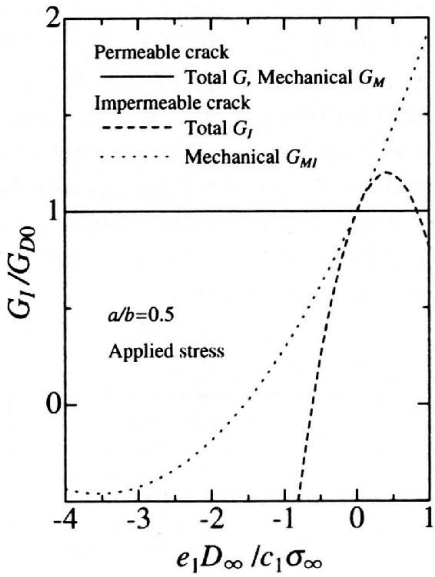

FIG. 6. Energy release rate versus electric displacement $e_1D_\infty/c_1\sigma_0$ (Case I).

θ_1 for Case II is found to be similar to that for Case I. Figure 9 shows the crack growth segment r_{1j} (energy density factor S_j) for the permeable crack under applied uniform displacement versus normalized electric displacement $e_1D_\infty/c_1\sigma_0$ (Case I) for $a/b = 0.5$ and $\theta_1 = 0$, where r_{1j} (S_j) has been normalized by the crack growth segment r_{1D0} (energy density factor S_{D0}) for $D_\infty = 0$. Also shown are data for the impermeable crack normalized by r_{1ID0} (S_{ID0}) that corresponds to the crack growth segment (energy density factor) for $D_\infty = 0$. The presence of positive electric displacement D_∞ leads to a decrease in the crack growth segment (energy density factor) for the permeable crack. In contrast, the crack growth segment (energy density factor) increases as the electric displacement D_∞ increases in the negative direction. Figure 10 shows the corresponding result for Case II. The data r_{1j} (S_j) and r_{1jI} (S_{jI}) have been normalized due to r_{1E0} (S_{E0}) and r_{1IE0} (S_{IE0}) for $E_\infty = 0$, respectively. For the permeable boundary condition, no difference in the effects of the electrical loads on crack propagation is found for the criteria (the stress intensity factor, total energy release rate, mechanical strain energy release rate and energy density factor). Figures 11 and 12 exhibit the dependence of the crack growth segment (energy density factor) for the permeable and impermeable cracks under applied uniform stress on $e_1D_\infty/c_1\sigma_\infty$ and $e_2E_\infty/\sigma_\infty$, respectively. Based on the energy density criterion for the impermeable crack, we cannot explain the experimental results.

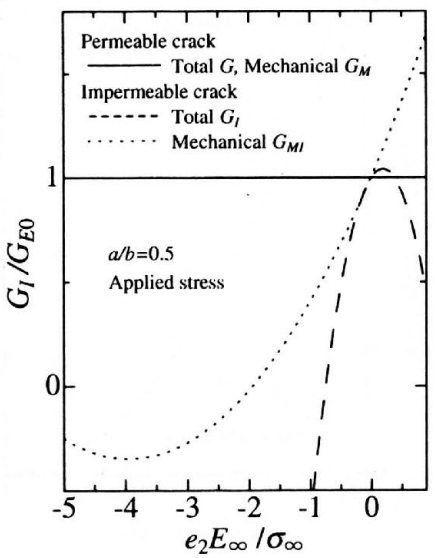

FIG. 7. Energy release rate versus electric field e_2E_∞/σ_0 (Case II).

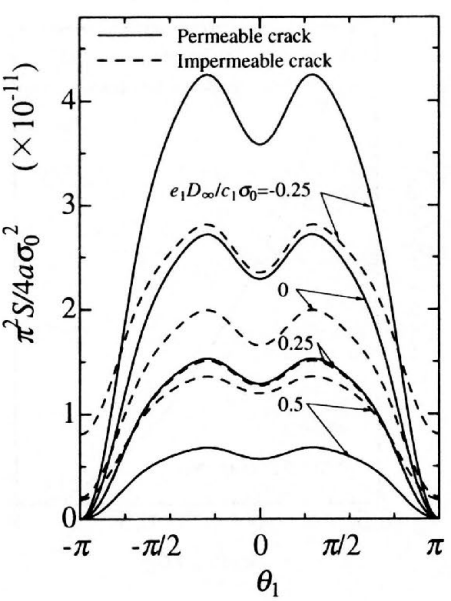

FIG. 8. Energy density factor versus angle θ_1 for a/b=0.5 (Case I).

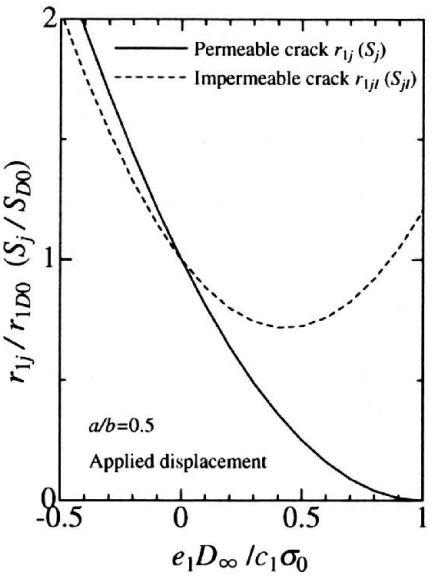

FIG. 9. Crack growth segment (energy density factor) versus electric displacement $e_1D_\infty/c_1\sigma_0$ (Case I).

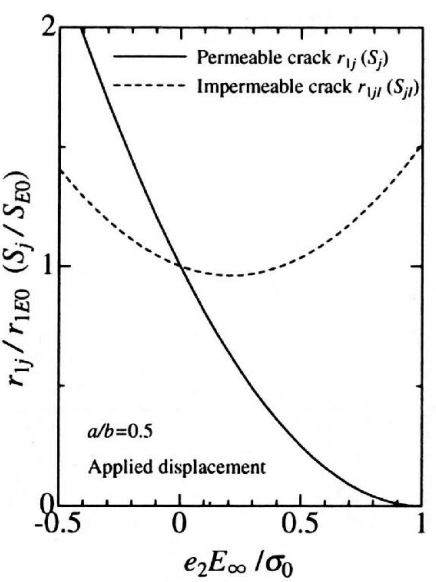

FIG. 10. Crack growth segment (energy density factor) versus electric field e_2E_∞/σ_0 (Case II).

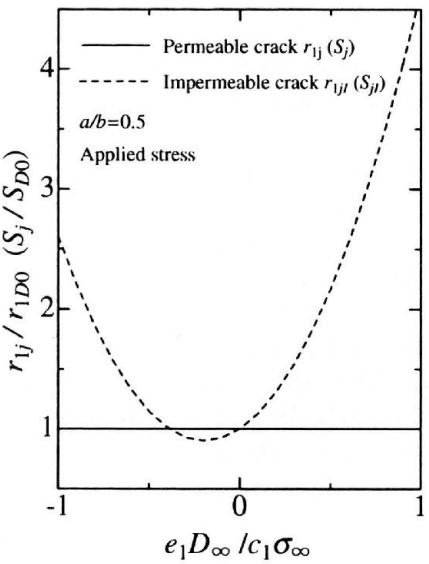

FIG. 11. Crack growth segment (energy density factor) versus electric displacement $e_1D_\infty/c_1\sigma_\infty$ (CaseI).

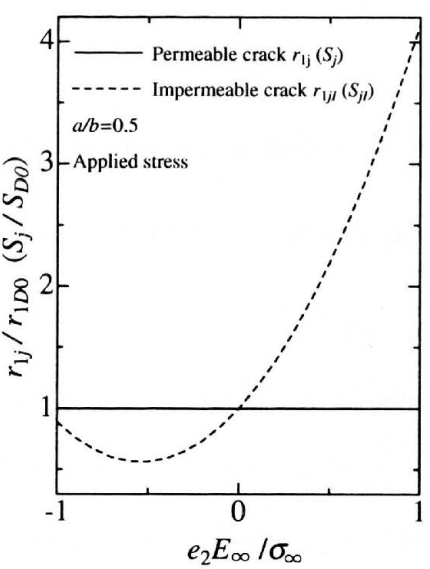

FIG. 12. Crack growth segment (energy density factor) versus electric field $e_2E_\infty/\sigma_\infty$ (Case II).

5. Conclusions

The electroelastic problem of a piezoceramic cylinder with a penny-shaped crack has been theoretically analyzed. The results are expressed in terms of the stress intensity factor, energy release rate and energy density factor. It is found that the stress intensity factor tends to increase with increasing crack-radius to cylinder-radius ratio, depending on the electrical boundary condition on the crack face. For the permeable boundary condition, positive electrical loads impede crack propagation in piezoelectric cylinder under applied displacement while negative electrical loads aid the crack propagation. The experimental study has shown that crack growth inhibition corresponds to a positive field. For applied stress, electric fields have no effect on crack propagation. No consensus is reached on the fracture criteria for the impermeable piezoelectric cracks, and the stress intensity factor, energy release rate and energy density factor criteria for the permeable crack are superior to the fracture criteria for the impermeable crack.

Acknowledgement

The work was supported by the Grant-in-Aid for Encouragement of Young Scientists from the Ministry of Education, Culture, Sports, Science and Technology of Japan

Appendix A

γ_j^2 $(j = 1, 2, 3)$ in Eqs. (3.1), (3.2) are the roots of the following characteristic equation:

$$a_0\gamma^6 + b_0\gamma^4 + c_0\gamma^2 + d_0 = 0, \tag{A.1}$$

where

$$\begin{aligned}
a_0 &= c_{44}(c_{33}\epsilon_{33} + e_{33}^2),\\
b_0 &= -2c_{44}e_{15}e_{33} - c_{11}e_{33}^2 - c_{33}(c_{44}\epsilon_{11} + c_{11}\epsilon_{33}) + \epsilon_{33}(c_{13} + c_{44})^2\\
&\quad + 2e_{33}(c_{13} + c_{44})(e_{31} + e_{15}) - c_{44}^2\epsilon_{33} - c_{33}(e_{31} + e_{15})^2,\\
c_0 &= 2c_{11}e_{15}e_{33} + c_{44}e_{15}^2 + c_{11}(c_{33}\epsilon_{11} + c_{44}\epsilon_{33}) - \epsilon_{11}(c_{13} + c_{44})^2\\
&\quad - 2e_{15}(c_{13} + c_{44})(e_{31} + e_{15}) + c_{44}^2\epsilon_{11} + c_{44}(e_{31} + e_{15})^2,\\
d_0 &= -c_{11}(c_{44}\epsilon_{11} + e_{15}^2)
\end{aligned} \tag{A.2}$$

and, $\gamma_j^{'2}$, a_j, b_j, $a_j^{'}$, $b_j^{'}$ $(j = 1, 2, 3)$ stand for the abbreviations:

$$\gamma_j^{'2} = \frac{1}{\gamma_j^2}, \tag{A.3}$$

$$a_j = \frac{(e_{31} + e_{15})(c_{33}\gamma_j^2 - c_{44}) - (c_{13} + c_{44})(e_{33}\gamma_j^2 - e_{15})}{(c_{44}\gamma_j^2 - c_{11})(e_{33}\gamma_j^2 - e_{15}) + (c_{13} + c_{44})(e_{31} + e_{15})\gamma_j^2}, \tag{A.4}$$

$$b_j = \frac{(c_{44}\gamma_j^2 - c_{11})a_j + (c_{13} + c_{44})}{e_{31} + e_{15}}, \tag{A.5}$$

$$a_j^{'} = -a_j\gamma_j^2, \tag{A.6}$$

$$b_j^{'} = -b_j. \tag{A.7}$$

Appendix B

The unknowns $B_j(\alpha)(j = 1, 2, 3)$ can be related to the new parameter as

$$B_1(\alpha) = \frac{1}{\Delta(\alpha)} \sum_{i=1}^{3} d_i \int_0^{\infty} \{M_{1i}(\alpha)G_i(s, \alpha) + N_{1i}(\alpha)G_i^{'}(s, \alpha), \}D(s)ds,$$

$$B_2(\alpha) = \frac{1}{\Delta(\alpha)} \sum_{i=1}^{3} d_i \int_0^{\infty} \{M_{2i}(\alpha)G_i(s, \alpha) + N_{2i}(\alpha)G_i^{'}(s, \alpha), \}D(s)ds, \tag{B.1}$$

$$B_3(\alpha) = \frac{1}{\Delta(\alpha)} \sum_{i=1}^{3} d_i \int_0^{\infty} \{M_{3i}(\alpha)G_i(s, \alpha) + N_{3i}(\alpha)G_i^{'}(s, \alpha), \}D(s), ds$$

where

$$G_i(s, \alpha) = \frac{2}{\pi} \frac{\gamma_i s^2}{s^2\gamma_i^2 + \alpha^2} J_0(bs),$$

$$G_i^{'}(s, \alpha) = \frac{2}{\pi} \frac{\gamma_i s}{s^2\gamma_i^2 + \alpha^2} J_1(bs), \tag{B.2}$$

$$M_{1i}(\alpha) = m_i\{q_2(\alpha)r_3(\alpha) - q_3(\alpha)r_2(\alpha)\},$$

$$M_{2i}(\alpha) = m_i\{q_3(\alpha)r_1(\alpha) - q_1(\alpha)r_3(\alpha)\},$$

$$M_{3i}(\alpha) = m_i\{q_1(\alpha)r_2(\alpha) - q_2(\alpha)r_1(\alpha)\},$$

(B.3)

$$N_{1i}(\alpha) = \frac{(c_{12} - c_{11})a_i}{b}\{q_2(\alpha)r_3(\alpha) - q_3(\alpha)r_2(\alpha)\}$$
$$+\frac{f_i}{\gamma_i^2}\{r_2(\alpha)p_3(\alpha) - r_3(\alpha)p_2(\alpha)\} + \frac{n_i}{\gamma_i^2}\{p_2(\alpha)q_3(\alpha) - p_3(\alpha)q_2(\alpha)\},$$

$$N_{2i}(\alpha) = \frac{(c_{12} - c_{11})a_i}{b}\{q_3(\alpha)r_1(\alpha) - q_1(\alpha)r_3(\alpha)\}$$
$$+\frac{f_i}{\gamma_i^2}\{r_3(\alpha)p_1(\alpha) - r_1(\alpha)p_3(\alpha)\} + \frac{n_i}{\gamma_i^2}\{p_3(\alpha)q_1(\alpha) - p_1(\alpha)q_3(\alpha)\},$$

$$N_{3i}(\alpha) = \frac{(c_{12} - c_{11})a_i}{b}\{q_1(\alpha)r_2(\alpha) - q_2(\alpha)r_1(\alpha)\}$$
$$+\frac{f_i}{\gamma_i^2}\{r_1(\alpha)p_2(\alpha) - r_2(\alpha)p_1(\alpha)\} + \frac{n_i}{\gamma_i^2}\{p_1(\alpha)q_2(\alpha) - p_2(\alpha)q_1(\alpha)\},$$

$$(i = 1, 2, 3);$$

(B.4)
$$\Delta(\alpha) = p_1(\alpha)\{q_2(\alpha)r_3(\alpha) - q_3(\alpha)r_2(\alpha)\} + p_2(\alpha)\{q_3(\alpha)r_1(\alpha)$$
$$- q_1(\alpha)r_3(\alpha)\} + p_3(\alpha)\{q_1(\alpha)r_2(\alpha) - q_2(\alpha)r_1(\alpha)\}$$

and

$$p_i(\alpha) = \alpha\gamma_i m_i I_0(\gamma_i'\alpha b) + \gamma_i^2 n_i I_1(\gamma_i'\alpha b),$$

(B.5)
$$q_i(\alpha) = f_i I_1(\gamma_i'\alpha b), \qquad (i = 1, 2, 3);$$

$$r_i(\alpha) = n_i I_1(\gamma_i'\alpha b),$$

$$m_i = c_{11}a_i - c_{13} + e_{31}b_i,$$

(B.6)
$$n_i = e_{15}(a_i\gamma_i^2 + 1) + \epsilon_{11}b_i \qquad (i = 1, 2, 3).$$

Appendix C

The impermeable boundary condition becomes

$$\begin{aligned} &D_z(r,0) = 0 && (0 \le r < a), \\ &\phi(r,0) = 0 && (a \le r \le b). \end{aligned} \tag{C.1}$$

The boundary condition of Eq. (2.8) leads to Eq. (3.6). Making use of mixed boundary conditions of Eqs. (2.9) and (C.1), two simultaneous dual integral equations are obtained:

$$\begin{cases} \displaystyle\int_0^\infty \alpha F_{11} D_1(\alpha) J_0(\alpha r) d\alpha + \int_0^\infty \alpha F_{12} D_2(\alpha) J_0(\alpha r) d\alpha \\ \qquad \displaystyle -\sum_{j=1}^{3} \int_0^\infty \alpha g_j \gamma_j B_j(\alpha) I_0(\gamma_j' \alpha r) d\alpha = -\frac{\pi}{2}\sigma_\infty \quad (0 \le r < a) \\ \displaystyle\int_0^\infty D_1(\alpha) J_0(\alpha r) d\alpha = 0 \quad (a \le r \le b); \end{cases} \tag{C.2}$$

$$\begin{cases} \displaystyle\int_0^\infty \alpha F_{21} D_1(\alpha) J_0(\alpha r) d\alpha + \int_0^\infty \alpha F_{22} D_2(\alpha) J_0(\alpha r) d\alpha \\ \qquad \displaystyle -\sum_{j=1}^{3} \int_0^\infty \alpha h_j \gamma_j B_j(\alpha) I_0(\gamma_j' \alpha r) d\alpha = -\frac{\pi}{2} D^* \quad (0 \le r < a) \\ \displaystyle\int_0^\infty D_2(\alpha) J_0(\alpha r) d\alpha = 0 \quad (a \le r \le b), \end{cases} \tag{C.3}$$

where

$$\begin{aligned} D_1(\alpha) &= \frac{1}{\gamma_1} A_1(\alpha) + \frac{1}{\gamma_2} A_2(\alpha) + \frac{1}{\gamma_3} A_3(\alpha), \\ D_2(\alpha) &= \frac{b_1}{\gamma_1} A_1(\alpha) + \frac{b_2}{\gamma_2} A_2(\alpha) + \frac{b_3}{\gamma_3} A_3(\alpha); \end{aligned} \tag{C.4}$$

$$F_{11} = \sum_{j=1}^{3} g_j d_j, \quad F_{12} = \sum_{j=1}^{3} g_j l_j, \quad F_{21} = \sum_{j=1}^{3} h_j d_j, \quad F_{22} = \sum_{j=1}^{3} h_j l_j, \tag{C.5}$$

(C.6) $$l_1 = \gamma_1(f_2 - f_3), \quad l_2 = \gamma_2(f_3 - f_1), \quad l_3 = \gamma_3(f_1 - f_2)$$

(C.7) $$D^* = \begin{cases} D_\infty & \text{(Case I)}, \\ c_2\sigma_0 + e_3 E_\infty & \text{(Case II)}, \end{cases}$$

(C.8) $$c_2 = \frac{e_{33}(c_{11} + c_{12}) - 2c_{13}e_{31}}{(c_{11} + c_{12})c_{33} - 2c_{13}^2}, \quad e_3 = \frac{2e_{31}}{c_{11} + c_{12}} + \epsilon_{33};$$

(C.9)
$$B_1(\alpha) = \frac{1}{\Delta(\alpha)} \sum_{i=1}^{3} \int_0^\infty \{M_{1i}(\alpha)G_i(s,\alpha) + N_{1i}(\alpha)G_i'(s,\alpha)\}\{d_i D_1(s) + l_i D_2(s)\}ds,$$

$$B_2(\alpha) = \frac{1}{\Delta(\alpha)} \sum_{i=1}^{3} \int_0^\infty \{M_{2i}(\alpha)G_i(s,\alpha) + N_{2i}(\alpha)G_i'(s,\alpha)\}\{d_i D_1(s) + l_i D_2(s)\}ds,$$

$$B_3(\alpha) = \frac{1}{\Delta(\alpha)} \sum_{i=1}^{3} \int_0^\infty \{M_{3i}(\alpha)G_i(s,\alpha) + N_{3i}(\alpha)G_i'(s,\alpha)\}\{d_i D_1(s) + l_i D_2(s)\}ds.$$

The unknowns $D_1(\alpha)$ and $D_2(\alpha)$ can be found by the same method of approach as in the permeable case. The results are

(C.10)
$$D_1(\alpha) = -\frac{\sigma_\infty}{F_{11}} a^2 \int_0^1 \Phi_1(\xi)\sin(a\alpha\xi)d\xi,$$

$$D_2(\alpha) = -\frac{\sigma_\infty}{F_{12}} a^2 \int_0^1 \Phi_2(\xi)\sin(a\alpha\xi)d\xi.$$

The functions $\Phi_1(\xi)$ and $\Phi_2(\xi)$ in Eqs. (C.10) are the solutions of the following simultaneous Fredholm integral equations of the second kind:

$$\Phi_1(\xi) + \Phi_2(\xi) + \int_0^1 \Phi_1(\eta) K_{11}(\xi,\eta)d\eta + \int_0^1 \Phi_2(\eta) K_{12}(\xi,\eta)d\eta = \xi,$$

$$\text{(C.11)} \qquad \frac{F_{21}}{F_{11}}\Phi_1(\xi) + \frac{F_{22}}{F_{12}}\Phi_2(\xi).$$

$$+ \int_0^1 \Phi_1(\eta) K_{21}(\xi,\eta)d\eta + \int_0^1 \Phi_2(\eta) K_{22}(\xi,\eta)d\eta = \frac{D^*}{\sigma_\infty}\xi.$$

The kernels $K_{ij}(\xi,\eta)(i,j=1,2)$ are given by

$$K_{11}(\xi,\eta) = \frac{4}{\pi^2 F_{11}} \sum_{j=1}^{3} g_j \gamma_j^2 \int_0^\infty \frac{1}{\Delta(\alpha)} \sum_{i=1}^{3} d_i \gamma_i' \{\gamma_i' \alpha M_{ji}(\alpha) K_0(\gamma_i' \alpha b)$$

$$- N_{ji}(\alpha) K_1(\gamma_i' \alpha b)\} \sinh(\gamma_i' a\alpha\eta) \sinh(\gamma_j' a\alpha\xi) d\alpha,$$

$$K_{12}(\xi,\eta) = \frac{4}{\pi^2 F_{12}} \sum_{j=1}^{3} g_j \gamma_j^2 \int_0^\infty \frac{1}{\Delta(\alpha)} \sum_{i=1}^{3} l_i \gamma_i' \{\gamma_i' \alpha M_{ji}(\alpha) K_0(\gamma_i' \alpha b)$$

$$- N_{ji}(\alpha) K_1(\gamma_i' \alpha b)\} \sinh(\gamma_i' a\alpha\eta) \sinh(\gamma_j' a\alpha\xi) d\alpha,$$

(C.12)

$$K_{21}(\xi,\eta) = \frac{4}{\pi^2 F_{11}} \sum_{j=1}^{3} h_j \gamma_j^2 \int_0^\infty \frac{1}{\Delta(\alpha)} \sum_{i=1}^{3} d_i \gamma_i' \{\gamma_i' \alpha M_{ji}(\alpha) K_0(\gamma_i' \alpha b)$$

$$- N_{ji}(\alpha) K_1(\gamma_i' \alpha b)\} \sinh(\gamma_i' a\alpha\eta) \sinh(\gamma_j' a\alpha\xi) d\alpha,$$

$$K_{22}(\xi,\eta) = \frac{4}{\pi^2 F_{12}} \sum_{j=1}^{3} h_j \gamma_j^2 \int_0^\infty \frac{1}{\Delta(\alpha)} \sum_{i=1}^{3} l_i \gamma_i' \{\gamma_i' \alpha M_{ji}(\alpha) K_0(\gamma_i' \alpha b)$$

$$- N_{ji}(\alpha) K_1(\gamma_i' \alpha b)\} \sinh(\gamma_i' a\alpha\eta) \sinh(\gamma_j' a\alpha\xi) d\alpha.$$

The stress intensity factor k_1 and electric displacement intensity factor k_D for the impermeable crack are obtained as

$$\text{(C.13)} \qquad k_1 = \frac{2}{\pi}\sigma_\infty \sqrt{a}\{\Phi_1(1) + \Phi_2(1)\},$$

$$k_D = \frac{2}{\pi}\sigma_\infty\sqrt{a}\left\{\frac{F_{21}}{F_{11}}\Phi_1(1) + \frac{F_{22}}{F_{12}}\Phi_2(1)\right\}. \tag{C.14}$$

Using the field distribution in front of the crack border, the total potential energy release rate G and mechanical strain energy release rate G_M for the impermeable crack are

$$\begin{aligned} G = -\frac{\pi}{2(F_{11}F_{22} - F_{12}F_{21})^2}\Bigg[\Bigg\{(F_{11}F_{22} - F_{12}F_{21})\sum_{j=1}^{3}\frac{s_j}{\gamma_j} \\ -\sum_{j=1}^{3}h_j s_j \sum_{j=1}^{3}\frac{b_j s_j}{\gamma_j}\Bigg\} k_1^2 \\ +\Bigg\{\sum_{j=1}^{3}h_j t_j \sum_{j=1}^{3}\frac{b_j s_j}{\gamma_j} + \sum_{j=1}^{3}h_j s_j \sum_{j=1}^{3}\frac{b_j t_j}{\gamma_j} - (F_{11}F_{22} - F_{12}F_{21})\sum_{j=1}^{3}\frac{t_j}{\gamma_j}\Bigg\} k_1 k_D \\ -\left(\sum_{j=1}^{3}h_j t_j \sum_{j=1}^{3}\frac{b_j t_j}{\gamma_j}\right) k_D^2\Bigg], \end{aligned} \tag{C.15}$$

$$G_M = -\frac{\pi}{2(F_{11}F_{22} - F_{12}F_{21})}\left\{\left(\sum_{j=1}^{3}\frac{s_j}{\gamma_j}\right) k_1^2 - \left(\sum_{j=1}^{3}\frac{t_j}{\gamma_j}\right) k_1 k_D\right\}, \tag{C.16}$$

where

$$\begin{aligned} s_j &= d_j F_{22} - l_j F_{21}, \\ t_j &= d_j F_{12} - l_j F_{11}. \end{aligned} \tag{C.17}$$

The energy density factor are expressible in the forms

$$S = S_M + S_E, \tag{C.18}$$

where

$$S_M = \frac{1}{8(F_{11}F_{22} - F_{12}F_{21})^2}(\beta_1 k_1^2 + \beta_2 k_1 k_D + \beta_3 k_D^2), \tag{C.19}$$

$$S_E = \frac{1}{8(F_{11}F_{22} - F_{12}F_{21})^2}(\beta_4 k_1^2 + \beta_5 k_1 k_D + \beta_6 k_D^2), \tag{C.20}$$

(C.21)

$$\beta_1 = \sum_{j=1}^{3} m_j s_j R_j^c(\theta_1) \sum_{j=1}^{3} a_j s_j R_j^c(\theta_1) + 2\sum_{j=1}^{3} \frac{f_j s_j}{\gamma_j} R_j^s(\theta_1) \sum_{j=1}^{3} \frac{s_j(a_j\gamma_j^2+1)}{\gamma_j} R_j^s(\theta_1)$$
$$- \sum_{j=1}^{3} g_j s_j R_j^c(\theta_1) \sum_{j=1}^{3} s_j R_j^c(\theta_1),$$

$$\beta_2 = -\sum_{j=1}^{3} m_j t_j R_j^c(\theta_1) \sum_{j=1}^{3} a_j s_j R_j^c(\theta_1) - 2\sum_{j=1}^{3} \frac{f_j t_j}{\gamma_j} R_j^s(\theta_1) \sum_{j=1}^{3} \frac{s_j(a_j\gamma_j^2+1)}{\gamma_j} R_j^s(\theta_1)$$
$$+ \sum_{j=1}^{3} g_j t_j R_j^c(\theta_1) \sum_{j=1}^{3} s_j R_j^c(\theta_1) - \sum_{j=1}^{3} m_j s_j R_j^c(\theta_1) \sum_{j=1}^{3} a_j t_j R_j^c(\theta_1)$$
$$- 2\sum_{j=1}^{3} \frac{f_j s_j}{\gamma_j} R_j^s(\theta_1) \sum_{j=1}^{3} \frac{t_j(a_j\gamma_j^2+1)}{\gamma_j} R_j^s(\theta_1) + \sum_{j=1}^{3} g_j s_j R_j^c(\theta_1) \sum_{j=1}^{3} t_j R_j^c(\theta_1),$$

$$\beta_3 = \sum_{j=1}^{3} m_j t_j R_j^c(\theta_1) \sum_{j=1}^{3} a_j t_j R_j^c(\theta_1) + 2\sum_{j=1}^{3} \frac{f_j t_j}{\gamma_j} R_j^s(\theta_1) \sum_{j=1}^{3} \frac{t_j(a_j\gamma_j^2+1)}{\gamma_j} R_j^s(\theta_1)$$
$$- \sum_{j=1}^{3} g_j t_j R_j^c(\theta_1) \sum_{j=1}^{3} t_j R_j^c(\theta_1),$$

$$\beta_4 = \sum_{j=1}^{3} \frac{n_j}{\gamma_j} s_j R_j^s(\theta_1) \sum_{j=1}^{3} \frac{b_j s_j}{\gamma_j} R_j^s(\theta_1) - \sum_{j=1}^{3} h_j s_j R_j^c(\theta_1) \sum_{j=1}^{3} b_j s_j R_j^c(\theta_1),$$

$$\beta_5 = -\sum_{j=1}^{3} \frac{n_j}{\gamma_j} t_j R_j^s(\theta_1) \sum_{j=1}^{3} \frac{b_j s_j}{\gamma_j} R_j^s(\theta_1) + \sum_{j=1}^{3} h_j t_j R_j^c(\theta_1) \sum_{j=1}^{3} b_j s_j R_j^c(\theta_1)$$
$$- \sum_{j=1}^{3} \frac{n_j}{\gamma_j} s_j R_j^s(\theta_1) \sum_{j=1}^{3} \frac{b_j t_j}{\gamma_j} R_j^s(\theta_1) + \sum_{j=1}^{3} h_j s_j R_j^c(\theta_1) \sum_{j=1}^{3} b_j t_j R_j^c(\theta_1),$$

$$\beta_6 = \sum_{j=1}^{3} \frac{n_j}{\gamma_j} t_j R_j^s(\theta_1) \sum_{j=1}^{3} \frac{b_j t_j}{\gamma_j} R_j^s(\theta_1) - \sum_{j=1}^{3} h_j t_j R_j^c(\theta_1) \sum_{j=1}^{3} b_j t_j R_j^c(\theta_1).$$

References

1. Y. SHINDO, K. TANAKA, F. NARITA, *Singular stress and electric fields of a piezoelectric ceramic strip with a finite crack under longitudinal shear,* Acta Mech., **120**, 31–45, 1997.

2. Y. SHINDO, K. WATANABE, F. NARITA, *Electroelastic analysis of a piezoelectric ceramic strip with a central crack*, Int. J. Engng Sci. **38**, 1–19, 2000.

3. Y. E. PAK, *Crack extension force in a piezoelectric material*, ASME J. Appl. Mech., **57**, 647–653, 1990.

4. Y. SHINDO, E. OZAWA, J. P. NOWACKI, *Singular stress and electric fields of a cracked piezoelectric strip*, Int. J. Appl. Electromagnetics Mater., **1**, 77–87, 1990.

5. R.M. MCMEEKING, *Electrostrictive stresses near crack-like flaws*, J. Appl. Math. Phys., **40**, 615–627, 1989.

6. F. NARITA, Y. SHINDO, *Mode I crack growth rate for yield strip model of a narrow piezoelectric ceramic body*, Theoret. Appl. Fract. Mech., **36**, 73–85, 2001.

7. Y. SHINDO, H. MURAKAMI, K. HORIGUCHI, F. NARITA, *Evaluation of electric fracture properties of piezoelectric ceramics using the finite element and single-edge precracked-beam methods*, J. Am. Ceram. Soc., **85**, 1243–1248, 2002.

8. S. B. PARK, C. T. SUN, *Fracture criteria for piezoelectric ceramics*, J. Am. Ceram. Soc., **78**, 1475–1480, 1995.

9. Y. SHINDO, M. OKA, K. HORIGUCHI, *Analysis and testing of indentation fracture behavior of piezoelectric ceramics under an electric field*, ASME J. Eng. Mater. Tech., **123**, 293–300, 2001.

10. G. C. SIH, Mechanics of Fracture Initiation and Propagation, Kluwer Academic Publishers, The Netherlands 1991.

11. G. C. SIH, J. Z. ZUO, *Multiscale behavior of crack initiation and growth in piezoelectric ceramics*, Theoret. Appl. Fract. Mech., **34**, 123–141, 2000.

Received March 18, 2003.

Arch. Mech., **55**, 3, pp. 305–324, Warszawa 2003

Fluctuating flow of a third order fluid past an infinite plate with variable suction

T. HAYAT, S. NADEEM, S.P. PUDASAINI[(1)], S. ASGHAR

Department of Mathematics, Quaid-i-Azam University
Islamabad, Pakistan.
[(1)] *Department of Mechanics, Institute of Fluid Mechanics, AG-III,*
Darmstadt University of Technology,
Hochschulstr. 1, D-64289, Darmstadt, Germany.
e-mail: pudasain@mechanik.tu-darmstadt.de, t_pensy@hotmail.com

THE TWO-DIMENSIONAL flow problem of a third order incompressible fluid past an infinite porous plate is discussed when the suction velocity normal to the plate, as well as the the external flow velocity, varies periodically with time. The governing partial differential equation is of third order and nonlinear. Analytic solution is obtained using the series method. Expressions for the velocity and the skin friction have been obtained in a dimensionless form. The results of viscous and second order fluids can be recovered as special cases of this problem. Finally, several graphs are plotted and discussed.

1. Introduction

THE OSCILLATING flows play an important role in many engineering applications. The study of such flows was first initiated by LIGHTHILL [1] who studied the effects of free stream oscillations on the boundary layer flows of viscous, incompressible fluid past an infinite plate. Thereafter STUART [2] extended it to study a two-dimensional flow past an infinite, porous plate with constant suction when the free stream oscillates in time about a constant mean. After the appearance of LIGHTHILL'S [1] classic paper on the response of skin friction in laminar flow due to fluctuations in the free stream, considerable interest has been developed in the subject of boundary layers which have a regular fluctuating flow superimposed on the mean boundary flow. A large number of papers dealing with this subject have appeared, cf. for example WATSON [3], MESSIHA [4], KELLY [5] and LAL [6]. The idea has been also extended to magnetohydrodynamic flows, SURYAPRAKASARO [7], and the elastico-viscous flows, KALONI [8], SOUNDALGEKAR and PURI [9] and PURI [10]. The boundary layer suction is a very effective method for prevention of the separation. The effects of different arrangements and configurations of the suction holes and slits on the undesired phenomenon of separation have been studied extensively by various scholars, and

have been compiled by LACHMAN [11]. In technological fields, the boundary layer phenomenon in non-Newtonian fluids has recently become a fascinating problem, under a wide range of geometrical, dynamical and rheological conditions.

Some experiments by BARNES *et al.* [12] confirmed that an increase in the flow rate is possible and that the phenomenon appears to be governed by the shear-dependent viscosity. In fact, in [13] WALTERS and TOWNSEND show that the mean flow rate is unaffected by second-order viscoelasticity. Although the second-order model is able to predict the normal stress differences which are characteristic of non-Newtonian liquids, it is not shear thinning or thickening, the shear viscosity is constant. Third-order model exhibits shear-dependent viscosity, for a simple-shearing motion ($u' = (\gamma y', 0, 0)$), where γ is the rate of strain. The relation between the shearing stress and the rate of strain is given by $S_{xy} = \mu \left(1 \mp T_s^2 \gamma^2\right) \gamma$, where T_s is the shear relaxation time (its reciprocal is the characteristic rate of strain at which the apparent shear viscosity noticeably decreases or increases), and μ is the lower limiting viscosity. Experiments made by BRUCE [14] has shown that there are materials that exhibit: (1) strong normal stresses but are weakly shear thinning or thickening (class 1 a, b); (2) roughly equal normal and shear effects (class 2 a, b); (3) weak normal stresses, but they are strongly shear thinning or thickening (class 3 a, b).

Since many years there has been much interest in the effect of a variable suction velocity on the flow field. Regarding the elasto-viscous (Walters liquid B$'$) model, SOUNDALGEKAR and PURI [9] obtained the perturbation solution for the fluctuating flow of the elasto-viscous fluids past an infinite plate with variable suction.

As far as the authors are aware, no attempt has been made to examine the effect of the variable suction velocity on the flow fields of third-order fluids past an infinite plate. In the present work such an attempt has been considered. Literature survey revealed no previous attempts on studying this problem, even in the constant suction velocity case. The external flow velocity in the present paper is taken as $U_0' \left[1 + \in e^{iw't'}\right]$ and the suction velocity is assumed to be of the form $v_0' \left[1 + \in A e^{iw't'}\right]$, where v_0' is a non-zero constant mean suction velocity, $\in$ is small and A is a positive constant such that $\in A \leq 1$. By neglecting higher powers of $\in$, approximate solutions are obtained for the velocity field in the boundary layer.

2. The constitutive model

The incompressible, homogeneous fluid of third order is a simple fluid of the differential type whose Cauchy stress tensor has the representation [15]

$$\mathbf{T} = -p\mathbf{I} + \mu\mathbf{A}_1 + \alpha_1\mathbf{A}_2 + \alpha_2\mathbf{A}_1^2 + \beta_1\mathbf{A}_3 + \beta_2\left(\mathbf{A}_1\mathbf{A}_2 + \mathbf{A}_2\mathbf{A}_1\right) + \beta_3\left(\mathrm{tr}\mathbf{A}_1^2\right)\mathbf{A}_1, \tag{2.1}$$

where $-p\mathbf{I}$ is the indeterminate part of the stress due to the constraint of incompressibility, $\mu, \alpha_1, \alpha_2, \beta_1, \beta_2$ and β_3 are material constants, and the tensors A_n, $n = 1, 2, 3$ are defined through [16]

$$\begin{aligned} &\mathbf{A}_1 = (\mathrm{grad}\mathbf{V}) + (\mathrm{grad}\mathbf{V})^T, \\ &\mathbf{A}_n = \left(\frac{\partial}{\partial t'} + \mathbf{V}.\nabla\right)\mathbf{A}_{n-1} + \mathbf{A}_{n-1}(\mathrm{grad}\mathbf{V}) + (\mathrm{grad}\mathbf{V})^T\mathbf{A}_{n-1}, \quad n > 1, \end{aligned} \tag{2.2}$$

where $\mathbf{V}$ is the velocity and t' is the time.

JOSEPH [17] proved that the rest state of fluids of grade n, $n \neq 1$, any is unstable in the spectral sense of linearized theory when the ratio of the coefficients of $\mathbf{A}_n$ and $\mathbf{A}_{n-1}$ in the constitutive equation is negative. Hence, if $\alpha_1 < 0$ then the above model exhibits unacceptable stability characteristics. On the other hand, Eq. (2.1) must be consistent with thermodynamics principles. The thermodynamic of fluid model by Eq. (2.1) has been the object of a detailed study by FOSDICK and RAJAGOPAL [18]. They have shown that the Eq. (2.1) to be compatible with thermodynamics, and the free energy to be minimum when the fluid is at rest, the material constants should satisfy the relations

$$\begin{aligned} &\mu \geq 0, \qquad \alpha_1 \geq 0, \qquad \beta_1 = \beta_2 = 0, \\ &\beta_3 \geq 0, \qquad -\sqrt{24\mu\beta_3} \leq \alpha_1 + \alpha_2 \leq \sqrt{24\mu\beta_3}. \end{aligned} \tag{2.3}$$

It is easy to see that the ratio of the coefficients of A_2 and A_3 in the form of $\mathbf{T}$, i.e. the "ratio" $\frac{\alpha_1}{0}$, does not satisfy neither the hypothesis of JOSEPH [17] nor the hypothesis of RENARDY [19], who assumed the coefficients α_{n-1} ($n \geq 5$ and here 3) of $\mathbf{A}_n$ is non-zero for instability. We also point out that the retarded motion approximation does not lead the models. Thus subject was clearly explained by DUNN and RAJAGOPAL [20]. Therefore, the model of Eq. (2.1) reduces to:

$$\mathbf{T} = -p\mathbf{I} + \mu\mathbf{A}_1 + \alpha_1\mathbf{A}_2 + \alpha_2\mathbf{A}_1^2 + \beta_3\left(\mathrm{tr}\mathbf{A}_1^2\right)\mathbf{A}_1. \tag{2.4}$$

The equation of motion, in the absence of body forces, is

$$\rho'\frac{d\mathbf{V}}{dt'} = \mathrm{div}\mathbf{T}, \tag{2.5}$$

where ρ' is the density of the fluid in the dimensional form and $\frac{d}{dt'}$ is the material derivative. The fluid is incompressible, thus only isochoric (i.e. volume preserving) flows are possible, i.e. the flow satisfies the constraints

$$\mathrm{div}\mathbf{V} = 0. \tag{2.6}$$

We consider a two-dimensional incompressible fluid flow along an infinite plane porous wall. The flow is independent of the distance parallel to the wall and the suction velocity normal to the wall is directed towards it and varies periodically with time about a non-zero constant mean value v_0'. The x'-axis is taken along the wall, y'-axis normal to the wall. Dash denotes dimensional quantities. Thus for the problem under consideration, we seek a velocity field of the form

$$\mathbf{V} = \left[u'\left(y', t'\right), v', 0\right], \tag{2.7}$$

where $v' < 0$ is the suction velocity.

From Eqs. (2.6) and (2.7)

$$\frac{\partial v'}{\partial y'} = 0. \tag{2.8}$$

It is evident from Eq. (2.8) that v' is a function of time only. Hence we consider v' in the form [4]

$$v' = -v_0'(1 + \in Ae^{i\omega' t'}). \tag{2.9}$$

The negative sign in Eq. (2.9) indicates that the suction velocity normal to the wall is directed towards the wall. In view of Eqs. (2.4), (2.7) and (2.9), Eq. (2.5) takes the form

$$\frac{\partial u'}{\partial t'} - v_0'(1 + \in Ae^{i\omega' t'})\frac{\partial u'}{\partial y'} = -\frac{1}{\rho'}\frac{\partial P'}{\partial x'} + \nu\frac{\partial^2 u'}{\partial y'^2} + \frac{\alpha_1}{\rho'}\left[\frac{\partial^3 u'}{\partial y'^2 \partial t'} - v_0'\left(1 + \in Ae^{i\omega' t'}\right)\frac{\partial^3 u'}{\partial y'^3}\right] + \frac{6\beta_3}{\rho'}\left(\frac{\partial u'}{\partial y'}\right)^2\frac{\partial^2 u'}{\partial y'^2}, \tag{2.10}$$

$$\frac{\partial v'}{\partial t'} = -\frac{1}{\rho'}\frac{\partial P'}{\partial y'}, \tag{2.11}$$

where

$$\nu = \frac{\mu}{\rho'},$$

$$P' = p' - (2\alpha_1 + \alpha_2)\left(\frac{\partial u'}{\partial y'}\right)^2.$$

From Eqs. (2.9) and (2.11), it is clear that $\frac{\partial P'}{\partial y'}$ is small in the boundary layer and can be neglected [9]. Hence the pressure is taken to be constant along any normal and is given by its value outside the boundary layer. If $U'(t')$ is the stream velocity parallel to the wall just outside the boundary layer, then

$$-\frac{1}{\rho'}\frac{\partial P'}{\partial x'} = \frac{dU'}{dt'}$$

and the Eq. (2.10) takes the form

$$\frac{\partial u'}{\partial t'} - v_0'\left(1+\in Ae^{i\omega' t'}\right)\frac{\partial u'}{\partial y'} = \frac{dU'}{dt'} + \nu\frac{\partial^2 u'}{\partial y'^2} + \frac{\alpha_1}{\rho'}\left[\frac{\partial^3 u'}{\partial y'^2 \partial t'} - v_0'\left(1+\in Ae^{i\omega' t'}\right)\frac{\partial^3 u'}{\partial y'^3}\right] + \frac{6\beta_3}{\rho'}\left(\frac{\partial u'}{\partial y'}\right)^2\frac{\partial^2 u'}{\partial y'^2}. \tag{2.12}$$

The boundary conditions are

$$u' = 0 \quad \text{at} \quad y' = 0 \quad \text{and} \quad u' = U'(t') \quad \text{as} \quad y' \longrightarrow \infty. \tag{2.13}$$

We introduce dimensionless quantities defined by

$$y = \frac{y' v_0'}{\nu}, \quad t = \frac{v_0'^2 t'}{4\nu}, \quad \omega = \frac{4\nu\omega'}{v_0'^2},$$
$$\alpha = \frac{\alpha_1 v_0'^2}{\rho\nu^2}, \quad u = \frac{u'}{U_0'}, \quad U = \frac{U'}{U_0'}, \quad \in_1 = \frac{6\beta_3}{\rho'\nu^3}U_0'^2 v_0'^2, \tag{2.14}$$

where U_0' is the reference velocity and ω' is the frequency. Equation (2.12) takes the dimensionless form

$$\frac{1}{4}\frac{\partial u}{\partial t} - (1+\in Ae^{i\omega t})\frac{\partial u}{\partial y} = \frac{1}{4}\frac{dU}{dt} + \frac{\partial^2 u}{\partial y^2} + \alpha\left[\frac{1}{4}\frac{\partial^3 u}{\partial y^2 \partial t} - \left(1+\in Ae^{i\omega t}\right)\frac{\partial^3 u}{\partial y^3}\right] + \in_1\left(\frac{\partial u}{\partial y}\right)^2\frac{\partial^2 u}{\partial y^2}, \tag{2.15}$$

subject to the conditions

$$u = 0 \quad \text{at} \quad y = 0 \quad \text{and} \quad u \longrightarrow U \quad \text{as} \quad y \longrightarrow \infty, \tag{2.16}$$

where

$$U = 1+\in e^{i\omega t}. \tag{2.17}$$

3. Perturbation solution

We note that the resulting equation of motion (2.15) is of the third order. Moreover, this equation is nonlinear as compared to the cases of the second order, elastic-viscous [9] and Newtonian flow [4] equations. As a result, it seems to be impossible to obtain the general solution in a closed form for arbitrary values of all parameters appearing in the nonlinear equation. Even in the case of constant suction and elastic-viscous fluid [8], all analytic solutions obtained so far are based on the assumptions that one or more of the parameters are zero or small. Therefore, we seek the solution of the problem as a power series expansion in the small parameters $\in_1$. Accordingly, we assumed that the velocity component u can be expanded in powers of $\in_1$ as follows:

$$u(y, \in_1) = u_0(y) + \in_1 u_1(y) + \ldots \tag{3.1}$$

Substituting Eq. (3.1) into Eq. (2.15) and the boundary conditions (2.16), and then collecting terms of the same powers of $\in_1$, one obtains the following systems of partial differential equations along with appropriate boundary conditions.

System of order zero

$$\frac{1}{4}\frac{\partial u_0}{\partial t} - (1 + \in Ae^{i\omega t})\frac{\partial u_0}{\partial y} = \frac{i\omega}{4} \in e^{i\omega t} + \frac{\partial^2 u_0}{\partial y^2} + \alpha\left[\frac{1}{4}\frac{\partial^3 u_0}{\partial y^2 \partial t} - (1 + \in Ae^{i\omega t})\frac{\partial^3 u_0}{\partial y^3}\right], \tag{3.2}$$

$$u_0 = 0 \quad \text{at} \quad y = 0 \quad \text{and} \quad u_0 \longrightarrow 1 + \in e^{i\omega t} \quad \text{as} \quad y \longrightarrow \infty. \tag{3.3}$$

System of order one

$$\frac{1}{4}\frac{\partial u_1}{\partial t} - (1 + \in Ae^{i\omega t})\frac{\partial u_1}{\partial y} = \frac{\partial^2 u_1}{\partial y^2} + \alpha\left[\frac{1}{4}\frac{\partial^3 u_1}{\partial y^2 \partial t} - (1 + \in Ae^{i\omega t})\frac{\partial^3 u_1}{\partial y^3}\right] + \left(\frac{\partial u_0}{\partial y}\right)^2 \frac{\partial^2 u_0}{\partial y^2}, \tag{3.4}$$

$$u_1 = 0 \quad \text{at} \quad y = 0 \quad \text{and} \quad u_1 \longrightarrow 0 \quad \text{as} \quad y \longrightarrow \infty. \tag{3.5}$$

Zeroth-order solution

We note that the zeroth order mathematical problem is same as that of SOUNDALGEKAR and PURI [9] except that $(-k)$ is replaced by α in Eq. (3.2). Thus, in order to avoid repetition, the details of calculations are omitted and the solution is directly given by

$$u_0(y,t) = 1 - e^{-y} - \alpha y e^{-y} + \in e^{i\omega t} \begin{bmatrix} 1 - Se^{-hy} - (1-S)e^{-y} + Lye^{-hy} \\ -\alpha \begin{pmatrix} (1-S)\, e^{-hy} \\ -(1-y)\, e^{-y} \end{pmatrix} \end{bmatrix}, \tag{3.6}$$

where

$$h = \left[\frac{\sqrt{1+i\omega}+1}{2}\right], \tag{3.7}$$

$$L = \frac{h^2\left(h + \frac{i\omega}{4}\right)\left(1 - \frac{4iA}{\omega}\right)}{\sqrt{1+i\omega}}, \tag{3.8}$$

$$S = 1 - \frac{4iA}{\omega}. \tag{3.9}$$

First-order solution

Now, let

$$u_1(y,t) = f_1(y) + \in e^{i\omega t} f_2(y). \tag{3.10}$$

Substituting Eqs. (3.6) and (3.10) in Eq. (3.4) and boundary conditions (3.5), comparing nonharmonic and harmonic terms and neglecting coefficients of $\in^2$, we get

$$\alpha \frac{d^3 f_1}{dy^3} - \frac{d^2 f_1}{dy^2} - \frac{df_1}{dy} = e^{-3y}(1 + \alpha y), \tag{3.11}$$

$$\alpha \frac{d^3 f_2}{dy^3} - \left(1 + \frac{i\omega\alpha}{4}\right)\frac{d^2 f_2}{dy^2} - \frac{df_2}{dy} + \frac{i\omega}{4} f_2 = A\frac{df_1}{dy} + B_1 - \alpha\left[A\frac{d^3 f_1}{dy^3} + B_2\right], \tag{3.12}$$

(3.13) $$\text{at} \quad y = 0 \quad \text{and} \quad y \longrightarrow \infty : f_1 = f_2 = 0,$$

where

(3.14) $$B_1 = e^{-3y}\left[\frac{A}{2} - 3(1-S)\right] + \frac{A}{6}e^{-y} + (h^2 S - 2hS)e^{-(h+2)y},$$

(3.15) $$B_2 = e^{-y}\left[\frac{A}{12}(9+2y) + 2 - \frac{A}{6}\right] - e^{-3y}\left[\frac{A}{4}(9+y^2-2y) - \frac{A}{6}(y-1) - \frac{9A}{2} - 1 + 3y + S - 2Sy\right] - e^{-(h+2)y}\left[2h(1-S) + 4hL - 2L - h^2 - h^2 Ly\right].$$

There have been several investigations devoted to study the existence and uniqueness of the solutions to the equations governing the flows of fluids of differential type [21–23]. These equations are usually higher order partial differential equations than the Navier–Stokes equations. Hence the issue of whether the "no-slip" boundary condition is sufficient to have a well-posed problem is very important. This question can not be answered by any generality for fluids of differential type of complexity n, for arbitrary n. However, if attention is confined to fluids of grade 2 or grade 3, one can provide some definite answers, while some partial answers are also possible for fluids of grade n [24].

Before proceeding with the solution of Eqs. (3.11) and (3.12), it would be interesting to remark here that although in the classical viscous case ($\alpha = 0$) we encounter differential equations of order two [2, 4], the presence of the material parameter of the second order fluid increases the order to three. It would therefore seem that the additional boundary condition must be imposed in order to get a unique solution. In order to overcome such a difficulty, several authors have studied an acceptable additional condition. FOSDICK and BERSTEIN [25] have studied the flow in the annular region between two porous rotating cylinders. They assumed one of the constants in the solutions to be zero. However, there is no apparent reason for such a choice. FRATER [26] has studied the asymptotic suction flow. Since only two of the coefficients in the solution can be found by the no-slip condition, he imposes an extra condition that the solution tends to the Newtonian value as the coefficient of the higher derivative in the equation approaches zero. However, the perturbation expansion may give correct results under certain conditions [27]. Thus following [8, 28], we overcome the difficulty in the present study using perturbation expansion for small material parameter α and assume the solution in the form as follows [28]:

(3.16) $$f_1 = f_{01} + \alpha f_{11} + O(\alpha^2),$$
$$f_2 = f_{02} + \alpha f_{12} + O(\alpha^2),$$

which is valid for small values of α only. Putting Eq. (3.16) in Eqs. (3.11) and (3.12) and equating the coefficient of α we obtain

$$\frac{d^2 f_{01}}{dy^2} + \frac{df_{01}}{dy} = -e^{-3y}, \tag{3.17}$$

$$\frac{d^2 f_{11}}{dy^2} + \frac{df_{11}}{dy} = -\frac{df_{01}^3}{dy^3} + ye^{-3y}, \tag{3.18}$$

$$\frac{d^2 f_{02}}{dy^2} + \frac{df_{02}}{dy} - \frac{i\omega}{4} f_{02} = B_1, \tag{3.19}$$

$$\frac{d^2 f_{12}}{dy^2} + \frac{df_{12}}{dy} - \frac{i\omega}{4} f_{12} = -\frac{d^3 f_{02}}{dy^3} - \frac{i\omega}{4}\frac{df_{02}}{dy} - B_2, \tag{3.20}$$

$$\begin{aligned} &f_{01} = f_{11} = f_{02} = f_{12} = 0 \text{ at } y = 0, \\ &f_{01} = f_{11} = f_{02} = f_{12} = 0 \text{ as } y \longrightarrow \infty. \end{aligned} \tag{3.21}$$

Solving Eqs. (3.17) to (3.20) under the boundary conditions (3.21), we have, in view of Eq. (3.16),

$$f_1 = \frac{1}{12}\left[e^{-y}\left\{2 + \alpha(9 + 2y)\right\} - e^{-3y}\left\{\alpha\left(9 + y^2 - 2y\right) + 2\right\}\right], \tag{3.22}$$

$$\begin{aligned} f_2 = {} & M_1\left(e^{-3y} - e^{-hy}\right) + N_1\left(e^{-y} - e^{-hy}\right) + P_1\left(e^{-(h+2)y} - e^{-hy}\right) \\ & - \alpha\begin{pmatrix} M_2\left(e^{-3y} - e^{-hy}\right) + N_2\left(e^{-y} - e^{-hy}\right) + P_2\left(e^{-(h+2)y} - e^{-hy}\right) \\ + \dfrac{i}{3\omega} e^{-3y}\left(36y - 24Sy + 3Ay^2 - 2Ay\right) \end{pmatrix}, \end{aligned} \tag{3.23}$$

where

$$M_1 = \frac{2\left[A - 6(1 - S)\right]}{24 - i\omega}, \quad N_1 = \frac{2iA}{3\omega}, \quad P_1 = \frac{\left(h^2 - 2h\right)S}{h^2 + 3h + 2 - \dfrac{i\omega}{4}}, \tag{3.24}$$

$$M_2 = \frac{i}{\omega}\left(36M_1 + 9A + 8 - 8S\right), \quad N_2 = \frac{-4}{3\omega^2}\left(12N_1 - 13A - 24\right), \tag{3.25}$$

$$P_2 = \frac{2h(1 - S) + 4hL - 2L - h^2 - h^2 L}{h^2 + 3h - 2 - \dfrac{i\omega}{4}}. \tag{3.26}$$

In view of Eqs. (3.10), (3.22) and (3.23), we have

$$u_1 = \frac{1}{12}\left[e^{-y}\{2+\alpha(9+2y)\} - e^{-3y}\{\alpha(9+y^2-2y)+2\}\right] + \epsilon e^{i\omega t}\begin{pmatrix} M_1\left(e^{-3y}-e^{-hy}\right)+N_1\left(e^{-y}-e^{-hy}\right) \\ +P_1\left(e^{-(h+2)y}-e^{-hy}\right) \\ -\alpha\begin{pmatrix} M_2\left(e^{-3y}-e^{-hy}\right)+N_2\left(e^{-y}-e^{-hy}\right) \\ +P_2\left(e^{-(h+2)y}-e^{-hy}\right) \\ +\frac{i}{3\omega}e^{-3y}\left(36y-24Sy+3Ay^2-2Ay\right) \end{pmatrix} \end{pmatrix}. \tag{3.27}$$

Now from Eqs. (3.6) and (3.27), the velocity field in the boundary layer is given by

$$u = 1-e^{-y}-\alpha y e^{-y} + \epsilon e^{i\omega t}\begin{pmatrix} 1-Se^{-hy}-(1-S)e^{-y}- \\ \alpha\left\{(1-S)e^{-hy}-(1-y)e^{-y}\right\} \\ +Lye^{-hy} \end{pmatrix} + \epsilon_1\frac{1}{12}\left[e^{-y}\{2+\alpha(9+2y)\} - e^{-3y}\{\alpha(9+y^2-2y)+2\}\right] + \epsilon_1\epsilon e^{i\omega t}\begin{pmatrix} M_1\left(e^{-3y}-e^{-hy}\right)+N_1\left(e^{-y}-e^{-hy}\right) \\ +P_1\left(e^{-(h+2)y}-e^{-hy}\right) \\ -\alpha\begin{pmatrix} M_2\left(e^{-3y}-e^{-hy}\right)+N_2\left(e^{-y}-e^{-hy}\right) \\ +P_2\left(e^{-(h+2)y}-e^{-hy}\right) \\ +\frac{i}{3\omega}e^{-3y}\left(36y-24Sy+3Ay^2-2Ay\right) \end{pmatrix} \end{pmatrix}. \tag{3.28}$$

The real, u_r, and the imaginary, u_i, parts of this expression, respectively, yield

$$u_r = 1-e^{-y}(1+\alpha y) + \frac{\epsilon_1}{12}\left[e^{-y}\{2+\alpha(2y+9)\} - e^{-3y}\{\alpha(y^2-2y+9)+2\}\right] + \epsilon\{M_r\cos(\omega t) - M_i\sin(\omega t)\}, \tag{3.29}$$

$$u_i = \epsilon\left(M_r\sin(\omega t) + M_i\cos(\omega t)\right), \tag{3.30}$$

where

$$M_r = m_{r_{10}} + \epsilon_1 m_{r_{11}}, \tag{3.31}$$

$$M_i = m_{i_{10}} + \epsilon_1 m_{i_{11}}. \tag{3.32}$$

The parameter functions $m_{r_{10}}, m_{i_{10}}, m_{r_{11}}$ and $m_{i_{11}}$ involved in u_r, u_i and M_r, M_i are explicitly computed, and are listed in the Appendix.

The other interesting aspect of the solution (3.28) is, however, the prediction of the shear stress near the wall. From Eq. (4) the expression for the shear stress is given by

$$(3.33) \qquad P'_{x'y'} = \mu \frac{\partial u'}{\partial y'} + \frac{\alpha_1}{\rho'}\left[\frac{\partial^2 u'}{\partial y' \partial t'} - v'_0\left(1+ \in Ae^{i\omega' t'}\right)\frac{\partial^2 u'}{\partial y'^2}\right] + 2\beta_3\left(\frac{\partial u'}{\partial y'}\right)^3,$$

which in virtue of Eq. (2.14) reduces to

$$(3.34) \qquad P_{xy} = \frac{P'_{x'y'}}{U'_0 v'_0 \rho'} = \frac{\partial u}{\partial y} + \frac{\alpha}{4}\left[\frac{\partial^2 u}{\partial y \partial t} - 4\left(1+ \in Ae^{i\omega t}\right)\frac{\partial^2 u}{\partial y^2}\right] + \frac{\in_1}{3}\left(\frac{\partial u}{\partial y}\right)^3.$$

where u is given by Eq. (3.28).

4. Discussions

In order to investigate the effects of the third order fluid on the velocity profile near the plate (both in case of constant and variable suction), we have plotted u_r against y in Figs. 1 to 4 for the different values of ϵ, ϵ_1, A, ω, α and $\omega t = \pi/2$. From Figs. 1 and 2 we observe that the velocity profile increases with fixed ω and large values of ϵ_1. Figure 3 is prepared to bring out the effects of the variable suction velocity on the separation of the fluid at the plate for large frequency. It is evident from this figure that velocity increases with an increase in ω, in A and ϵ_1, the third order fluid parameter. Further, for fixed ϵ_1, increase in ϵ, A and ω increases the velocity and then the two velocities coincide (see Fig. 4).

In Figs. 5 to 9 the fluctuating parts are plotted for different values of ϵ, ϵ_1, ω, α, A and for $\omega t = \pi/2$. For $A = 0$, it is noted that an increase in ϵ_1 with fixed ϵ and ω (Fig. 5) leads to a decrease in M_r, but with increase in ϵ_1 and for $\epsilon = 0.2$ and $\omega = 10$, M_r is almost the same. Figure 6 shows the effect of ϵ_1 in case of variable suction. In this case, it is noted that increase in ϵ_1 leads to a decrease in M_r first then the curves tend to coincide. Further, it is clear from Fig. 7 that for $\epsilon_1 = 0.7$ and increase in A and ω, results in a decrease in M_r, and ultimately the curves are almost the same. In case of non-Newtonian fluids at large ω and increase in ϵ_1 there is a fall of M_i (Fig. 8), which is not observed in Newtonian fluids. From Fig. 9, one can conclude that an increase in A and ω leads to an increase in M_i first; then there arises a decrease, then increase and finally it reaches zero level.

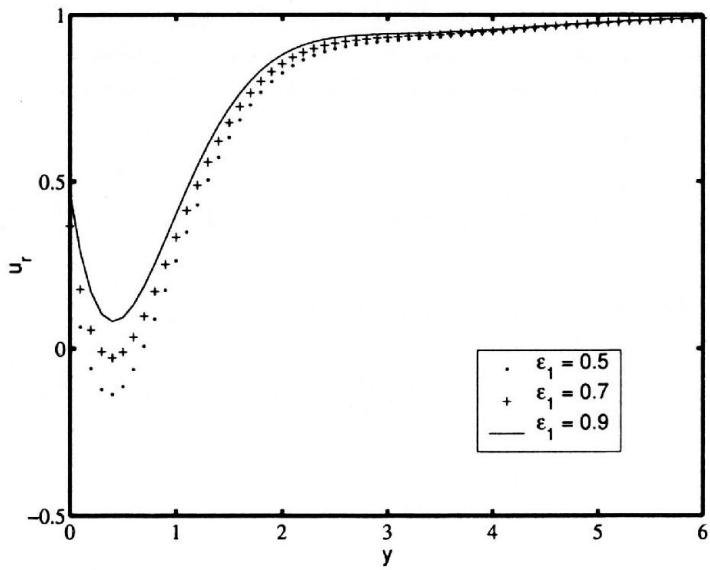

FIG. 1. Graphs for the parameter values $\alpha = 0.7, \epsilon = 0.5, \omega t = \pi/2, A = 0, \omega = 10$.

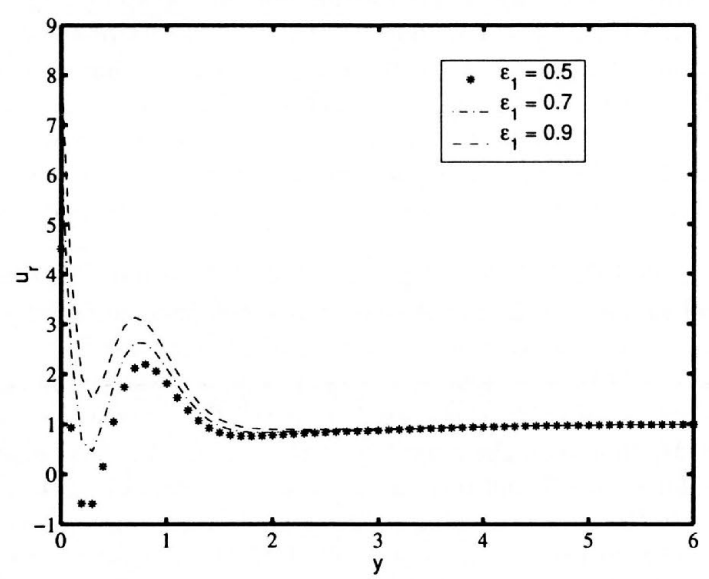

FIG. 2. Graphs for the parameter values $\alpha = 0.8, \epsilon = 0.5, \omega t = \pi/2, A = 0, \omega = 100$.

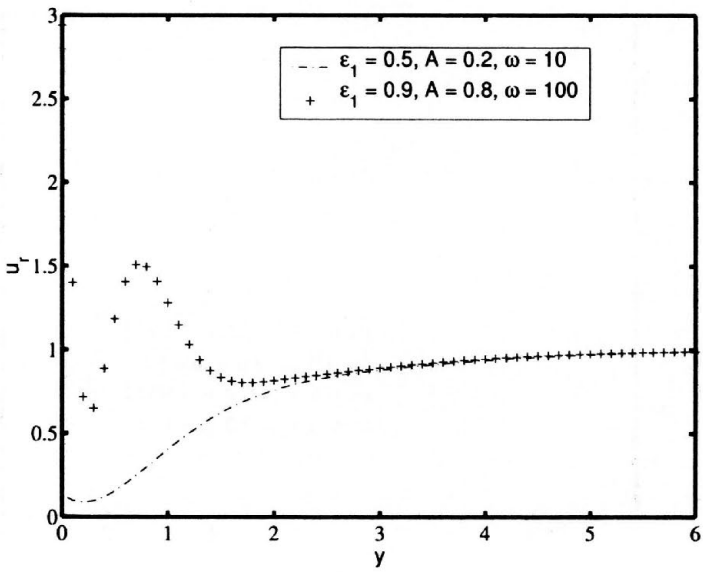

FIG. 3. Graphs for the parameter values $\epsilon = 0.2, \alpha = 0.8, \omega t = \pi/2$.

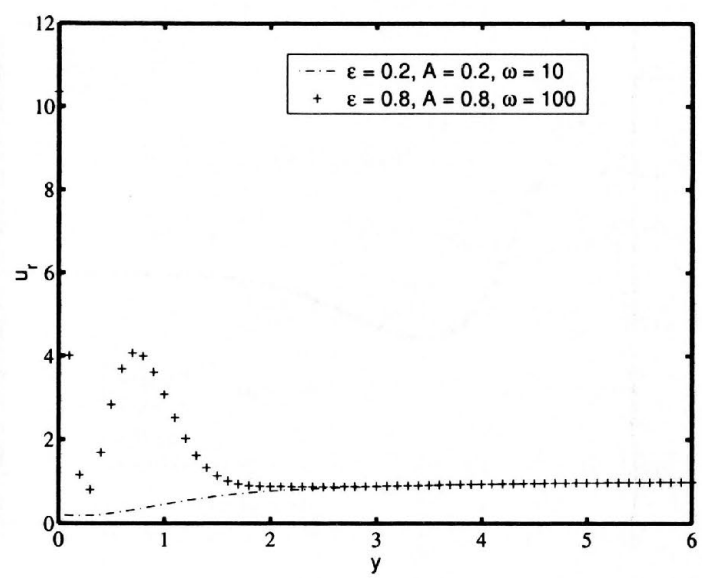

FIG. 4. Graphs for the parameter values $\epsilon_1 = 0.7, \alpha = 0.9, \omega t = \pi/2$.

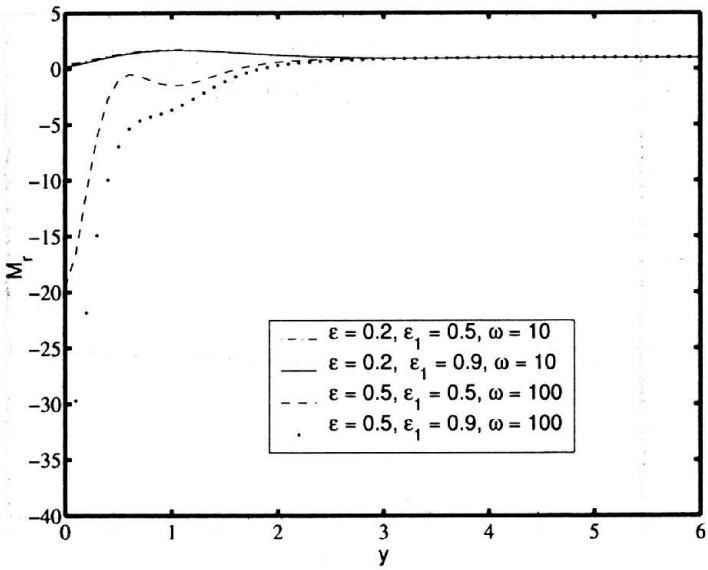

FIG. 5. Graphs for the parameter values $\alpha = 0.6, A = 0, \omega t = \pi/2$.

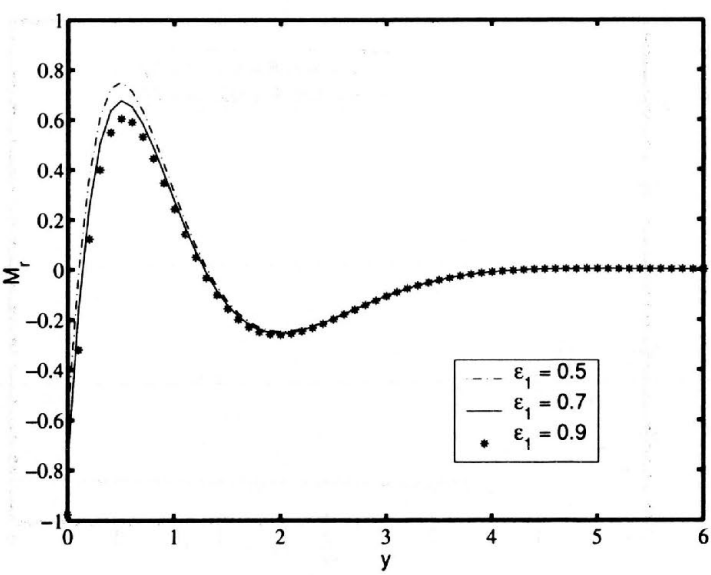

FIG. 6. Graphs for the parameter values $\alpha = 0.7, \omega t = \pi/2, \epsilon = 0.2, A = 0.4, \omega = 10$.

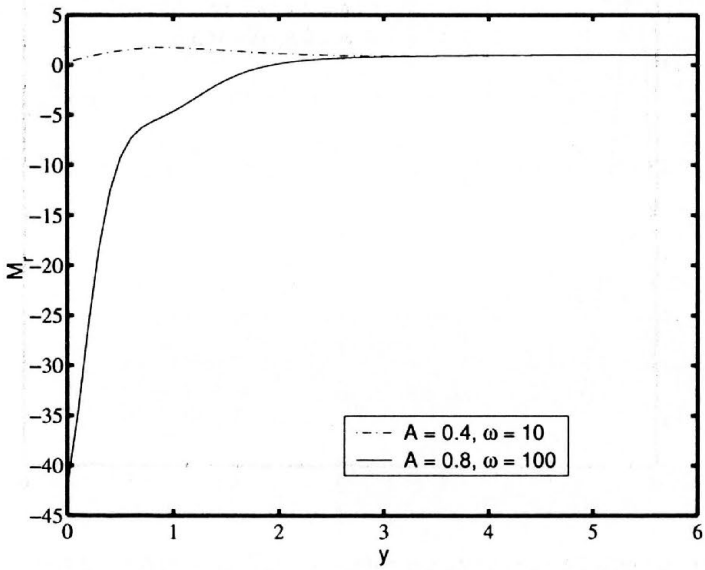

FIG. 7. Graphs for the parameter values $\alpha = 0.9, \omega t = \pi/2, \epsilon = 0.2, \epsilon_1 = 0.7$.

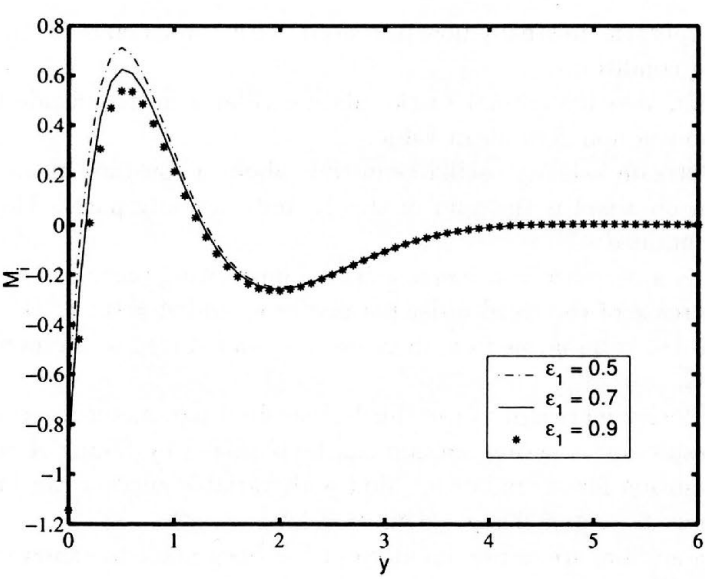

FIG. 8. Graphs for the parameter values $\alpha = 0.8, \omega t = \pi/2, \epsilon = 0.2, A = 0.4, \omega = 10$.

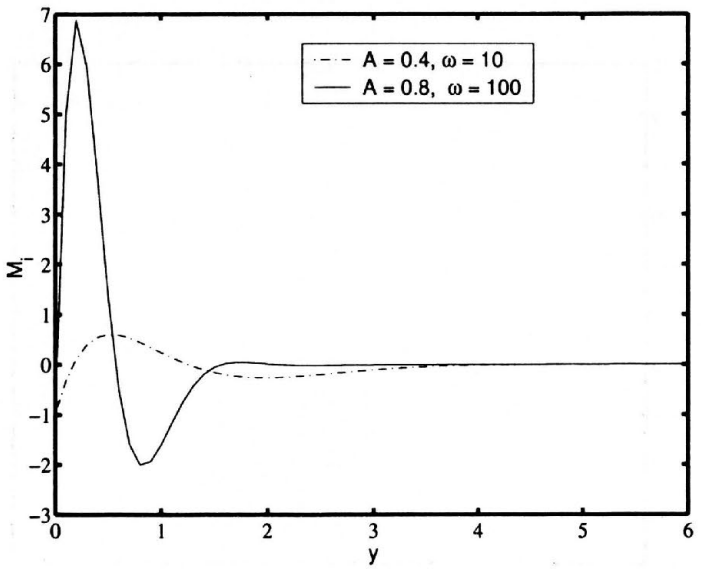

FIG. 9. Graphs for the parameter values $\alpha = 0.7, \omega t = \pi/2, \epsilon = 0.2, \epsilon_1 = 0.9$.

5. Conclusions

In this paper, the unsteady flow past an infinite porous plate is studied under the following conditions:
(i) the suction velocity normal to the plate oscillates in magnitude but not in direction about a non-zero mean value,
(ii) the free stream velocity oscillates in time about a constant mean value.
The solution obtained is the sum of steady and unsteady parts. The following results are obtained:

1. There is a decrease and increase in the fluctuating parts M_r and M_i with the increase of the third order parameter ϵ_1 and $A \neq 0$.
2. Increase of variable suction, increase in ϵ_1 and A lead to an increase in the velocity.
3. The velocity increases as the third order fluid parameter increases.
4. The results for constant suction can be obtained by taking $A = 0$.
5. The solution for second-order fluid with variable suction can be obtained as a special case of this problem by taking $\epsilon_1 = 0$.

As far as the authors are aware, no attempt has been made to examine the effect of variable suction velocity for second order fluids. However, a second order fluid exhibits normal stresses but is not shear thinning; the shear viscosity is constant. The third order approximation of a simple fluid exhibits shear-dependent

viscosity. Keeping this fact in view, the problem considered for the third order fluid in this paper is more general.

Appendix

Equation (3.28) is a very complex algebraic equation. In order to split it into real and imaginary parts, for brevity, we define the following list of parameters:

$$m_{r_1} := \sqrt{\frac{1+\sqrt{1+\omega^2}}{2}}, \qquad m_{i_1} := \sqrt{\frac{-1+\sqrt{1+\omega^2}}{2}},$$

$$m_{r_2} := \frac{1}{2} + \frac{1}{2} m_{r_1}, \qquad m_{i_2} := \frac{1}{2} m_{i_1},$$

$$m_{r_3} := \frac{m_{r_1}}{m_{r_1}^2 + m_{i_1}^2}, \qquad m_{i_3} := -\frac{m_{i_1}}{m_{r_1}^2 + m_{i_1}^2},$$

$$m_{r_4} := m_{r_3}(R_4 + 4BR_3) - m_{i_3}(R_3 - 4BR_4),$$

$$m_{i_4} := m_{r_3}(R_3 - 4BR_4) + m_{i_3}(R_4 + 4BR_3),$$

$$m_{r_5} := 96A/R_5, \qquad m_{i_5} := 2A(\omega - (24)^2/\omega)/R_5,$$

$$m_{r_6} := \{R_6(R_7 + 4BR_8) + R_9(R_8 - 4BR_7)\} / (R_6^2 + R_9^2),$$

$$m_{i_6} := \{R_6(R_8 - 4BR_7) - R_9(R_7 + 4BR_8)\} / (R_6^2 + R_9^2),$$

$$m_{r_7} := -\frac{1}{\omega}(36m_{i_5} + 32B), \quad m_{i_7} := \frac{1}{\omega}(36m_{r_5} + 9A),$$

$$m_{r_8} := \frac{4}{3\omega^2}(13A + 24), \qquad m_{i_8} := -\frac{32A}{3\omega^3},$$

$$m_{r_9} := \{(-8Bm_{i_2} + 4R_{10} - R_{11} - R_{12})R_{16} + (8Bm_{r_2} + 4R_{13} - 2R_{14} - R_{15})R_9\} \div (R_{16}^2 + R_9^2),$$

$$m_{i_9} := \{(8Bm_{r_2} + 4R_{13} - 2R_{14} - R_{15})R_{16} - (-8Bm_{i_2} + 4R_{10} - R_{11} - R_{12})R_9\} \div (R_{16}^2 + R_9^2),$$

$$m_{r_{10}} := 1-e^{-m_{r_2}y}(\cos(m_{i_2}y)-4B\sin(m_{i_2}y))-\alpha\big(4Be^{-m_{r_2}y}\sin(m_{i_2}y)-(1-y)e^{-y}\big) + ye^{-m_{r_2}y}(m_{r_4}\cos(m_{i_2}y)+m_{i_4}\sin(m_{i_2}y)),$$

$$m_{i_{10}} := e^{-m_{r_2}y}(4B\cos(m_{i_2}y)+\sin(m_{i_2}y))-4Be^{-y}-4B\alpha e^{-m_{r_2}y}\cos(m_{i_2}y) + ye^{-m_{r_2}y}(m_{i_4}\cos(m_{i_2}y)-m_{r_4}\sin(m_{i_2}y)),$$

$$m_{r_{11}} := (m_{r_5}-\alpha m_{r_7})\big(e^{-3y}-e^{-m_{r_2}y}\cos(m_{i_2}y)\big)-(m_{i_5}-\alpha m_{i_7})e^{-m_{r_2}y}\sin(m_{i_2}y) - \alpha m_{r_8}\big(e^{-y}-e^{-m_{r_2}y}\cos(m_{i_2}y)\big)-(2B/3+m_{i_8})e^{-m_{r_2}y}\sin(m_{i_2}y) + 32\alpha Ae^{-3y}/\omega^2+(m_{r_6}-\alpha m_{r_9})e^{-2y},$$

$$m_{i_{11}} := (m_{r_5}-\alpha m_{r_7})e^{-m_{r_2}y}\sin(m_{i_2}y)+(m_{i_5}-\alpha m_{i_7})\big(e^{-3y}-e^{-m_{r_2}y}\cos(m_{i_2}y)\big) - \alpha m_{r_8}e^{-m_{r_2}y}\sin(m_{i_2}y)+(2B/3-\alpha m_{i_8})\big(e^{-y}-e^{-m_{r_2}y}\cos(m_{i_2}y)\big) - \big(12y+3Ay^2-2Ay\big)\alpha e^{-3y}/(3\omega)+(m_{i_6}-\alpha m_{i_9})e^{-2y},$$

where

$$\begin{aligned}
R_1 &:= m_{r_2}^2-m_{i_2}^2, \quad R_2 := m_{i_2}+\omega/4, \quad R_3 := 2m_{r_2}^2m_{i_2}+R_1R_2,\\
R_4 &:= m_{r_2}R_1-2m_{r_2}m_{i_2}R_2, \quad R_5 := (24)^2+\omega^2, \quad R_6 := R_1+3m_{r_2}+2,\\
R_7 &:= R_1-2m_{r_2}, \quad R_8 := 2m_{r_2}m_{i_2}-2m_{i_2}, \quad R_9 := 2m_{r_2}m_{i_2}+3m_{i_2}-\omega/4,\\
R_{10} &:= m_{r_2}m_{r_4}-m_{i_2}m_{i_4}, \quad R_{11} := 2m_{r_4}+R_1,\\
R_{12} &:= m_{r_4}R_1-2m_{r_2}m_{i_2}m_{i_4}, \quad R_{13} := m_{i_2}m_{r_4}+m_{r_2}m_{i_4},\\
R_{14} &:= m_{i_4}+m_{r_2}m_{i_2}, \quad R_{15} := m_{i_4}R_1+2m_{r_2}m_{i_2}m_{i_4}, \quad R_{16} := R_1+3m_{r_2}-2,\\
B &:= A/\omega.
\end{aligned}$$

The parameter functions $h, L, S, M_1, M_2, N_1, N_2, P_1$ and P_2 of Eqs. (3.7)–(3.9) and (3.24)–(3.26) can now be expressed in terms of these m_rs and m_is as follows:

$$h=\frac{1}{2}+\frac{1}{2}m_{r_1}+i\frac{1}{2}m_{i_1}=m_{r_2}+im_{i_2}, \qquad L=m_{r_4}+im_{i_4}, \qquad S=1-i4B,$$

$$M_1=m_{r_5}+im_{i_5}, \qquad M_2=m_{r_7}+im_{i_7}, \qquad N_1=i2B/3,$$

$$N_2=m_{r_8}+im_{i_8}, \qquad P_1=m_{r_6}+im_{i_6}, \qquad P_2=m_{r_9}+im_{i_9}.$$

Substituting the values of these parameters, Eq. (3.28) can be split into real and imaginary parts (the calculation is very lengthy and tedious but straightforward), u_r and u_i, as given in Eqs. (3.29) and (3.30), with

$$M_r=m_{r_{10}}+\epsilon_1 m_{r_{11}}, \qquad M_i=m_{i_{10}}+\epsilon_1 m_{i_{11}}.$$

References

1. M. J. LIGHTHILL, *The response of laminar skin friction and heat transfer to fluctuations in the stream velocity*, Proc. R. Soc. Lond. A, 224, 1, 1954.
2. J. T. STUART, *A solution of the Navier-Stokes and energy equations illustrating the response of skin friction and temperature of an infinite plate thermometer fluctuations in the stream velocity*. Proc. Roy. Soc. Ser. A, 231, 116, 1955.
3. J. WATSON, *A solution of the Navier Stokes equation*, Quart. J. Mech. Appl. Math. **11**, 302, 1958.
4. S. A. S. MESSIHA, *Laminar boundary layers in oscillatory flow along an infinite plate with variable suction*, Proc. Camb. Phil. Soc. **62**, 329, 1966.
5. R. E. KELLY, *The flow of viscous fluid past a wall of infinite extent with time dependent suction*, Quart. J. Mech. Appl. Math., **18**, 287, 1965.
6. K. LAL, *A note on the unsteady flow along infinite flat plate with time dependent suction*, Indian J. Maths., **11**, 2, p. 51, 1969.
7. U. SURYAPRAKASARAO, *The response of laminar skin friction and heat transfer to fluctuations in the stream velocity in the presence of a transverse magnetic field*, ZAMM, **43**, 127, 1963.
8. P. N. KALONI, *Fluctuating flow of an elastico-viscous fluid past a porous flat plate*, Phys. Fluids, **10**, 1344, 1967.
9. V. M. SOUNDALGEKAR and P. PURI, *On fluctuating flow of an elastico viscous fluid past an infinite plate with variable suction*, J. Fluid Mech., **35**, 3, p. 561, 1969.
10. P. PURI, *Fluctuating flow of a viscous fluid on a porous plate in a rotating medium*, Acta Mech., **21**, 153, 1975.
11. G. V. LACHMAN, *Boundary layer and flow control*, Its principles and application, Vols. I and II Pergamon Press, Oxford 1961.
12. H. A. BARNESS, P. TOWNSEND and K. WALTERS, *Flow of a non-Newtonian liquids under varying pressure gradient*, Nature, 224, 585, 1969.
13. K. WALTERS and P. TOWNSEND, Proc. 4th Int. Congress on Rheology, S. ONOGI [Ed.], **4**, p. 471, Tokyo 1970.
14. C. BRUCE, Ph. D. Dissertation, Stanford 1969.
15. M. E. ERDOGAN, *Unsteady viscous flow between eccentric rotating disks*, Acta Mech., **108**, 179, 1995.
16. C. TRUESDELL and W. NOLL, *The nonlinear field theories of mechanics*, Handbuchder Physic, Vol. III/3, Springer, Berlin 1965.
17. D. D. JOSEPH, Arch. Rat. Mech. Anal., **75**, 251, 1981.
18. R. L. FOSDICK and K. R. RAJAGOPAL, *Thermodynamics and stability of fluids of third grade*, Proc. R. Soc. Lond., A 339, 377, 1980.
19. M. RENARDY, Arch. Rat. Mech. Anal., **79**, 21, 1983.
20. J. E. DUNN and K. R. RAJAGOPAL, *Fluids of differential type: critical review and thermodynamic analysis*, Int. J. Engng. Sci., **33**, 689, 1995.

21. K.R. RAJAGOPAL, *On creeping flow of a second order fluid*, J. Non-Newtonian Fluid Mech., **15**, 239, 1984.

22. K.R. RAJAGOPAL and P.N. KALONI, *Some remarks on boundary conditions for flow of fluids of differential type*, [in:] B.C. BUNABY [Ed.], *Continuum Mech. and its applications, hemisphere*, New York, 1989.

23. K.R. RAJAGOPAL and A.S. GUPTA, *An exact solution for the flow of a non-Newtonian fluid past a porous plate*, **19**, 158, 1984.

24. K.R. RAJAGOPAL, *On boundary conditions for the fluids of differential type*, [in:] A. SEQUEIRA [Ed.], *Navier-Stokes Equations and Related Nonlinear Problems*, Plenum Press, New York 1995.

25. R.L. FOSDICK and B. BERSTEIN, *Non-uniqueness of second order fluid under steady radial flow in annuli*, **7**, 555–569, 1969.

26. K.R. FRATER, *On solutions of some boundary value problems arising in elastico-viscous fluid mechanics*, ZAMP, **21**, 134, 1970.

27. M.E. ERDOGAN, *On the flow of a non-Newtonian fluid past a porous flat plate*, ZAMM, **55**, 99, 1975.

28. D.W. BEARD and K. WALTERS, *Elastico-viscous boundary layer flows*, Proc. Camb. Phil. Soc., **60**, 667, 1964.

Received September 16, 2002; revised version January 31, 2003.